Identification of UGT-Isoform Specific Substrates and Inhibitors and their Effect on Drug Metabolism and Systemic Levels of Bile Acids

THESIS

Submitted in partial fulfilment

of the requirements for the degree of

DOCTOR OF PHILOSOPHY

by

T V RADHAKRISHNA MULLAPUDI

ID. No. 2017PHXF0108H

Under the Supervision of

Prof. PUNNA RAO RAVI

BIRLA INSTITUTE OF TECHNOLOGY AND SCIENCE, PILANI

2024

BIRLA INSTITUTE OF TECHNOLOGY AND SCIENCE, PILANI

CERTIFICATE

This is to certify that the thesis titled "**Identification of UGT-Isoform Specific Substrates and Inhibitors and their Effect on Drug Metabolism and Systemic Levels of Bile Acids**" submitted by **T V Radhakrishna Mullapudi**, ID No. **2017PHXF0108H**, for an award of a PhD from the Institute, embodies original work done by him under my supervision.

Signature of the Supervisor: 

Name in capital letters: PUNNA RAO RAVI

Designation : Professor

Date : 29-Mar-2024

Acknowledgements

It has always been my understanding that research involves more than experiments on animals or in a laboratory. Throughout my journey, I have worked on self-education through constant interaction with fellow researchers, asking myself questions, developing data and reflecting on my findings. Several individuals provided encouragement, advice, and timely guidance along the way.

My deepest gratitude goes out to Prof. Punna Rao Ravi, my doctoral supervisor. I was always encouraged to explore different research possibilities while pursuing my thesis objectives by Prof. Punna Rao Ravi. My outlook on research has completely changed as a result of his freedom to explore several interdisciplinary avenues. Being able to work with Prof. Punna Rao Ravi has been a great honour for me. The exemplary qualities he possesses in terms of research acumen and strict moral and ethical code of conduct should be emulated.

I am excited to extend my heartfelt gratitude to Prof. V. Ramgopal Rao, Vice Chancellor, BITS Pilani, Prof. G. Sundar, Director, BITS Pilani Hyderabad Campus, Mr. Col Soumyabrata Chakraborty (Retd)., Registrar, BITS Pilani, Prof. Yogeeswari, Dean, General Administration and Prof. Venkata Vamsi Krishna Venuganti, Associate Dean, AGSRD, for their invaluable assistance in facilitating the successful completion of my research project.

I am extremely grateful to Prof. Sajeli Begum, Head, Department of Pharmacy, for her unwavering support and for making it possible for me to work at the institute. I would also like to express my heartfelt appreciation to Prof. Onkar Kulkarni and Prof. D. Sriram, my Doctoral Advisory Committee (DAC), providing their invaluable feedback and guidance throughout this project. I am deeply grateful for the support received from other faculty members of Department of Pharmacy, namely Prof. Swati Biswas, Prof. Balram Ghosh, Prof. Arti Dhar,

Dr. Akash Chaurasiya, and Dr. Nirmal Jayabalan in assisting me with any challenges that arose during my research work.

I am filled with immense gratitude towards Mr. Ganapathi Thipparapu from Pharmajen Laboratories Pvt Ltd for not only being a colleague but also a dear friend. During the challenging times, his unwavering support has alleviated much of the stress I faced. Our conversations often centre around our work in the field of science, which leads to dynamic discussions, debates, and disagreements, making our time at BITS and Pharmajen Labs truly captivating.

I am incredibly appreciative of the guidance and assistance provided by my colleagues and lab mates, including Dr. Chandra Teja U, Dr. Avantika Dalvi, Ms. Ekta Prasanthi B., Dr. Mohammed Shareef, Ms. Radhika Mahajan, Ms. Swagata Sinha, and many others. Additionally, I extend my gratitude to Dr. Rimpy Diwan and Mr. Pradeep Rawat for their unwavering support and invaluable guidance during their time at BITS Pilani Hyderabad Campus.

I am filled with gratitude for the assistance given by the non-teaching personnel, particularly the lab technicians, such as Mrs. Saritha, Mrs. Rekha, Mrs. Sunita and Mr. Rajesh of Department of Pharmacy as well other staff members including store employees, librarian and security personnel. I extend my thanks to Mr. Uppalaiah, Mr. Mallesh, Mr. Narasimha and Mr. Kumar, the Central Analytical Laboratory (CAL) technicians for their support in this endeavor.

My sincere thanks to my parents, Mr. MVS Bhaskara Rao and Late Mrs. Sita Rathnam, and family members who understood the challenges that come with pursuing doctoral research and provided their unconditional support and encouragement, which uplifted my spirit during difficult times.

Abstract

Uridine diphosphate glucuronosyl transferases (UGTs) are important phase-II metabolic enzymes that catalyse the conjugation of glucuronic acid from uridine diphosphate glucuronic acid to either xenobiotic or endogenous molecules, commonly referred to as 'glucuronidation' metabolism. Glucuronidation involves in the detoxification and elimination of toxic hydrophobic compounds by converting them into hydrophilic glucuronide metabolites that are excreted from body. At least one in ten of the top two hundred prescription drugs having glucuronidation as an important clearance pathway and this number is being constantly increasing and thus UGTs are attracting more attention in the drug metabolism and pharmacokinetics research field. Involvement of cytochrome P450 (CYP) enzymes in metabolic drug-drug interactions (DDIs) have been extensively studied and Food and Drugs Administration (FDA) has already issued guidance for evaluation of *in vitro* and clinical DDIs using classified substrates, inhibitors and inducers for various CYPs. But the paucity of such guidance by regulatory agencies exists until a recent M12 draft guidance for drug interactions studies for UGTs. However, the challenges still exist in the form of limited number of selective substrates, inhibitors/inducers to study UGT-mediated DDIs *in vitro* and *in vivo.* Moreover, it is noteworthy to consider the intestinal metabolism in addition to hepatic first pass clearance. Although compounds that are identified as substrates or inhibitors of certain UGTs *in vitro*, the potential to result in clinically significant DDIs is not warranted and this could be evaluated using animal models at preclinical stage, because solubility, permeability, gut metabolism, effective concentration etc. determine drug fate *in vivo*. Hence, identification of such sensitive index substrates (victims) and index inhibitors/inducers (perpetrators) of various UGT isoforms is ongoing research.

Among all UGT isoforms UGT1A1 and UGT1A3 are important isoforms in metabolic clearance of many drugs and in the detoxification of endogenous molecules such as bilirubin and bile acids. Bilirubin is glucuronidated to form mono- and di-glucuronides by UGT1A1 and inhibition of this isoenzyme causes hyperbilirubinemia. While, UGT1A3 is the major isozyme involved in the glucuronidation of bile acids and its inhibition may leads to increased hydrophobic toxic bile acid accumulation in the body and results in cholestasis and other bile acid related metabolic diseases. Atazanavir, a UGT1A1 inhibitor, resulted in clinically significant hyperbilirubinemia, but the effect of inhibition of UGT1A3 on the bile acid profiles was hitherto unexplored. Moreover, inhibition of UGT1A1/UGT1A3 clearance pathway on systemic bilirubin and bile acids homeostasis was not studied till date.

In this context, in the current research work we aimed to identify suitable selective substrates and inhibitors and to establish a robust and convenient *in vitro* methodology to be used for routine screening of substrates and inhibitors of UGT1A1 and UGT1A3 isoforms. Further to identify a common substrate and common inhibitor of these isoforms to establish an *in vivo* rat model to investigate possible substrates or inhibitors for their potential to yield a significant drug interaction when given in combination. Finally, we aimed to develop and validate a simultaneous UHPLC-MS/MS method of seven major bile acids in order to investigate the hitherto unexplored effect of UGT inhibition on the systemic bilirubin and bile acids levels in rat model to understand the role of UGTs in regulation of endogenous molecules homeostasis and to highlight the importance of drug-endobiotic interaction (DEI) potential of UGT inhibitors. To our knowledge this is the first report to discuss the effects of UGT inhibition on bilirubin and bile acid homeostasis.

As the initial objective of this research work, an optimized *in vitro* methodology was developed in human liver microsomes (HLM), human intestinal microsomes (HIM) and human

recombinant UGT1A1 and UGT1A3 Supersomes™ (rUGT) as enzyme sources. Herein, HLM and HIM represent hepatic and intestinal metabolism, respectively. β-estradiol and chenodeoxycholic acid (CDCA) were used as selective substrates and, atazanavir (HLM)/zafirlukast (HIM), and lithocholic acid were used as inhibitors for UGT1A1 and UGT1A3 isoforms, respectively. Alamethicin was used to activate microsomes and uridine diphosphate glucuronic acid (UDPGA) was used as cofactor for glucuronidation reactions. The incubation mixture consisted of 50 mM of Tris-HCl buffer (pH 7.4), 5 mM of $MgCl_2$, 10 µg/mL of alamethicin and 0.25 mg/mL of microsomes or Supersomes^{TM} (HLM/HIM/rUGTs), various concentrations of either substrates or inhibitors and 5 mM of UDPGA in 100 µL reaction volume. A novel approach of preparation of a master mix containing buffer, $MgCl_2$, microsomes/Supersomes™ and alamethicin was employed to mitigate experimental errors and this mix was kept on ice for 15 min. Enzyme kinetics studies were conducted by transferring 94.25 µL of this mix into each well of 96-deep well plate and 0.75 µL of various concentrations of substrates were added and preincubated at 37 ºC for 5 min and the reaction was initiated by adding 5 µL of prewarmed UDPGA and incubated at 37 ºC for 40 min and stopped the reaction by adding 300 µL of ice-cold acetonitrile containing telmisartan as internal standard. The supernatants were collected after centrifugation and analysed by LC-MS/MS. Similar approach was employed for enzyme inhibition studies except the addition of 0.25 µL of substrates at the concentrations of their respective K_m/S_{50} values, and 0.5 µL of different concentrations of inhibitors to the preincubation reaction mixture. LC-MS/MS methods for β-Estradiol 3-β-D-glucuronide and CDCA 24-Acyl-β-D-glucuronide metabolites were developed and used in kinetic or inhibition studies. β-estradiol followed allosteric sigmoidal kinetics in all three systems while CDCA followed Michaelis-Menten kinetics in HLM and substrate inhibition kinetics in other systems tested. The K_m/S_{50} values of β-estradiol were found to be 21.3±0.5 µM, 25.8±1.7 µM, and 22.3±0.6 µM; of CDCA were found to be 63.2±3.0 µM, 43.3±3.1 µM,

and 88.6±18.7 µM in HLM, rUGTs and HIM, respectively. The K_i values of CDCA were calculated as 424.2±61.1 µM and 500.1±234.3 µM in rUGT and HIM respectively. Further, IC_{50} values of atazanavir in rUGT and HLM were 0.16±0.09 µM and 0.54±0.07 µM respectively. Zafirlukast's IC_{50} in HIM was 16.70±3.64 µM against β-estradiol glucuronidation. Whereas, IC_{50} values of lithocholic acid were found to be 1.68±0.56 µM, 1.84±0.15 µM, 12.42±1.47 µM in HLM, rUGT and HIM, respectively. This methodology is appropriate for identification of isoform specific substrates and inhibitors covering hepatic and intestinal metabolism with the inclusion of recombinant UGTs, HLM and HIM in a simple, optimized and similar assay conditions. Moreover, the results from this study can be used to derive relative activity factors (RAF) or intersystem extrapolation factors (ISEF) for these UGT isoforms which can be used to calculate fraction metabolized in liver and intestine during prediction of clinical DDIs of other compounds.

To achieve the second objective of this research work, an attempt was made to establish an *in vivo* rat model that can be applied for the assessment of UGT1A1/UGT1A3 mediated *in vivo* DDIs. After identification of either substrates or inhibitors *in vitro*, the magnitude of *in vivo* DDI potential is assessed in animals to determine if they cause clinically significant DDIs or not. We have identified ezetimibe as a common victim as it is majorly and extensively metabolized by these two isoforms with similar reaction velocities in both intestine and liver tissues fractions. Also, we identified zafirlukast as a common inhibitor that inhibits both UGT1A1/UGT1A3 mediated glucuronidation. Surprisingly, no UGT-mediated metabolic DDIs were reported for ezetimibe even though glucuronidation is the major clearance pathway. The drug interaction potential of zafirlukast on ezetimibe metabolism is not yet reported and for the first time the current research work reveals this potential drug interaction. Prior to conducting a DDI study in rats, enzyme kinetics profile of ezetimibe using various

concentrations (0.073 – 53.33 µM) and, inhibitory potential of zafirlukast (0.247-540 µM) on ezetimibe (1 µM) glucuronidation were evaluated in HLM using above mentioned *in vitro* methods with the modification in the incubation time (10 min). In enzyme kinetics studies, ezetimibe phenoxy glucuronide metabolite was quantified (product formation approach) and in enzyme inhibition studies ezetimibe was quantified (substrate remaining approach). In addition, ezetimibe effect on zafirlukast exposure also assessed. Male SD rats were divided in to victim only, perpetrator only and victim + perpetrator groups (n=3). Victim group was administered with ezetimibe, perpetrator group was administered with zafirlukast, and victim + perpetrator group received ezetimibe + zafirlukast (co-administration) at 10 mg/kg body weight and 5 mL/kg dose volume for both drugs. Blood samples were collected at 0.25, 0.5, 1, 2, 4, 6, 8 and 24 h post dose from retro orbital plexus under slight isoflurane anaesthesia. Ezetimibe and zafirlukast plasma concentrations were analysed by UHPLC-MS/MS and pharmacokinetics parameters were calculated using Phoenix WinNonlin® software. *In vitro* results indicate that ezetimibe followed substrate inhibition kinetics with K_i value of 67.49±17.56 µM and the apparent K_m and V_{max} values were found to be 13.23±2.37 µM and 14275±1633 ng/min/mg protein, respectively. Due to higher reaction velocity and substrate inhibition properties of ezetimibe, the concentration used in the inhibition studies was far below the K_m values. Meanwhile IC_{50} value of zafirlukast was calculated as 16.41±3.65 µM. From the mean plasma concentration-time curve profiles, C_{max} of ezetimibe was increased 3.48-folds (248.47%) while $AUC_{0\text{-last}}$ was increased 2.34-folds (133.80%) with zafirlukast co-administration. No apparent change in the pharmacokinetics profile of zafirlukast was observed when given in combination with ezetimibe. These results indicate that zafirlukast is capable of inhibiting UGT1A1/UGT1A3 isoforms in rat. Since zafirlukast is a pan-UGT inhibitor it can be used to estimate total cumulative UGT mediated clearance of new chemical entities. Since

ezetimibe is a common substrate of UGT1A1/UGT1A3 isoforms it can be used to identify dual inhibitors for these isoforms.

The *in vivo* studies confirmed that zafirlukast can inhibit both UGT1A1 and UGT1A3 in rat and it can be used as a suitable inhibitor to study the effect of UGT inhibition on the homeostasis of bile acids and bilirubin in rat. A robust and validated bioanalytical method is a prerequisite for accurate quantification of systemic bile acids. Hence, a UHPLC-MS/MS method was developed and validated for simultaneous estimation of seven major bile acids in rat plasma. UHPLC system (Nexera 40D-XS, Shimadzu Corporation, Kyoto, Japan) coupled with a SCIEX QTRAP® 4500 mass analyser attached with Turbo V™ and electrospray ionization probe with negative mode (Sciex, MA, USA) was used. Water containing 0.1% v/v formic acid (aqueous) and acetonitrile (organic) were used as mobile phases at a flow rate of 0.45 mL/min and chromatographic separation was achieved on Acquity UPLC® HSS T3 column (1.8 µm, 2.1 × 100 mm) by optimized gradient method with 2 µL sample within 10 min runtime. Pseudo-MRM was employed and the area ratio of analyte to the respective deuterated internal standards was used to calculate analyte concentration. The method was validated for selectivity, specificity, carryover, extraction recovery, matrix effect, linearity, accuracy & precision, stability, reinjection reproducibility and dilution integrity using charcoal stripped rat plasma as surrogate matrix with a simple precipitation method as per FDA M10 guidance for bioanalytical method development and validation and, applied to study the effect of an FXR agonist, ivermectin, on bile acid levels in rats. The developed method was proved to be robust and accurate for the precise quantification of specified bile acids in rat plasma.

Finally, the developed method was utilized to assess the bile acid homeostasis upon UGT1A1/UGT1A3 inhibition by zafirlukast in male SD rats. Zafirlukast was administered to six rats by oral route at dose of 10 mg/kg and a dose volume of 5 mL/kg once-daily for seven

days. Blood samples were collected at 0.25, 0.5, 1, 2, 4, 8, 24 h on day-0 and on day-7 from each animal from retro orbital plexus under slight isoflurane anaesthesia. Similarly, blood was collected before and after 7-days drug exposure at single time point for bilirubin estimation. Plasma bile acids were quantified by UHPLC-MS/MS method and the area under the curves (AUC) were calculated using Phoenix WinNonlin® software. Serum total bilirubin was estimated by diazonium method. Surprisingly, the total bilirubin levels were not affected by 7-days zafirlukast exposure. While interesting results were observed for bile acids levels. The plasma exposure levels of CA, CDCA and DCA were significantly reduced by 73.59% (P=0.023), 88.50% (P=0.026) and 56.50% (P=0.044), respectively, in the day-7 samples compared to day-0 samples. Statistically no significant difference (P>0.05) was observed in the plasma levels of GDCA, Tα-MCA and Tβ-MCA levels in the study. Interestingly, TDCA levels were significantly increased by 223.10% (P=0.040) with zafirlukast exposure. These results indicate that UGT inhibition results in the altered bile acid profiles via unrecognized mechanisms. The underlying mechanisms for these changes in bile acid homeostasis can be explained by the assumption of involvement of ligand activated nuclear receptors such as farnesoid-X-receptor (FXR), constitute-androstane-receptor (CAR) and aryl hydrocarbon receptor (AhR) etc. by feed-forward or feedback mechanisms. In detail, the increased levels of bile acids as a result of inhibited UGT1A3 mediated glucuronidation, in turn activate these receptors. This possibility is further supported by the fact that CDCA, CA and DCA are potent endogenous FXR agonists while Tβ-MCA is an FXR antagonist. Literature also reported that activation of FXR by both endogenous and exogenous agonists resulted in the induction of UGT1A3 enzyme expression, which leads to the increased glucuronidation of bile acids. The specific decrease in the unconjugated bile acids may be because of UGT1A3 induction, which specifically involves in the glucuronidation at C-24 position of bile acids. In contrast, lithocholic acid mediated activation of FXR reduced the expression of UGT2B7 which

glucuronidates C-3 position of bile acids. Moreover, the decrease in the primary bile acids (CA, CDCA) may be resulted by FXR negative feedback regulation to inhibit bile acid biosynthesis via small heterodimer partner (SHP), fibroblast growth factor 15/19 (FGF15/19) that block CYP7A1, a rate limiting enzyme in bile acid synthesis from cholesterol. Conclusively, these results indicate that either inhibition or induction of UGTs by drug candidates may potentially alter the disposition of endobiotics with clinical significance. Herein, we suggest that evaluating such kind of drug-endobiotic interactions can offer more insights into the understanding of drug effects on metabolic fate and homeostasis of endogenous molecules.

In summary, we have established *in vitro* methodology to identify UGT1A1 and/or UGT1A3 substrates and inhibitors. These methods can be used for routine high throughput screening of inhibitors of these isoforms. Further these results can be employed to calculate *in vivo* scaling factors during clinical DDI predictions. The *in vivo* rat model of DDI can be advantageous in the assessment of the magnitude of either substrates or inhibitors of these isoforms to cause clinically significant DDIs. The changes in the systemic bile acid levels by any existing drug or novel chemical entities can be evaluated using the validated UHPLC-MS/MS method. The bioanalytical method also used in exploratory research works such as investigating bile acid related pathophysiological conditions in the preclinical settings. The observed results from the drug-endobiotic interactions of zafirlukast on systemic bile acid levels suggest that changes in the disposition of endobiotics due to altered UGT metabolism represent a potential issue to be considered and further research is expected to unravel the underlying distinct mechanisms of the paradoxical results obtained. Preference should be given to this kind of research work where critical endobiotic imbalance implicates with occurrence of metabolic diseases. Thus, adverse reactions will be predicted or prevented by dose adjustments or proper labelling of drug products in the clinic.

Table of contents

List of tables

List of figures

List of abbreviations and symbols

Acronym/Symbol	Abbreviation/Meaning
%	Percentage
%bias	Percentage relative error
%RSD	Percentage Relative standard deviation
°	Degree (angle)
°C	Degree Celsius
µg	Micro gram
µL	Microliter
µm	Micrometre
Å	Angstrom
ACN	Acetonitrile
AUC	Area under the curve
$AUC_{0-\infty}$	Area under the curve from t=0 to t=infinity
AUC_{0-t}	Area under the curve from t=0 to t=a specific sampling point
$AUC_{0-tlast}$	Area under the curve from t=0 to t=last sampling point
BA	Bile acid
BLQ	Below limit of quantification
CI	Confidence Interval
cm	Centimetre
cm^2	Square-Centimetre
C_{max}	Concentration maximum or peak concentration
CPCSEA	Committee for the purpose of control and supervision of experiments on animals
Da	Daltons
DMSO	Dimethyl sulfoxide
EDTA	Ethylenediaminetetraacetic acid (disodium salt)
FDA	Food and Drugs Administration
h	Hour(s)
HPLC	High performance liquid chromatography
UPLC	Ultra performance liquid chromatography
HQC	High quality control
IVM	Ivermectin
IV	Intravenous
IAEC	Institutional Animal Ethics Committee
ICH	International Conference on Harmonization
IS	Internal standard
Kg	Kilogram
V	Volts
L	Litre

LLOQ	Lower limit of quantification
LOD	Limit of detection
LOQ	Limit of quantification
LQC	Low quality control
MeOH	Methanol
M	Molarity
m/z	Mass to charge ratio
mg	Milligram
min	Minute
mL	Millilitre
mm	Millimetre
mM	Millimolar
MQC	Medium quality control
MRT	Mean residence time
n	Number of replicates
NCA	Non-compartmental analysis
ng	Nanogram
nm	Nanometre
pH	Negative log of H^+ ion concentration
DMPK	Drug Metabolism and Pharmacokinetics
pKa	Negative log of acid dissociation constant
PRESS	Predicted residual error sum of squares
QC	Quality control
R^2	Regression coefficient
R^2_{adjusted}	Regression coefficient of the model adjusted for significant terms
$R^2_{\text{Predicted}}$	Regression coefficient of the predicted model for a response
RH	Relative humidity
rpm	Rotations per minute
R_t	Retention time
SD	Standard deviation
SEE	Standard error of estimate
Sec	Seconds
$t_{1/2}$	Elimination half life
T_{max}	Time taken to reach maximum plasma concentration
ULOQ	Upper limit of quantification
v/v	Volume/volume
VSS	Volume of distribution at steady state
w/v	Weight/volume
α	Alpha
β	Beta
σ	Standard Deviation of y-intercepts

ADME	Absorption, distribution, metabolism and elimination
DME	Drug metabolizing enzymes
DDI	Drug-drug interaction
CYP	Cytochrome P450
IVIVC	*In vitro-in vivo*-correlation
AO	Aldehyde oxidase
XO	Xanthin oxidase
MAO	Monoamine oxidase
FMO	Flavin monooxygenase
UGT	Uridine 5’ diphospho glucuronosyl transferases
SULT	Sulfotransferases
NAT	N-acetyltransferase
GST	Glutathione S transferases
UDPGA	Uridine diphospho glucuronic acid
kb	Kilo base
LC-MS	Liquid chromatography-mass spectrometry
HLM	Human liver microsomes
HIM	Human intestinal microsomes
HKM	Human kidney microsomes
GI	Gastrointestinal
HNF	Hepatocyte nuclear factor
FOXA1	Forkhead Box A1
SP1	Specific protein 1
CDX2	Caudal type homeobox 2
AhR	Aryl hydrocarbon receptor
Nrf2	Nuclear factor erythroid 2-related factor 2
CAR	Constitutive androstane receptor
PXR	Pregnane X receptor
FXR	Farnesoid X receptor
PPAR	Peroxisome proliferator-activated receptor
NCE	Novel chemical entity
M-3-G	Morphine-3-glucuronide
M-6-G	Morphine-6-glucuronide
AZT	zidovudine
HDI	Herb-drug interaction
IC_{50}	Half-maximal inhibitor concentration
MOA	Methylophiopogonanone A
TDI	Time dependent inhibition
K_m	Substrate concentration at half of the V_{max} (Michaelis-Menten constant)
V_{max}	Maximum reaction velocity

K_i	Inhibition constant
LC-MS/MS	Liquid chromatography-tandem mass spectrometry
ISEF	Intersystem extrapolation factor
f_m	Fraction metabolism
CA	Cholic acid
CDCA	Chenodeoxycholic acid
DCA	Deoxycholic acid
GDCA	Glycodeoxycholic acid
TDCA	Taurodeoxycholic acid
Tα-MCA	Tauro alpha muricholic acid
Tβ-MCA	Tauro beta muricholic acid
rUGT	Recombinant UGT
S_{50}	Half maximal substrate concentration
™	Trade mark
®	Registered mark
kPa	Kilo pascal
MRM	Multiple reaction monitoring
CC	Calibration curve
MM	Michaelis-Menten
AS	Allosteric sigmoidal
SI	Substrate inhibition
$S_{y.x}$	Standard error of estimate values
V	Velocity
n	Hill coefficient
CL_{int}	Intrinsic clearance
AICc	Akaike's Information Criterion, corrected
pmol	Picomole
nM	Nanomole
ng	Nanogram
CPIC	Clinical Pharmacogenetics Implementation Consortium
PBPK	Physiological based pharmacokinetics
NPC1L1	Niemann-Pick C1-like 1
CCSEA	Committee for control and supervision of experiments on animals
BITS	Birla institute of technology and science
ESI	Electrospray ionization
K_{el}	Elimination rate constant
psi	Pound-force for square inch
TEM	Source temperature
CUR	Curtain gas
GS	Nebulizing gas
%CV	Percent co-efficient of variation

RSD	Relative standard deviation
P	Probability
BACS	Bile acid coenzyme A (CoA) synthetase
BAAT	Bile acid-CoA:amino acid N-acetyltransferase
LCA	Lithocholic acid
DEI	Drug-endobiotic interaction
TCDD	2,3,7,8-tetrachlorodibenzo-p-dioxin
NAFLD	Non-alcoholic fatty liver disease
UDCA	Ursodeoxycholic acid
SD	Sprague-Dawley
PVDF	Polyvinylidene difluoride
UFLC	Ultrafast liquid chromatography

1

Introduction

1.1 Drug metabolism

Drug metabolism and pharmacokinetics (DMPK) is an essential part of the drug discovery and development process. *In vitro* and *in vivo* investigation of DMPK profiles of the drug candidates ensure the development of safe and effective drug products. Absorption, distribution, metabolism, and excretion (ADME) properties of a drug affect the pharmacokinetic parameters and the pharmacodynamic outcomes [1-3]. Oral delivery is the route of choice for administration of any drug substance. Following oral administration of a drug product, the drug is absorbed through gastro-intestinal membranes and enters the liver via portal vein. In the liver, the drug is exposed to various drug metabolizing enzymes (DMEs) and metabolized to different metabolites [4,5]. The optimum elimination of drug via biotransformation is desirable for an ideal drug candidate to maintain sufficient systemic concentrations to elicit the pharmacological effect. But in certain circumstances such as in polypharmacy, the drug concentrations can either drop significantly below its minimum effective concentration (MEC) or exceed the therapeutic window. If the drug concentration is below its MEC, the pharmacological effect is lost and on the other hand if the drug concentration exceeds the therapeutic window, it leads to side effects and toxic buildup in the body. This occurs mainly when the DMEs of the drug are modulated, either by inhibition or by induction, by the co-administered drugs. Induction of DMEs leads to increase in their metabolizing enzyme expression which results in the increased metabolism of their substrate drugs and subsequent decreases in substrate drug's concentration in the body. While inhibition of DMEs results in diminished metabolism of drugs that are being metabolized by the DMEs thereby leading to increase in the levels of those drugs in the body. In polypharmacy or concomitant use of multiple drugs in patients to treat complex disease conditions, there is a possibility of the above-mentioned metabolism related drug interactions due to inhibition or

induction of any specific enzyme that is responsible for the metabolism of either drug. In both the cases, either dose or dosing regimen may be modified for the drugs to avoid undesirable clinical outcomes [6-8]. Therefore, caution should be taken while administering more than one drug in combination for cumulative health benefits. Biotransformation, chemical alterations of a substance in the body, either for clearance or bioactivation, is an important parameter which influences the pharmacokinetics, safety and efficacy of drugs [2]. Investigation of drug metabolism to determine its metabolic stability is the initial step to know the rate at which the drug is metabolized to its corresponding metabolite(s). The identification of metabolizing enzymes and respective metabolites is important to know which enzyme is responsible for the major metabolic clearance of a drug. This information is essential to understand the metabolic profile and to assess the possible drug-drug interactions (DDIs) of that particular drug [3].

Extensive research has been done in characterization of various DMEs, such as cytochrome P450 (CYP) enzymes, in the drug metabolism. The reaction phenotyping protocols of various CYPs have been developed over the years and are routinely used in the current drug discovery projects [4, 5]. Majority of drugs are metabolized by CYP enzymes via the phase-I metabolic reactions. Phase-I metabolic reactions of a drug involve oxidation or reduction or hydrolysis of the drug. The enzymes responsible for these phase-I metabolic reactions include CYP enzymes, aldehyde oxidase (AO), xanthine oxidase (XO), monoamine oxidases (MAO), flavin containing monooxygenases (FMO) and hydrolases. Phase-II metabolic reactions also play significant role in the metabolic clearance of several drugs. These reactions involve the conjugation of a drug with an appropriate molecule via glucuronidation, sulfation, methylation, acetylation, amidation, glutathione conjugation and fatty acid conjugation. These reactions are carried out by uridine 5’ diphospho glucuronosyl transferases (UGTs), sulfotransferases (SULT), N-acetyltransferase (NAT), glutathione S transferases (GST) etc. [6, 7]. In recent

years, several researchers have been working on phase-II metabolism of drugs in the context of achieving better *in vitro* and *in vivo* correlations (IVIVC) and to study possible drug interactions involving phase-II metabolic reactions [8-10]. Hence, it is highly recommended to consider phase-II metabolizing enzymes in the complete metabolic profiling of drugs.

Both phase-I and phase-II reactions make the parent compound more polar so that it is easily eliminated from body through urine or bile or feces. The metabolites formed by phase-I reactions may undergo elimination directly or they can further undergo phase-II metabolism to form conjugated metabolites. Phase-II metabolic reactions are majorly involved in the detoxification of toxic endogenous or exogenous compounds. Endogenous compounds such as bilirubin and unconjugated bile acids are conjugated by either glucuronidation or sulfate conjugation reactions and eliminated from the body in urine or feces. Therefore, such phase-II conjugation reactions play an important role in the homeostasis of endogenous compounds [11, 12] which are eliminated from the body by metabolic clearance processes. Phase-II metabolizing enzymes are gaining significant attention due to their involvement in the drug metabolism, detoxification, homeostasis of endogenous compounds and protection from reactive moieties [13].

1.2 Uridine 5' diphospho glucuronosyl transferases (UGTs)

Uridine 5' diphospho glucuronosyl transferases (UGTs) are the crucial and major DMEs involved in the phase-II metabolism of several drugs. In the glucuronidation conjugation reaction, glucuronic acid moiety is added to the hydroxyl group or carboxylic acid group or amine group of the substrate (exogenous/endogenous compound or the metabolite formed from phase-I reaction) to form more polar glucuronide metabolites of the substrate. This conjugation reaction involves the covalent linkage of glucuronic acid from uridine diphospho glucuronic acid (UDPGA) to any of the above-mentioned functional groups of the substrate moiety. The

mechanism of a typical glucuronidation reaction is depicted in Figure 1.1 [1, 14]. A myriad of drugs belonging to various therapeutic classes are metabolized by glucuronidation conjugation reaction.

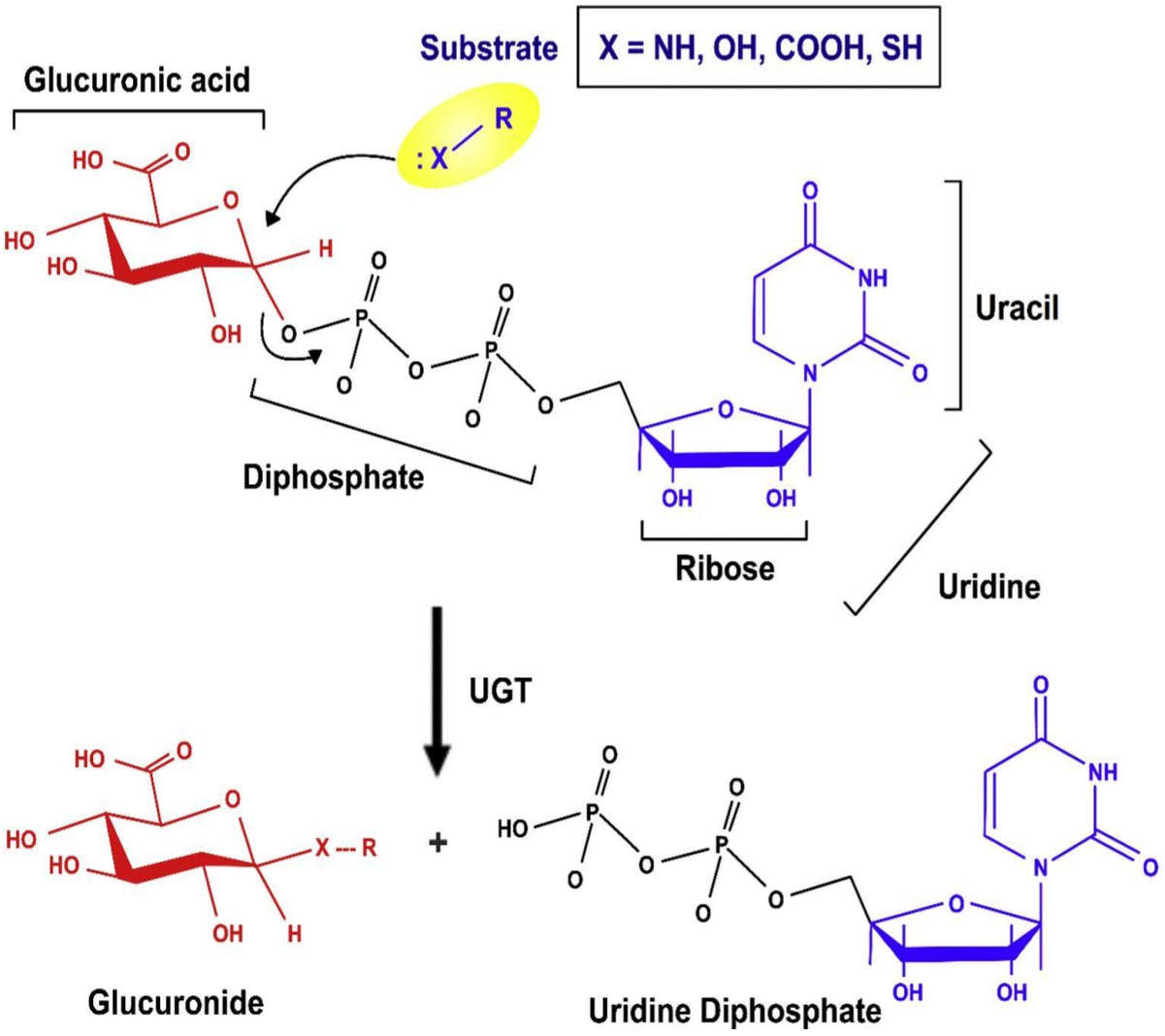

Figure 1.1 Mechanism of glucuronidation conjugation reaction [1].

In human, UGT superfamily is classified into family 1 (subfamily 1A), family 2 (subfamily 2A, 2B), family 3 (subfamily 3A) and family 8 based on the amino acid sequence. The classification of UGT enzymes is represented in Figure 1.2. A 200-kb locus on chromosome 2q37 encodes UGT1A genes in humans and each of these genes consists one of the 13 unique first exons spliced to 4 common distal exons. Hence, each UGT1A enzyme has a unique N-

terminal domain (286 amino acids) but an identical C-terminal domain (245 amino acids) compared to other UGT1A enzyme. Among the UGT1A subfamily, 9 active enzymes, namely, UGT1A1, UGT1A3, UGT1A4, UGT1A5, UGT1A6, UGT1A7, UGT1A8, UGT1A9 and UGT1A10 enzymes are encoded by the UGT1A locus. Though the data on protein activity of UGT1A5 is published but it is equivocal. The UGT2A1 and UGT2A2 genes are encoded by a unique first exon which is spliced to 5 common exons. The UGT2A3 and 7 enzymes of the UGT2B subfamily (UGT2B4, UGT2B7, UGT2B10, UGT2B11, UGT2B15, UGT2B17 and UGT2B28) are encoded by different genes which have 6 unique exons. Therefore, these proteins differ in their amino acid sequence and the greatest dissimilarity appears in sequence of N-terminal residues. The two enzymes of UGT3A subfamily, UGT3A1 and UGT3A2, are encoded by tandemly arranged genes. Only one enzyme, UGT8A1, is present in the UGT8 family [22,23].

The UGT enzymes are transmembrane proteins that are present in the smooth endoplasmic reticulum and nuclear compartments. The entire protein along with its active site is present within the lumen of endoplasmic reticulum. The UGT enzymes are majorly distributed in liver followed by intestine and kidney as given in Table 1. Except the UGT1A5, UGT1A7, UGT1A8, UGT1A10 enzymes in the UGT1A subfamily and UGT2A1 enzyme in the UGT12A subfamily, the messenger ribonucleic acid (mRNA) expression of all the isoforms is observed in the liver. The presence of UGT1A1, UGT1A3, UGT1A4, UGT1A6, UGT1A9, UGT2B4, UGT2B7, UGT2B10, UGT2B15 and UGT2B17 protein expression in human liver microsomes (HLM) is confirmed by multiple advanced proteomic analysis such as liquid chromatography coupled with tandem mass spectrometry (LC-MS/MS). Further, the enzyme activities of UGT1A1, UGT1A3, UGT1A4, UGT1A6, UGT1A9, UGT2B7 and UGT2B15 in human liver microsomes (HLMs) showed significant correlation with protein expression. Human kidney

microsomes (HKMs) expressed mRNA of UGT1A6, UGT1A9 and UGT2B7 enzymes. Gastro-intestinal tract (GIT) including stomach, small intestine and colon exhibited the mRNA expression of UGT1A1, UGT1A3, UGT1A4, UGT1A6, UGT2B7, UGT2B15 and UGT2B17 but interestingly, UGT1A7, UGT1A8 and UGT1A10 are exclusively expressed in GIT as the expression of these isoforms is absent in HLMs and HKMs. Since most of the important family of UGT enzymes are expressed in the liver, intestine and kidney tissues, isoforms belonging to UGT1A and UGT2A are differentially expressed in lungs, mammary glands, ovaries, prostate and testis [14-17]. As there are differences in the mRNA and relative protein expressions across these tissues, it is necessary to quantify the protein content of each enzyme system and correlate with each other. Further, the development of relative activity factors across the tissues can be highly advantageous in extrapolation of *in vitro* data to *in vivo* predictions or *in vitro-in vivo* correlation (IVIVC) [18-20]. Apart from the differential tissue distribution, polymorphism can also play role in metabolism and toxicity. Age, gender, ethnicity etc. can also affect the expression and activity of UGT enzymes. Moreover, polymorphic allele can cause metabolism related diseases due to imbalance of homeostasis of endogenous biological molecules [21, 22]. Hence caution should be taken while designing metabolic or drug interaction studies of drugs that are inhibitors or substrates of UGT enzymes.

Table 1.1 Distribution of UGT isoforms in liver, intestine, and kidney in humans

Tissue	**Types of UGT isoforms present in the tissue**
Liver	UGT1A1, 1A3, 1A4, 1A6, 1A9, 2B4, 2B7, 2B10, 2B15, 2B17
Intestine	UGT1A1, 1A3, 1A4, 1A6, 2B7, 2B15, 2B17, 1A7, 1A8, 1A10
Kidney	UGT1A6, 1A9, 2B7

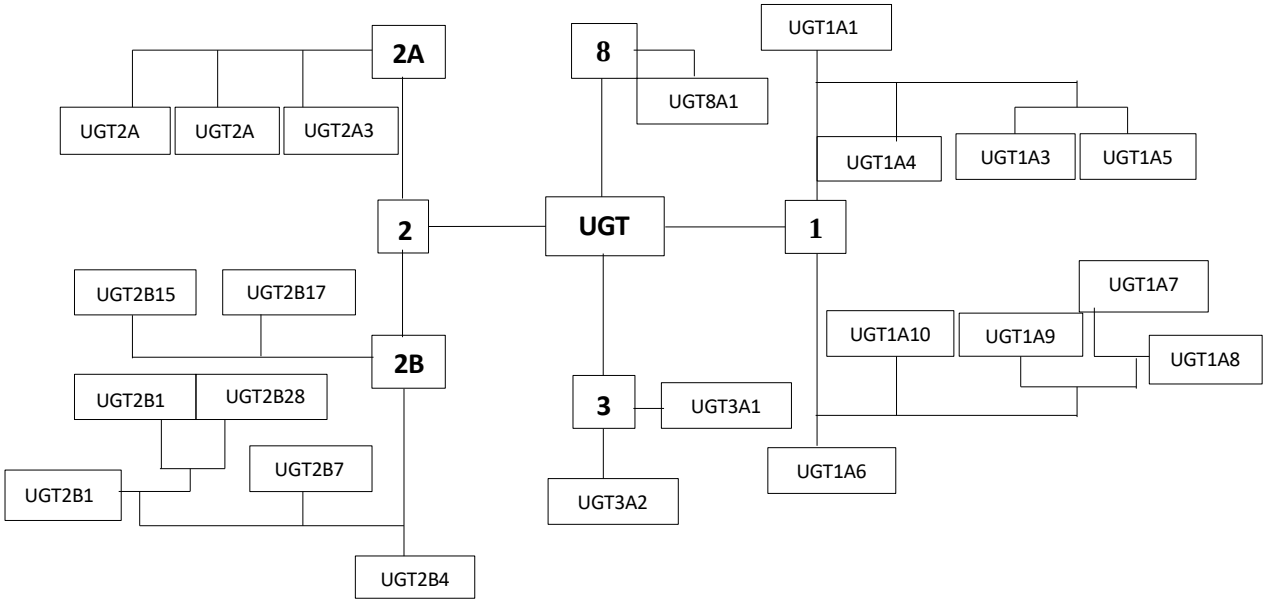

Figure 1.2 Classification of human UGT enzymes

The differential expression of UGTs in different organs or in the same organ in different individuals creates large variations among different populations. As a result, this could lead to differences in glucuronidation capabilities and finding the reason for this variation can help in evaluation of drug toxicity or potential drug interactions [23]. So far, several mechanisms have been identified that regulate the expression of UGTs, but the important mechanisms include epigenetic, tissue specific or ligand specific transcription factor regulation. The epigenetic regulation of UGTs can be exemplified by the absence of UGT1A1 in kidney and UGT1A10 in liver due to hyper-methylation of their respective promoters in the chromosome. Conversely, hypo-methylation of the promoters of UGT1A10 and UGT1A1 is associated with their presence in intestine and liver respectively [14, 24].

Apart from the chromatin modifications, various transcription factors like hepatocyte nuclear factor family (HNF1α and HNF4), ubiquitous tissue specific factors (Forkhead Box A1 (FOXA1), Specific Protein 1 (Sp1) and Caudal type homeobox 2 (Cdx2)) and chemical ligand

modulated transcription factors (Aryl hydrocarbon receptor (AhR) and Nuclear factor erythroid 2-related factor 2 (Nrf2)) and nuclear receptor superfamily (Farnesoid X receptor (FXR), Pregnane X receptor (PXR), Constitutive androstane receptor (CAR), Liver X receptor (LXR) and Peroxisome Proliferator-Activated Receptor (PPAR)) are involved in the transcriptional regulation of UGTs. HNF1α, the liver enriched transcription factor, was found to regulate the expression of UGT1 and UGT2 in liver. The proximal promoters of UGT1A1, UGT1A3, UGT 1A4, UGT2B7 and UGT2B17 genes have the binding sites for HNF1α activation. Other transcriptional factors also involve in the modulation of HNF1α mediated transcriptional upregulation. For example, interaction of organic cation transporter 1 (Oct-1) with HNF1α results in the enhanced UGT2B7 activation, while activation of UGT2B17 transcription via HNF1α was inhibited by pre-B cell homeobox 2. Another liver transcription factor, HNF4α, is also shown to regulate UGT1A1, UGT1A3 and UGT1A9. However, UGT1A9 expression is dependent on HNF1α, which enhances the activity or binding capacity of HNF4α. In the gastrointestinal tract, HNF1α binds to the proximal promoters of UGT1A8, UGT1A9, UGT1A10 and UGT2B7 genes to upregulate their expression. Intestinal specific transcription factor, Cdx2, augments the HNF1α mediated activation of UGT1A8, UGT1A9 and UGT2B7 by adjacent binding. Due to the absence of both Cdx-2 and Cdx-2 adjacent binding site in UGT1A7 (located in upper GIT), no regulation is mediated by Cdx-2. Further, UGT expression along the GIT is differentially regulated by other factors like Sp1 [14, 25, 26].

Steroidal hormones, like estradiol and dihydrotestosterone, have shown to upregulate the androgen glucuronidating UGTs, UGT2B15 and 2B17, by oestrogen response element of proximal gene promoter in the breast tissue. Conversely, UGT2B15 and UGT2B17 are down regulated in prostate cells by binding of dihydrotestosterone to androgen receptors. The hormone dependent activated and basal expression of these genes are majorly affected by Fork

head Box A1 transcription factor [27-29]. Like steroidal hormone receptors, other transcription factors also participate in the regulation of UGT gene expression which are activated by chemical ligands. These include androstane receptors (UGT1A1), PXR (UGT1A1, UGT1A3, UGT1A4 and UGT1A6), FXR (positively regulation of UGT2B4 and negative regulation of UGT2B7), LXR (UGT1A1), PPARα (UGT1A1, UGT1A3, UGT1A4, UGT1A6, UGT1A9 and UGT2B4), AhR (UGT1A1, UGT1A3, UGT1A4, UGT1A6 and UGT1A9) and Nrf2 transcription factor (UGT1A1) [30-39].

1.3 Contribution of UGTs in drug metabolism

The physicochemical properties of the new chemical entities (NCEs) that are developed in the recent years are significantly different from the earlier molecules. The NCEs in the recent years have larger molecular size, structurally more complex, high lipophilic and have more hydrogen bond acceptors or donors compared to the earlier drug substances [40, 41]. For most of the currently marketed drug substances, CYP metabolism is the major clearance pathway. Glucuronidation conjugation is also gaining importance as a metabolism and detoxification pathway in the current drug discovery. Some drugs (ezetimibe, morphine, dabigatran) are metabolised by UGT enzymes to form their respective glucuronide metabolites which are pharmacologically active [42-45]. Similarly, the glucuronide metabolites of few drugs such as gemfibrozil and clopidogrel cause the inactivation of CYP enzymes resulting in drug interactions [46]. Modulation (either inhibition or induction) of UGT enzymes may lead to occurrence of DDIs of drugs that are metabolized by UGTs. To evaluate the UGT-mediated DDI risk of NCEs, it is important to investigate the contribution of UGTs in their metabolism and to assess their potential for UGT modulation (inhibition or induction).

In DDIs mediated by UGTs, any drug can be considered as a victim drug if it is metabolized by a greater extent via glucuronidation conjugation reaction. A drug can be considered as a perpetrator if it potentially inhibits or induces UGT enzyme(s). Co-administration of the victim and perpetrator drugs can result in metabolism based DDIs, where the pharmacokinetic properties of the victim drug can be significantly altered compared to when the victim drug is administered alone. For the *in vitro* reaction phenotyping and enzyme inhibition studies human liver, intestinal and kidney microsomes are used while hepatocytes are used in addition to the above enzymes systems for the enzyme induction studies [47, 48]. Although *in vitro* assays help in identifying possible inhibitors, substrates and inducers, the corresponding inhibition or induction effects sometimes may not be exhibited in the *in vivo* experiments. This could be due to various factors playing a role in the *in vivo* studies such as dose, dosing volume, systemic average concentrations, other metabolizing enzymes, transporters, plasma protein or tissue binding, substrate or enzyme specificity etc. [49-51]. Hence, caution must be taken when making decisions based on *in vitro* UGT metabolism based DDI results.

Over the years, several molecules are reported to be UGT substrates or inhibitors, and the list of substrates and inhibitors of UGTs for *in vitro* studies are presented in table 2. The inhibitor compounds were identified based on inhibition of glucuronidation conjugation reactions of different UGT substrates from *in vitro* evaluations. Among the substrates some of them are also glucuronidated by multiple UGT isoforms. This kind of substrate overlapping is challenging for the identification of isoform specific inhibitors. Similarly, few of the inhibitors also inhibit multiple isoforms and hence isoform specific inhibition of UGTs has become arduous task. Interestingly some drugs such as testosterone are substrates of both CYP and UGT enzymes and thus require specific metabolites of CYP/UGT mediated reactions are

required to understand the magnitude of metabolism by various enzymes. Similarly, inducers like rifampin also induce CYP enzymes [52-55].

Table 1.2 List of substrates and inhibitors for UGTs (*in vitro* studies)

UGT Isoform	Substrates	Inhibitors
UGT1A1	β-Estradiol, PF-06409577	Nilotinib, Regorafenib
UGT1A3	Telmisartan	-
UGT1A4	Trifluoperazine, 1'-Hydroxymidazolam	Hecogenin
UGT1A6	Deferiprone, 5-Hydroxytryptophol, Serotonin	-
UGT1A9	Mycophenolic acid, Propofol	Magnolol, Niflumic acid
UGT2B7	Morphine, Zidovudine	16α- and 16β-Phenyllongifolol*, fluconazole**
UGT2B10	Cotinine, RO5263397	Desloratadine
UGT2B15	S-Oxazepam	-
UGT2B17	Testosterone	Imatinib

*16α- and 16β-Phenyllongifolol also inhibit UGT2B4. Their effects on UGT2B10 remains unknown.
** Fluconazole also inhibits UGT2B10 and UGT2B17.

Table 1.3 List of substrates and inhibitors for UGTs (clinical studies)

UGT Isoform	Substrates	Inhibitors
UGT1A1	Bictegravir, Cabotegravir, Dolutegravir, SN-38 (active metabolite of irinotecan)	Atazanavir*
UGT1A4	Lamotrigine (also by UGT2B7), Pexidartinib	Probenecid**, Valproic acid (also inhibit UGT2B7)
UGT1A9	Canagliflozin, Dapagliflozin, Ertugliflozin	Mefenamic Acid
UGT2B7	Bempedoic acid, Indomethacin, Naproxen, Zidovudine	Probenecid
UGT2B15	Lorazepam, Oxazepam	Probenecid

* Atazanavir is also an inhibitor of CYP3A. ** Probenecid is an inhibitor of OAT1 and OAT3 transporters.

Table 1.4 List of inducers for UGTs (clinical studies)

UGT Isozyme	Inducers
UGT1A1	Carbamazepine, Efavirenz, Phenobarbital, Rifampin, St. John's wort, Tipranavir combined with ritonavir
UGT1A4	Carbamazepine, Lopinavir combined with ritonavir, Phenobarbital, Phenytoin, Rifampin
UGT1A9	Rifampin
UGT2B7	Rifampin
UGT2B15	Rifampin, Phenytoin

UGT mediated clinical DDIs were reported for both inhibition and induction mediated mechanisms. Area under the plasma concentration-time curve (AUC) of victim drugs in the presence and absence of perpetrator drug is assessed to identify clinical DDIs. AUC_{Ratio} is defined as the ratio of the AUC of victim in presence and absence of perpetrator (AUC_{Ratio} = $AUC_{(+)\ Perpetrator}$ /$AUC_{(-)\ Perpetrator}$) which reflects the change in the systemic exposure of victim drug. If a drug has more than 50% contribution by glucuronidation conjugation in its overall elimination process, alteration of this glucuronidation conjugation by about 30% by perpetrator drug can lead to clinically significant DDI. While, for those drugs whose UGT-clearance accounts for less than 50% of its total systemic clearance, a significant change in the glucuronidation conjugation should be caused by the perpetrator to observe clinically significant DDI between the victim and the perpetrator. However, an arbitrary threshold of ≥ 30% change in AUC of the victim by the perpetrator is considered as clinically significant DDI. Based on the mechanism by which the perpetrator affects the metabolism of victim, the systemic levels of the victim can either increase or decrease. Inhibition of the UGT enzymes by the perpetrator causes an increase in the systemic exposure of the victim while enzymes induction results in decrease in the systemic exposure of the victim.

A summary of few DDIs mediated via the UGT enzymes is presented in the following sections. Bictegravir is a novel strand-transfer integrase inhibitor used in the treatment of human immunodeficiency virus (HIV) infection. It is majorly metabolized by UGT1A1 and CYP3A enzymes and is proposed to be a victim drug. When bictegravir (single dose of 75 mg) is administered in combination with atazanavir, a potent UGT1A1 inhibitor (at 300 mg or 400 mg once daily) in phase 2 and phase 3 clinical studies, the plasma AUC of bictegravir increased by 306–315% compared to when it is administered alone. Therefore, bictegravir is recommended not to be co-administered with atazanavir [56]. Atazanavir is also reported to

increase the systemic exposure of dolutegravir, molidustat, raltegravir (UGT1A1 substrates) with the AUC_{Ratio} of 1.91, 2.08 and 1.32-2.51, respectively. Though there is an increase in the AUC of the victim drugs (dolutegravir, molidustat, raltegravir) by perpetrator (atazanavir), no undesirable clinical outcomes are observed and the drug combinations were well-tolerated in human subjects [57]. In another clinical DDI, co-administration of faldaprevir with raltegravir is reported to cause a significant increase in the AUC of raltegravir (by 2.7 folds) compared to when raltegravir is administered alone. Faldaprevir is reported to inhibit UGT1A1, the enzymes which is primarily involved in the metabolic clearance of raltegravir. Therefore, faldaprevir acts a perpetrator and raltegravir as a victim and the DDI between the two drug is mediated via the UGT1A1 enzymes [58]. In the above examples, it is clearly evident that inhibition of the UGT enzymes by the perpetrator drug can cause a significant increase in the systemic exposure of the victim drug.

There are also few reports of DDIs where the perpetrator drug caused induction of the UGT enzymes which resulted in a significant reduction in the systemic exposure of the victim drug. Dolutegravir is reported to undergo metabolic clearance primarily by UGT1A1 enzyme. When dolutegravir is co-administered with efavirenz or carbamazepine, the systemic exposure of dolutegravir decreased significantly due to the induction of UGT1A1 enzymes by efavirenz or carbamazepine. The AUC_{Ratio} values of dolutegravir are found to be 0.43 and 0.51 when co-administered with efavirenz and carbamazepine, respectively. Therefore, to address the issue of systemic exposure of dolutegravir (victim drug), the dosing frequency of dolutegravir is increased to twice daily instead of once daily [59, 60]. In another such DDI, the systemic levels of canagliflozin are found to decrease significantly when co-administered with rifampicin. Canagliflozin is metabolized by UGT1A9 and UGT2B4 enzymes. Rifampicin causes induction of different isoforms of UGT enzymes. Co-administration of canagliflozin with rifampin

resulted in the induction of UGT isozymes, some of which are involved in the metabolic clearance of canagliflozin. Although this combination was well-tolerated, close monitoring of glycaemic control is recommended when the two drugs are co-administered [61].

In addition to DDIs, a myriad of UGT mediated herb-drug interactions (HDIs) are also reported in the literature. Many natural compounds belonging to diversified chemical classes like flavonoids, coumarins, terpenes, lignanes, anthraquinones and alkaloids are identified as possible UGT substrates and/or inhibitors. Natural compounds having hydroxy, carboxylic acid, amine and thiol groups are generally suitable substrates for UGT enzymes. Unlike drug molecules herbal derived phytochemicals exhibit more overlapping as substrates or inhibitors for multiple UGT isoforms [55]. A list of UGT substrates and inhibitors from herbal sources were presented in Table 1.5. The wide use of natural products as alternative or complementary therapies to the drug therapies increases the probability of HDIs in patients which can be of clinical significance.

Table 1.5 UGT substrates and inhibitors derived from natural products

Substrates	**Inhibitors**
Sakuranetin, oroxylin A, apigenin, diosmetin, erlodictyol, luteolin, isoneochamaejasmin A, icariside, isofraxidin, fraxetin, esculetin, betulin, tanshinone IIa, magnolol, emodin, salvianolic acid A, vasicine	Isoliquiritlgenin, cyanidins, deoxyschizandrin, schisantherin A, sauchinone, cryptotanshinone, dihydrotanshinone I, demethylzeylasteral, 20(S)-protopanaxatriol, cycloastragenol, bakuchlol, mangiferin, norathyriol

Sauchinone, a bioactive lignan in Saururus chinensis, is reported to inhibit multiple UGT enzymes like UGT1A1, UGT1A3, UGT1A6 and UGT2B7 with inhibitory concentration (IC_{50}) values of f 8.83, 43.9, 0.758 and 0.279 µM, respectively. Co-administration of sauchinone with zidovudine in mice resulted in an increase in the plasma AUC of zidovudine (a UGT substrate)

by 152% compared to when zidovudine is administered alone [62]. Myricetin, a food derived flavanol, has shown potent inhibition against UGT1A1, UGT1A3, UGT1A6, UGT1A7 and UGT1A10 enzymes. It can potentially cause significant HDIs with drugs which are known to undergo metabolic clearance via any of the above enzyme systems [63]. Methylophiopogonanone A (MOA) is identified as a pan-UGT probe substrate as it readily undergoes O-glucuronidation by various human UGT enzymes. MOA can be used as an *in vitro* tool to investigate UGT mediated metabolic reactions and DDIs [64]. Strong inhibition of UGT1A6 and UGT2B7 mediated glucuronidation was observed with celastrol, a pentacyclic nortriterpen quinone [65]. Icariin, a prenylated flavonol glycoside (a type of flavonoid), is reported to inhibit intestinal UGT1A3, UGT1A4 and UGT1A7 enzymes [66]. Deoxyschizandrin and schisantherin A, which are major bioactive lignans isolated from Fructusschisandrae, showed moderate inhibitory effect on UGT1A3 in the *in vitro* studies [67]. Piceatannol, a naturally occurring polyphenolic stilbene found in various fruits and vegetables, is reported to have inhibitory effect on UGT1A6, UGT1A7, UGT1A8 and UGT1A9 enzymes [68]. All the above phytochemicals can potentially cause clinically significant HDIs with drugs which undergo metabolic clearance by the UGT enzymes that the phytochemicals either inhibit or induce.

The UGT mediated clearance of a compound cannot be calculated solely based on the hepatic clearance but accounting the extrahepatic clearance from intestinal and/or renal tissues can predict the overall clearance and produce accurate results in DDI evaluations [69]. Non-UGT mediated metabolism pathways and transporters also contribute to the overall DDI risk, hence it is mandatory to check for those mechanisms too [70, 71]. Moreover, discrepancies occur between *in vitro* and *in vivo* results because of drug/metabolite momentum in systemic or enterohepatic circulation and excretion in *in vivo* whereas these steps are absent in *in vitro*

setup [72, 73]. In addition, altered expression of various metabolic enzymes in case of intestinal, hepatic and renal disorders may cause DDIs and hence caution must be exercised while prescribing drugs to such patients. Development of *in vitro* systems employing suitable selective substrates, inhibitors and inducers can predict glucuronidation contribution of a drug's clearance and knowing more about transcription factors of UGTs, genotyping human UGTs enable accurate labelling of drugs.

1.4 Overview of metabolic DDIs evaluation

The metabolic DDIs between two co-administered drugs can arise due to either inhibition or induction of the enzymes involved in the metabolic clearance of one drug (victim) by the other drug (perpetrator). To assess if a NCE is victim of enzyme inhibition or induction of a perpetrator, it is important to identify which enzyme is responsible for the metabolism clearance of the NCE during its development process. Initial investigation of metabolic stability of NCE is performed to identify metabolites' profiles and their metabolic pathways. If any metabolic pathway contributes more than 25% of the NCE's overall metabolism, then it is recommended to characterize the specific isoforms of the enzymes which are responsible for that metabolism. Several experimental procedures are involved in the characterization of metabolic enzyme involved in the metabolic clearance of a drug [74]. The first step is to perform a simple metabolic stability assay in liver microsomes with and without enzyme-specific cofactors. This will help to identify the type of metabolites (oxidation, glucuronidation, sulfation or glutathione conjugation etc.) formed during the metabolic reaction of the NCE. Based on the metabolites formed, suitable analytical methods are developed for those metabolites in the further investigations. In the next step, protein and time linearity tests were carried out to optimize the protein concentration and incubation time based on the metabolites

formed. Further, employing these optimized incubation conditions, enzyme kinetics were studied to determine V_{max} and K_m. V_{max} is the maximum rate of enzyme catalysed reaction at substrate saturation while K_m is the ability of a substrate to saturate the enzyme in a predefined reaction condition at the half-maximum velocity. There are mainly four types of enzyme kinetics models that are shown in Figure 1.3 [1].

In the further investigation to find out which isoform is responsible for specific metabolite formation; specific recombinant enzyme systems are used to phenotype the metabolic reactions. Finally, the drug is incubated in microsomes with an isoform specific inhibitor and compared the percentage inhibition of product formation with respective to vehicle control which further confirms the reaction phenotyping and enzyme characterization. The outcome of all these experimental procedures is highly dependent on the quality and efficiency of enzyme sources (recombinant enzymes or microsomes), optimized experimental conditions (substrate/inhibitor concentrations, incubation period, protein concentration etc.) and analytical methods used on the study. In addition, isoform specific probe substrates and inhibitors warrant accurate and reliable results during identification of metabolic pathways [1, 16, 75].

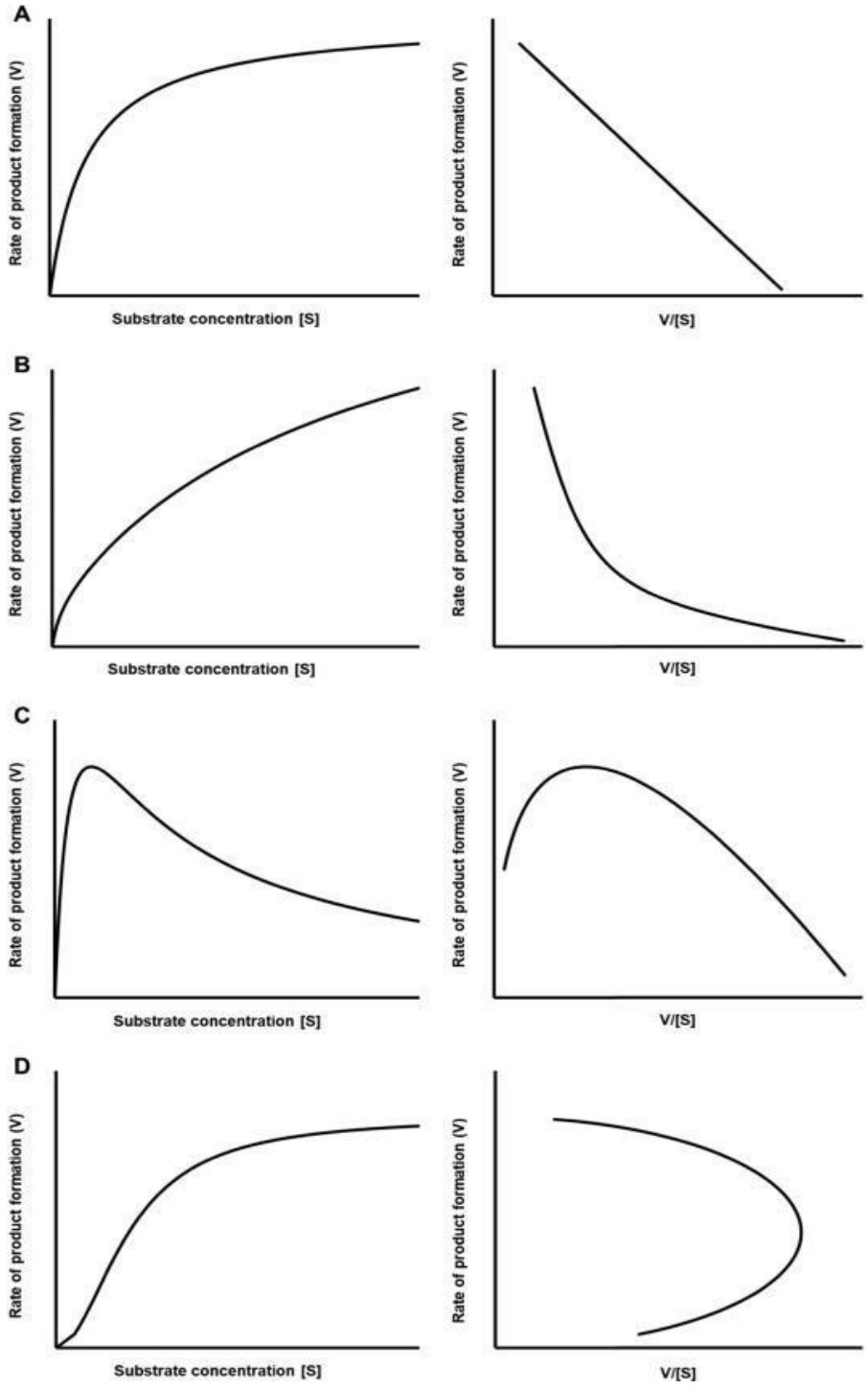

Figure 1.3 Enzyme kinetics models (on the left-hand side) and their respective Eadie-Hofstee plots used (on the right-hand side) in the analysis of data obtained from the *in vitro* studies (A) Michaelis-Menten (MM), (B) biphasic kinetics (C) substrate inhibition (SI) and (D) allosteric sigmoidal (AS) [1].

Enzyme inhibition can be either direct/reversible inhibition or time-dependent inhibition (TDI) or mechanism-based inhibition (MBI). If pre-incubation of inhibitor with the metabolizing system leads to the enhanced inhibition (reversible) of enzyme than without pre-incubation, it is referred to as TDI. The involvement of a mechanism of irreversible inhibition by reactive metabolites that are formed during pre-incubation of inhibitor with metabolic enzyme system is defined as MBI (a subset of TDI). In TDI or MBI, the test compound is converted to a degradation product or metabolite which in turn inhibits any of the metabolic enzymes [76]. Though there are some published reports on DDIs due to TDI or MBI of CYP enzymes, TDI of UGT enzymes are very few.

Most of the DDIs involving UGTs are due to the direct or reversible inhibition of the enzymes which can occur via three different mechanisms. They include competitive, non-competitive, and uncompetitive inhibition. In the competitive inhibition both substrate (victim) drug and inhibitor (perpetrator) drug compete for the same binding pocket. The effect of this type of enzyme inhibition can be minimized by increasing the substrate concentration over inhibitor, so that a greater number of substrate molecules occupy the binding site. In the non-competitive inhibition, the enzyme contains either two or multiple binding sites (orthosteric and allosteric), wherein one site is occupied by substrate and the other site(s) is/are occupied by the inhibitor. The effect of this type of inhibition cannot be minimized by increasing the substrate concentration. In the uncompetitive inhibition, the inhibitor binds to the substrate-enzyme complex and inhibits the formation of product by trapping the substrate in the enzyme-substrate-inhibitor complex. The type of inhibition mechanism can be distinguished by employing different substrate/inhibitor concentrations in the enzyme kinetics assays. The reduction in the substrate K_m (substrate concentration at half of the maximum reaction velocity)

and overall V_{max} (maximum reaction velocity) can be influenced by the inhibitory constant (K_i) [75].

The experimental protocol for the determination of UGT enzyme inhibition involves the incubation of substrate at a suitable/appropriate concentration with the enzyme in presence and absence of different concentrations of the inhibitor and followed by measuring either the formation of UGT metabolite of the substrate or the substrate remaining in the incubation at different time points. The formation of glucuronide metabolite decreases with increase in the concentration of inhibitor if the test compound shows enzyme inhibition. If the substrate remaining in the incubation is being examined in the *in vitro* metabolic study, the substrate remaining in the incubation increases with increase in the concentration of inhibitor.

The half-maximal inhibitory concentration (IC_{50}) can be calculated by plotting the logarithmic concentration of inhibitor and percentage control activity. Further, to determine the inhibition constant of enzyme-inhibitor complex and to exactly know which type of inhibition was involved, different concentrations of substrate and different concentrations of inhibitor are incubated with enzyme and the resulting data can be used to determine the K_i and type of inhibition. Eadie-Hofstee and sigmoidal non-linear regression equations are generally used to draw enzyme kinetics and inhibition profiles [1, 77]. The substrates used in the inhibition assay should be selective to the specific UGT isoform and the substrate and its glucuronide metabolite should be commercially available with feasibility of rapid and sensitive analytical method [1]. The ideal substrate concentration used in the assay should be at or below (less than 5-folds below) the K_m value of substrate to ensure linear reaction kinetics. It is suggested to use low protein concentration to prevent non-specific binding. Use of a positive control is highly recommended to evaluate the assay performance in such *in vitro* studies [75].

However, it is possible that some chemicals or drugs induce the expression of phase-I and phase-II drug metabolizing enzymes as well as transporters. Upregulation of respective genes or increase in the rate of synthesis of an enzyme can be assessed quantitatively by measuring the mRNA levels or by specific enzyme activity by real time quantitative polymerase chain reaction (RT-qPCR) and liquid chromatography-tandem mass spectrometry (LC-MS/MS), respectively, using fresh or cryopreserved hepatocytes [78, 79]. As mentioned earlier, several nuclear receptors and transcriptions factors involve in the regulation of enzyme expression. When a drug binds to these nuclear receptors, the corresponding enzymes can be induced which enhance the metabolism of their substrate drugs. This phenomenon is applicable to either perpetrator drug itself or to victim drug in monotherapy or in co-administration of drugs. It results in the reduced concentrations of those parent drugs and increased concentrations of metabolites. In both the cases it may result in diminished pharmacological effectiveness (due to sub-therapeutic levels) and may produce toxicity (due to accumulation of toxic metabolites). Both mRNA expression and catalytic activity measurements are necessary as there are possibilities of changes in the expression of protein because of post translational modifications. For the successful assessment of enzyme induction in both methods, suitable primers for the specific isoform and reference gene primers as well as suitable selective isoform specific probe substrates along with their glucuronide metabolites are essentially required [80]. Quantitative measurement of protein expression levels for each specific isoform must be performed in either cell fractions such as microsomes (per mg) or in tissues such as liver (per gram) by using advanced LC-MS/MS based proteomics analysis. These values can be employed in the estimation of intersystem extrapolation factors (ISEFs) or in the calculation of fraction metabolized (f_m) *in vivo* for better correlation with the *in vitro* data [19].

1.5 Bile acids

1.5.1 Biosynthesis of bile acids

Bile acids are a group of molecules which are steroidal acids with similar but not identical structures. The bile acids found in human have 24 carbon atoms. They are synthesized in the liver from cholesterol via two major pathways, the classical pathway, and the alternative pathway. Cholic acid (CA) and chenodeoxycholic acid (CDCA) are the two major bile acids synthesized by the classical pathway. In the alternative pathway, only chenodeoxycholic acid is synthesized (Figure 1.4). In the classical pathway, CYP7A1 is the rate limiting enzyme that initiates the synthesis of bile acids from cholesterol. In the alternative pathway, CYP27A1 is the first enzyme, among the various enzymes, involved in the synthesis of CDCA. The classical pathway accounts for more than 90% of total bile acid synthesis in human and about 70% of total bile acid synthesis in murine species. In the classical pathway, CYP8B1 is one of the critical enzymes involved in the synthesis of CA which determines the hydrophobicity of the resultant bile acid pool. In murine species, CYP2C70 is responsible for conversion of CDCA to murine specific α-muricholic acid and β-muricholic acid. Further these bile acids (CA and CDCA in humans; CA, CDCA, α-muricholic acid and β-muricholic acid in murine species) are conjugated with either glycine or taurine. Glycine conjugation is more predominant than taurine conjugation in human whereas taurine conjugation is more prominent in murine species.

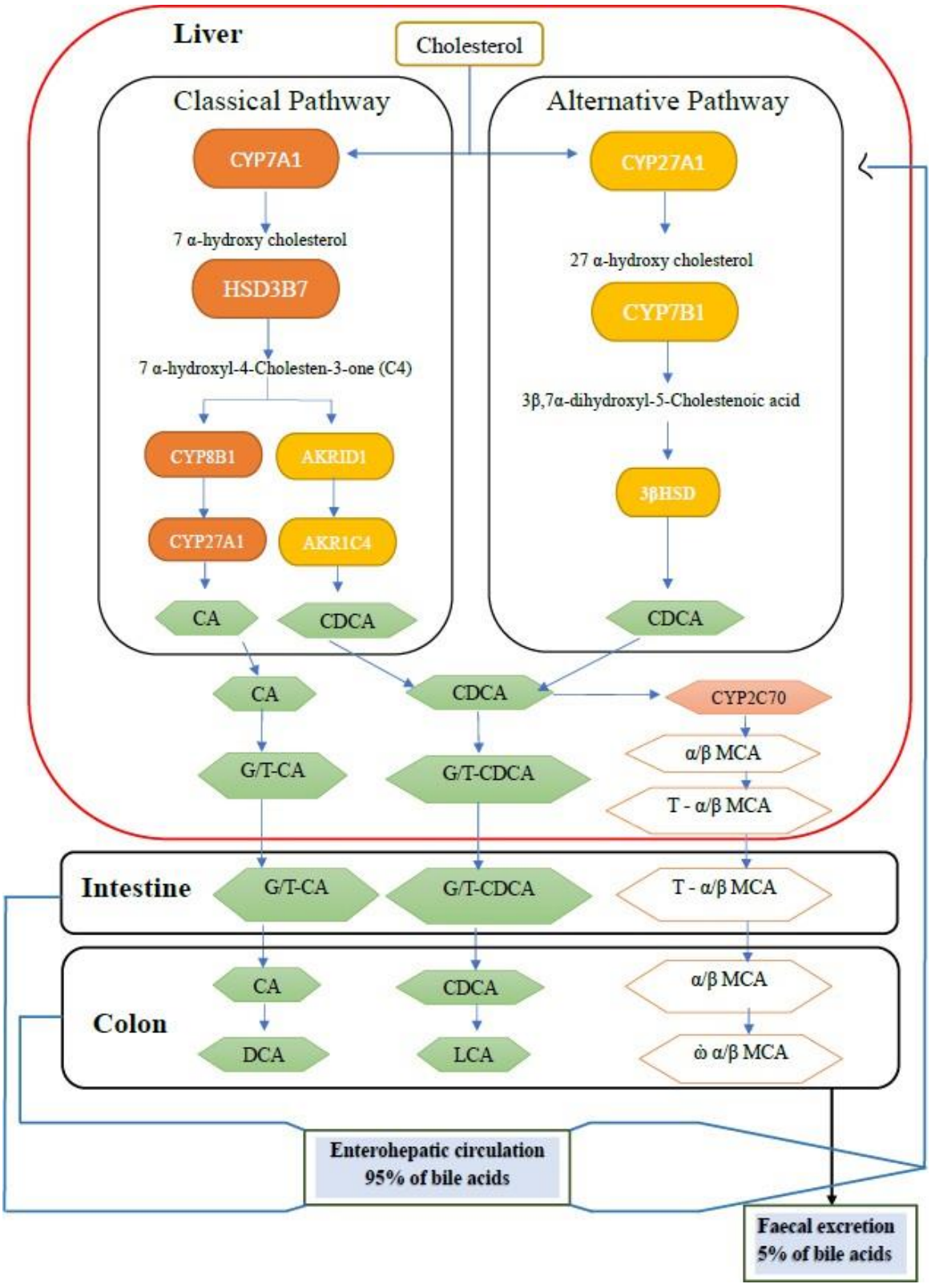

Figure 1.4 Biosynthesis and metabolism of bile acids in the liver and gastro-intestinal tract

1.5.2 Transportation of bile acids

Conjugated bile acids are secreted into the bile canaliculi via bile salt export pump (BSEP) transporter and stored in gallbladder. In bile, almost all the bile acids are present in conjugated form and if any unconjugated bile acids are secreted into the bile they may be absorbed from the biliary ductules back to sinusoidal blood and to the liver. Both the glycine/taurine-conjugated bile acids are then secreted into the gastrointestinal tract via the bile duct into duodenum. Most of the conjugated bile acids are reabsorbed in the distal ileum by apical sodium-dependent bile acid transporter (ASBT). Both unconjugated and conjugated bile acids are transported from enterocytes into portal vein by organic solute transporter α/β (OSTα/β), while the multidrug resistance protein 2 and multidrug resistance protein 3 (MRP2 and MRP3) facilitate the transport of sulphated/glucuronidated bile acids into portal vein and into the gut lumen, respectively. Active uptake of conjugated bile acids from the portal blood by hepatocytes is mediated by sodium taurocholate co-transporting polypeptide (NaTCP) and unconjugated bile acids are up taken via organic anion transport protein 1B1/1B3 family [81].

1.5.3 Regulation of bile acids homeostasis

Bile acid homeostasis is tightly regulated. Any impairment of bile flow or accumulation of bile acids leads to cholestasis and bile acid toxicity. Bile acids can regulate their own biosynthesis and transport by binding to various bile acid receptors such as FXR. Further, hormones, cytokines, growth factors, oxysterols, xenobiotics and even diurnal rhythms are also known to influence the biosynthesis and transport of bile acids. As endogenous natural agonists of FXR, bile acids activate FXR in the enterocytes (of the intestine) that leads to expression of FGF15 (in mice) or FGF19 (in humans) endocrine polypeptide. This polypeptide circulates through the portal flow to the hepatocytes where it binds with β-Klotho protein and fibroblast growth

factor-4 receptor that eventually repress the expression of CYP7A1 resulting in a decrease in the synthesis of bile acids. Meanwhile, in the liver cells, activation of hepatocyte specific FXR results in the production of short heterodimer partner (SHP) which also supresses the CYP71A expression and thereby reducing the biosynthesis of bile acids from cholesterol. This process is called negative feedback mechanism [82, 83].

1.5.4 Functional roles of bile acids

Bile acids are released from the gall bladder, via the biliary duct, into the luminal fluids of the GIT following the consumption of food. They play an important role in the emulsification and/or solubilization of cholesterol, triglycerides and fat-soluble vitamins present in the food and help in their absorption into systemic circulation. However, the role of bile acids is not just limited to the intestinal absorption of fat-soluble nutrients. Researchers have been unravelling the physiological role of bile acids in central nervous system, cardiovascular system, regulation of inflammatory reactions, influencing the hypothalamic–pituitary–adrenal axis, involvement in pathogenesis of intestinal diseases, liver diseases and lung diseases and growth of tumour cells [84]. Bile acids are also reported to play an important role in the regulation of energy, glucose and lipid metabolism, in the immune system modulation and in the detoxification reactions. Such a diversity in the physiological effects of bile acids is due to the activation of various receptors by the bile acids. Bile acids are reported to activate several receptors, including, FXR, PXR, CAR, LXR, vitamin D receptor (VDR), Takeda G-protein-coupled receptor (TGR5), muscarinic acetylcholine receptor and sphingosine-1-phosphate receptor2. Hormone-like actions of bile acids are mediated by these receptors in various tissues in controlling homeostasis of different endogenous molecules [84].

1.5.5 Biotransformation of bile acids

During the residence in the intestine, the conjugated bile acids undergo deconjugation and hydrolysis by the gut microbiota that results in the formation of secondary bile acids such as deoxycholic acid (DCA) from CA and, lithocholic acid (LCA) from CDCA. These secondary bile acids are passively absorbed from intestine. Unconjugated bile acids are metabolized in the enterocytes either by glucuronidation or by sulfation. Only 5% of bile acids are excreted in the faeces and *de novo* synthesis compensates this lost pool. Bile acids undergo biotransformation by CYP enzymes (specifically CYP3A4), UGT enzymes (specifically UGT1A1/UGT1A3/UGT2B7) and SULT enzymes (specifically SULT2A1) via hydroxylation, glucuronidation and sulfation, respectively [85].

1.6 Problem identification and research objectives

Several endogenous molecules act as substrates or inhibitors or inducers of specific DMEs and/or transporters. A classic example is bilirubin which acts as a substrate of UGT1A1 enzymes and produces glucuronide metabolites during its clearance mechanism [86]. Different unconjugated bile acids have been proposed to be substrates and inhibitors for UGT1A3 enzymes. For instance, chenodeoxycholic acid acts as a substrate of UGT1A3 but in contrast, taurolithocholic acid acts as an inhibitor of UGTs [87, 88]. Estradiol, a steroidal hormone, is known to be a probe substrate for UGT1A1 isoform [89]. Some endogenous ligands are also reported to act as inducers by binding and activating the nuclear receptors that are crucial for DMEs transcription. Progesterone, present in high concentrations during pregnancy, is involved in the upregulation of UGT1A1 expression by PXR-mediated UGT1A1 promoter activation and thereby causes an increase in the oral clearance of labetalol in pregnant women [90]. In addition to the detoxification of bilirubin and bile acids, these metabolic enzymes

(UGT1A1 and UGT1A3) also involve in the metabolic clearance of other xenobiotics or endobiotics. Inhibition of these enzymes by xenobiotics can leads to the manifestation of drug-induced cholestasis or altered bile acid homeostasis. Even though numerous studies are reported by both industry and academia on the drug/herb/food-drug interactions, special focus is needed to explore the effect of endogenous ligands on DMEs and the mechanisms thereof to provide immense insights in the DMPK science in relation to endobiotic homeostasis. Significant attention is required to investigate the role of endogenous ligands such as hormones, bile acids, phospholipids and neurotransmitters in drug metabolism and toxicity studies due to their implications in drug interactions and diseases modifications. These ligands may act as biomarkers and can also be exploited to investigate pathophysiology or therapeutic strategies in certain metabolic diseases by studying any deviations in their normal/healthy physiological concentration limits. Hence, it is imperative to address these kind of research questions during the pre-clinical development of the NCEs. In this regard, from the perspective of xenobiotic interactions with drug metabolizing enzymes, extensive research is expected in the field of drug-endobiotic interactions (DEIs) mediated via UGT enzymes. Despite the growing importance and contribution of UGT enzymes in the overall clearance of biologically important molecules, there were no reports on how modulation of UGT enzymes by drug candidates results in the alteration of bilirubin and bile acid levels in the systemic circulation. Exploring the mechanisms by which these DEIs are occurring is highly important. Such research findings may give rise to potential insights and pave roads to therapeutic applications in gastrointestinal and hepatobiliary diseases. The current research work aims to contribute to this research area by addressing how inhibition of UGT enzymes (specifically UGT1A1 and UGT1A3) can affect the bilirubin and bile acid homeostasis in a systematic approach. As on date, there is very

limited work reported in this area and provides a huge opportunity to explore as a priority area of research in academics as well as the pharmaceutical industry.

The UGT isoforms, specifically UGT1A1 and UGT1A3 isoforms, are involved in the metabolic clearance of bilirubin and bile acids. Inhibition of these specific isoforms can potentially alter homeostasis of bile acids and bilirubin [91]. A systematic method is required to study the effect of a drug (or an NCE) which has the potential to inhibit UGT1A1 and UGT1A3 isoforms and the subsequent alteration in the homeostasis of bile acids and bilirubin. First, *in vitro* studies have to be conducted to identify the suitable substrates and inhibitors for the two UGT isoforms using various enzyme systems. Based on the data obtained from the *in vitro* studies, *in vivo* studies have to be conducted in suitable animal models to confirm the victim and/or perpetrator drugs. In addition, robust analytical methods should be developed and validated for the accurate measurement of the bile acids as well as the various victim and perpetrator drugs as well as their used in the *in vitro* and *in vivo* studies.

The objectives envisaged for the current research work were as follows.

1. To establish *in vitro* methodology for UGT1A1 and UGT1A3 enzyme kinetic and enzyme inhibition studies using selective substrates and inhibitors.
2. To conduct the *in vivo* drug-drug interaction study mediated by UGT1A1 and UGT1A3 isoforms in rat model using selected victim and perpetrator drugs.
3. To develop and validate a UHPLC-MS/MS method for simultaneous quantification of seven selected bile acids in rat plasma.
4. To investigate the effect of UGT1A1 and UGT1A3 inhibition on the plasma levels of the seven selected bile acids and bilirubin in rat model.

2

In vitro methodology for UGT1A1 and UGT1A3 enzyme kinetic and inhibition studies using selective substrates and inhibitors

2.1 Introduction

Uridine-5'-diphospho-glucuronosyltransferase enzymes (UGTs) play an essential role in the phase-II metabolism of xenobiotics and endobiotics at the intestinal level [92]. A large number of exogenous compounds such as pharmaceutical drugs, chemical carcinogens, environmental pollutants, phytochemicals, dietary substances and endogenous compounds such as bilirubin, steroidal hormones, thyroid hormones, bile acids, and fat-soluble vitamins are metabolized via the transfer of glucuronic acid from co-factor UDP-glucuronic acid (UDPGA) to UGTs [93-95]. These reactions are commonly called glucuronidation conjugation reactions and account for approximately 35% of the phase II reactions [95]. Among the top two hundred approved drugs, one drug out of every ten is metabolized by UGT enzymes, which denotes their importance in drug metabolism [96]. The classification of important UGTs and their sites of expression are shown in Figure 2.1 [97-101].

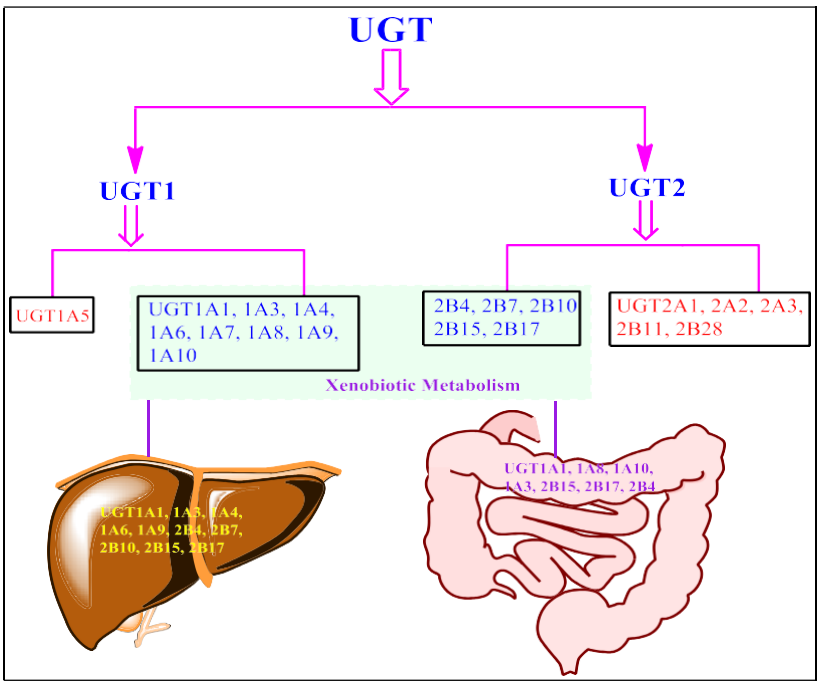

Figure 2.1 Classification of UGT isoforms with their distribution in liver and intestine

Among all the isoforms, inhibition of UGT1A1 and UGT1A3, either in the liver or intestinal tissue, leads to potential drug-drug interactions (DDIs), resulting in toxicity in the body [102-104]. For example, bilirubin is known to be metabolized by UGT1A1 mediated glucuronidation [89] and inhibition of UGT1A1 leads to elevated bilirubin levels (an endogenous by-product of heme metabolism) in the systemic circulation and causes hyperbilirubinemia [103]. While the inhibition of UGT1A3 reduces the glucuronidation of bile acids, such as CDCA, it increases the concentration of bile acids in plasma and liver, leading to bile acid-induced hepatotoxicity [102]. In hepatic disease conditions, the elevated bile acids, due to their UGT inhibitory properties, can interfere with the metabolism of xenobiotics and other endobiotics and alter their pharmacokinetic and pharmacodynamic profile [105-108]. DDIs mediated by hepatic UGT isozymes are well established in the literature [109]. One such well noted DDI mediated by hepatic UGTs is the 2.5-fold increase in plasma exposure of lamotrigine in the presence of valproic acid. In addition, valproic acid is also reported to inhibit the glucuronidation of zidovudine and lorazepam by UGT enzymes [110]. All these studies were reported based on the DDIs observed by inhibition of hepatic UGTs rather than the intestinal UGTs. Cuoto et al reported the presence of UGT1A3 in the mucosal samples of human jejunum and ileum using quantification concatemer-based targeted proteomics. But Fallon et al did not mention its presence in intestinal microsomes and Akazawa et al did not reported about UGT1A3 expression in microsomal membrane fractions of human small intestine. Amidst this uncertainty, study of UGT1A3 isoform in human intestinal microsomes may be essential to predict gut wall metabolism and related DDIs for orally administered drugs. [111-113]. Thorough literature review has shown that UGT mediated interactions at the intestinal level are not well studied till date [110, 114]. This is primarily due to the lack of

appropriate and robust *in vitro* experimental methods to elucidate the DDIs mediated by UGTs present in intestine.

Several research groups have developed and optimized the *in vitro* assay conditions to predict DDIs mediated by UGTs at the hepatic or intestinal level using HLM or HIM or recombinant isozymes independently. The conditions reported in these research works differ in terms of incubation conditions, protein concentration, incubation time, etc., therefore lacking standard experimental conditions to follow in evaluating the potential DDIs of new molecules [94, 95, 115-118]. Moreover, none of the earlier reported *in vitro* assay conditions to predict DDIs mediated by UGTs has evaluated the DDIs using three enzyme systems (HLM, HIM, rUGTs) and compared data across the three enzyme systems.

Therefore, this current thesis chapter aimed to develop *in vitro* assay systems using HLM, HIM and rUGTs under similar assay conditions and correlate the clearances of the substrates at hepatic and intestinal levels with respect to optimized assay conditions. Further, the UGT mediated inhibition potential of atazanavir, zafirlukast and lithocholic acid was also investigated in the assay systems. This work would be considered with special interest in the literature as we have compared the K_m or S_{50} values for β-estradiol, CDCA in HLM, HIM and rUGTs in one standardized assay conditions and determined the IC_{50} values for selective UGT inhibitors.

2.2 Materials and methods

2.2.1 Materials

β-estradiol, β-estradiol 3-(β-D-glucuronide) sodium salt, UDPGA, alamethicin, atazanavir sulfate and ammonium acetate were purchased from Sigma-Aldrich (Bangalore, India). Molecular biology grade tris base and magnesium chloride ($MgCl_2$) were purchased from Sisco

Research Laboratories (Mumbai, India). Lithocholic acid, CDCA, zafirlukast and telmisartan were obtained from TCI Chemicals (Hyderabad, India). Pooled human liver microsomes were procured from Invitrogen (NY, USA), HLM were from Xenotech (Kansas, USA), and recombinant UGT1A1 and UGT1A3 Supersomes™ were purchased from Corning® Inc., (NY, USA), respectively. Chenodeoxycholic acid 24-acyl-β-D-glucuronide was purchased from Toronto Research Chemicals (Toronto, Canada). dimethyl sulfoxide (Merck India), acetonitrile (Merck India), methanol (Merck India) was purchased.

2.2.2 Preparation of reagents

Tris-HCl (50 mM) buffer, pH 7.4, was prepared in ultrapure Milli-Q water. $MgCl_2$ (100 mM) and UDPGA (100 mM) were prepared using 50 mM Tris-HCl buffer (pH 7.4) as the solvent. Alamethicin (5 mg/mL) stock solution was prepared in ethanol. HLM, rUGTs and HIM were supplied as 20 mg/mL, 5 mg/mL and 10 mg/mL, respectively. Different concentrations of substrates/inhibitors or authenticated glucuronide standards were prepared in DMSO as the solvent.

2.2.3 Enzyme kinetics studies for determining the K_m or S_{50} of substrates

Enzyme kinetic studies were conducted to determine the K_m or S_{50} of β-estradiol and CDCA, which are substrates for UGT1A1 and UGT1A3 respectively. The K_m or S_{50} values of β-estradiol and CDCA were determined in HLM, HIM and rUGTs. Preliminary protein and time-course linearity experiments were conducted and the following conditions were employed in the experiments. The reaction mixture contained 50 mM of Tris buffer (pH 7.4), 5 mM of $MgCl_2$, 10 µg/mL of Alamethicin and 0.25 mg/mL of microsomes or Supersomes™ (HLM/HIM/rUGTs), various concentrations of substrates and 5 mM of UDPGA in 100 µL of

total reaction volume. The enzyme kinetic studies were conducted in triplicate in a 96-well plate, equilibrated at 37 ºC. A master mix, sufficient for the number of reactions, containing Tris-HCl buffer, $MgCl_2$, microsomes/ Supersomes™ and alamethicin was prepared and kept on ice bath for 15 min. 94.25 µL of the above reaction mixture was added to each of the labelled wells. 0.75 µL of various concentrations of substrate (β-estradiol or CDCA) was added to the corresponding wells, and the 96-well plate was then placed in an orbital shaking incubator (with shaking at 500 rpm) for 5 min to equilibrate the contents of the wells to 37 ºC. Following the equilibration, 5 µL of 100 mM UDPGA was added to the wells. The contents in the wells were mixed gently by pipetting and incubated at 37 ºC for 40 minutes. The 96-well plate was removed from the orbital shaking incubator at the end of reaction time, and the reaction was terminated in the wells by adding 300 µL of ice-cold acetonitrile containing telmisartan. Telmisartan was added as the internal standard (IS) in the analysis of samples. The 96-well plate was then placed on a benchtop orbital shaker (MAXQ2000, Thermo Scientific, MA, USA) for 15 min shaking at 250 rpm at room temperature. Then, the plate was centrifuged at 4000 rpm for 20 min using a centrifuge (SORVALL ST 8 Thermo Scientific, MA, USA). The supernatant obtained from each of the wells was collected and analysed by LC-MS/MS (Shimadzu-8040).

For calibration curves of authenticated glucuronide metabolites, the mixtures were also prepared in the same manner as explained above to avoid the matrix effect in the analysis. In brief, 99.25 µL of the master mix prepared above and 0.75 µL of glucuronide standard concentration were added into respective wells and precipitated immediately with 300 µL of ice-cold acetonitrile containing IS, and the remaining process remained the same as mentioned above.

2.2.4 Enzyme inhibition studies for determining the IC_{50} values of inhibitors

Based on the results obtained from the enzyme kinetic studies of β-Estradiol and CDCA, enzyme inhibition studies were conducted using selective inhibitors. The inhibitory effect of atazanavir or zafirlukast on the metabolism of β-Estradiol by UGT1A1 and the effect of lithocholic acid on the metabolism of CDCA by UGT1A3 were studied in three enzyme systems (HLM, HIM, respective rUGTs) to determine their corresponding IC_{50} values. The reaction mixture for enzyme inhibition studies contained 50 mM Tris-HCl buffer (pH 7.4), 5 mM $MgCl_2$, alamethicin (at a concentration of 10 µg/mL) and HLM or HIM or rUGTs at a concentration of 0.25 mg/mL, substrates and various concentrations of inhibitor in a total volume of 100 µL. All the reactions were conducted in triplicates in a 96-well plate, which was equilibrated at 37 ºC. A master mix, sufficient for the number of reactions, containing Tris-HCl buffer, $MgCl_2$, microsomes/ Supersomes™ and alamethicin was prepared and kept on ice bath for 15 min. 94.25 µL of the above reaction mixture was added to each of the labelled wells. 0.25 µL of the substrate (β-estradiol or CDCA) and 0.5 µL of various concentrations of inhibitors (atazanavir/zafirlukast as inhibitors in the case of β-estradiol and lithocholic acid as an inhibitor in the case of CDCA) or DMSO (vehicle control) were added to the corresponding wells, and the 96-well plate was then placed in an orbital shaking incubator (with shaking at 500 rpm) for 5 min to equilibrate the contents of the wells to 37 ºC. Following the equilibration, 5 µL of 100 mM UDPGA was added to the wells. The contents in the wells were mixed gently, and 96-well plate was placed back in the orbital shaking incubator and incubated at 37 ºC for 40 minutes. The 96-well plate was removed from the orbital shaking incubator at the end of reaction time, and the reaction was terminated in the wells by adding 300 µL of ice-cold acetonitrile containing IS. The 96-well plate was then placed on a benchtop orbital shaker for

15 min shaking at 250 rpm at room temperature. Then, the plate was centrifuged at 4000 rpm for 20 min in a centrifuge. The supernatant obtained from each of the wells was collected and analysed by LC-MS/MS.

2.2.5 Instrumentation and bioanalysis of the samples

The two glucuronide metabolites formed in the enzyme kinetic studies and enzyme inhibition studies were quantified against their respective authentic reference standards. Calibration curves for each of the glucuronide metabolites were developed using authentic reference standards on LC-MS/MS instrument. The LC-MS/MS instrument consisted of Shimadzu chromatographic separation unit (Prominence UFLC, Shimadzu Corp, Kyoto, Japan) coupled with Shimadzu 8040 triple quadrupole mass analyzer (Shimadzu Corp, Kyoto, Japan). Data acquisition and integration were carried out using LC-MS Lab Solutions software (Shimadzu Corp, Kyoto, Japan). Calibrated automated micropipettes were used for the preparation of all the samples during the analysis. The aqueous phase used in the mobile phase was filtered through a 0.22 µm Millipore® (MA, USA) filtration membrane while the samples were filtered using a 0.22 µm polyvinylidene difluoride (PVDF) syringe filter (Millipore® MA, USA) before the analysis.

Chromatographic separation was achieved on the reverse phase Luna C18 (4.6 × 100 mm, 5 µm) column (Phenomenex, USA). The mobile phase comprises a mixture of aqueous phase (solvent A: 10 mM ammonium acetate buffer with 0.1% formic acid) and an organic phase (solvent B: 100% LCMS grade methanol). Samples were analyzed under gradient conditions (30:70 aqueous: organic) at a mobile phase flow rate of 0.8 mL/min. The injection volume was 10 µL. LC acquisition time was set to 4 min. Autosampler and column oven temperatures were set at 4 and 50 °C, respectively.

The mass spectrometer (Shimadzu-8040) was operated in negative ESI mode, with DGU-20A3R solvent degasser, CBM-20A controller, two LC-20AD pumps, SIL-20ACHT autosampler, collision gas (Argon) at 230 kPa, DL temperature of 250 °C, and nebulizer gas at a flow rate of 3 L/min. Ultrahigh pure (99.95% purity) Argon gas was used as CID gas. The optimized multiple reaction monitoring (MRM) transitions and compound dependent parameters viz., dwell time, collision energy, Q1 Pre-Bias and Q3 Pre-Bias for the glucuronide metabolites are presented in Table 2.1.

The linearity of the method was determined by using a $1/x^2$ weighted least square regression analysis of standard plots. The method was linear and the linearity range for β-Estradiol 3-β-D-glucuronide and CDCA 24-Acyl-β-D-glucuronide was 50-40000 ng/mL and 6-6000 ng/mL respectively. The overall correlation coefficient was observed was ≥0.9956 and 0.9975 for β-Estradiol 3-β-D-glucuronide and CDCA 24-Acyl-β-D-glucuronide respectively. Sensitivity of the method was established at LLOQ level for both the analytes β-Estradiol 3-β-D-glucuronide and CDCA 24-Acyl-β-D-glucuronide found to be 50 ng/mL and 6 ng/mL respectively. Precision of the method was expressed as coefficient of variation (% CV). It was evaluated by the % CV at different concentration levels, the overall precision was found to be 10.23 – 11.42 and 9.32 – 10.54% for β-Estradiol 3-β-D-glucuronide and CDCA 24-Acyl-β-D-glucuronide. The accuracy was calculated as the absolute value of the ratio of the calculated mean values of the different concentration levels to their respective nominal values and expressed as percentage, The % mean accuracy found to be 90.14-110.45% and 89.24 – 92.14% for β-Estradiol 3-β-D-glucuronide and CDCA 24-Acyl-β-D-glucuronide respectively. The matrix effect for the method was assessed by post column infusion method, there was no suppression or enhancement at the retention time of analytes. The percentage recovery of β-Estradiol 3-β-

D-glucuronide and CDCA 24-Acyl-β-D-glucuronide was determined at two concentration levels by comparing the mean peak area of both the analytes in extracted samples with freshly prepared un-extracted samples, respectively. The overall mean recoveries for both the analytes found to be 70.21 & 75.12 % and 85.12 & 82.01% respectively. Figure 2.4a - 2.4f represents the chromatograms of blank, estradiol-glucuronide and CDCA-glucuronide metabolites.

2.3 Data analysis

Enzyme kinetics and enzyme inhibition studies were performed in triplicate, and the data obtained from the studies is presented in the form of mean with standard deviation (mean ± SD). The data obtained from enzyme kinetics studies fit various kinetic models, namely, Michaelis-Menten (MM) kinetics (Eq. 1), Substrate Inhibition (SI) kinetics (Eq. 2) and Allosteric Sigmoidal (AS) kinetics (Eq. 3) using GraphPad Prism 6 software (GraphPad Software Inc, CA, USA). The best fit model for each enzyme and substrate combination was selected based on the Eadie-Hofstee plots, and using various statistical parameters like R^2, adjusted R^2, the absolute sum of squares (SS), standard error of estimate values ($S_{y.x}$) and Akaike information criterion corrected (AICc).

$$V = \frac{V_{max}[S]}{K_m+[S]} \qquad \text{Eq. 1 (Michaelis-Menten kinetics)}$$

$$V = \frac{V_{max}[S]}{((K_m+[S]).(1+[S])/K_i)} \qquad \text{Eq. 2 (Substrate Inhibition kinetics)}$$

$$V = \frac{V_{max}[S]^n}{((S_{50})^n+[S]^n)} \qquad \text{Eq. 3 (Allosteric Sigmoidal kinetics)}$$

Where 'V' is the velocity of the kinetic reaction, '$[S]$' is the substrate concentration, 'V_{max}' is the maximum velocity of the kinetic reaction, 'S_{50}' or 'K_m' is the substrate concentration where the velocity of the kinetic reaction is 50% of 'V_{max}'. 'K_i' is the substrate inhibition constant, and 'n' is the Hill coefficient.

Table 2.1 Incubation conditions for UGT1A1 and UGT1A3 assays and analytical parameters

Incubation conditions	β-Estradiol (UGT1A1)		Chenodeoxycholic Acid (UGT1A3)	
	Kinetic assay	Inhibition assay	Kinetic assay	Inhibition assay
Pooled human liver microsomes				
Protein concentration (mg/mL)	0.25	0.25	0.25	0.25
Substrate concentration (μM)	0.65-160	-	0.65-480	-
Inhibitor concentration range (μM)		0.03-20		0.03-20
Incubation time (min)	40	40	40	40
Recombinant UGT				
rUGT concentration (mg/mL)	0.25	0.25	0.25	0.25
Substrate concentration (μM)	0.21-480	-	0.21-480	-
Inhibitor concentration Range (μM)	-	0.01-20	-	0.01-20
Incubation time (min)	40	40	40	40
Pooled human Intestine microsomes				
Protein concentration (mg/mL)	0.25	0.25	0.25	0.25
Substrate concentration (μM)	0.21-480	-	1.9-480	-
Inhibitor concentration Range (μM)	-	0.8-60	-	0.8-60
Incubation time (min)	40	40	40	40
Analytical method conditions	Analyte			
	β-Estradiol 3-β-D-glucuronide		CDCA 24-Acyl-β-D-glucuronide	
Internal standard:	Telmisartan			
Internal standard: final conc.	500 ng/mL			
Injection volume	10 μL			
Flow rate	0.8 mL/min			
Mobile phase				
System	A: 10mM Ammonium Acetate with 0.1 % Formic acid; B: Methanol (100%)			
Isocratic elution (B:A)	80:20			
Mass spectrometer conditions				
Mode	Negative			
DL temperature (°C)	250			
Nebulizing Gas Flow (L/min)	3			
Heat Block Temperature (°C)	400			
Drying Gas Flow (L/min)	10			
Dwell Time (mSec)	100		100	
Q1 Pre-Bias (V)	32		20	
Q3 Pre-Bias (V)	20		35	
Collision energy	23		28	
Analyte *m/z* transition	447.05→113.05		567.20 → 391.25	
Internal standard *m/z* transition	515.20 → 276.20		515.20 → 276.20	
*R*t (min)	1.7		2.7	
Standard curve range -HLM and rUGT	50-10000ng/mL	50-10000ng/mL	50-6000ng/mL	50-6000ng/mL
Standard curve range –HIM	50-40000 ng/mL	50-40000ng/ml	50-6000ng/mL	6-6000ng/ml

In the *in vitro* enzyme kinetics studies, intrinsic clearance (CL_{int}) of any substrate is the intrinsic ability of an enzyme to metabolize the substrate, which is also referred to as the enzyme activity. The maximum velocity of the reaction and the MM constant are used to obtain the enzyme activity or CL_{int} (Eq. 4).

$$CL_{int} = V_{max}/K_m \quad \text{Eq. 4}$$

Where, 'CL_{int}' is the intrinsic clearance

For the calculation of IC_{50} data of UGT inhibitors, the percentage activity data obtained by comparing the product formation with a test compound to DMSO vehicle control, and the inhibition data was also estimated using GraphPad Prism 6 (GraphPad Software Inc., CA, USA) applying nonlinear regression (curve fit) and four parameter logistic curve fitting (Eq.5). The IC_{50} values were reported as the mean of triplicate values (Mean ± standard deviation).

$$Y = Bottom + (Top - Bottom)/(1 + 10^{(LogIC50 - X) * HillSlope}) \quad \text{Eq. 5}$$

Where 'X' is the logarithmic value of dose or concentration of substrate used in the study, 'Y' is the response, Top and Bottom are the values of top and bottom of the plateaus obtained in the study (which have the same units as Y) and '$LogIC_{50}$' is the logarithmic value of half-maximal dose or concentration of inhibitor.

2.4 Results

2.4.1 Enzyme kinetics studies for determining the K_m or S_{50} of substrates

In the enzyme kinetic studies, reaction rate constant (K_m/ S_{50} / K_i) and maximal reaction velocity (V_{max}) for substrates were determined based on the rate of formation of glucuronide metabolite in the metabolic reactions. The goodness of fit of various models (MM, SI and AS)

for each enzyme-substrate pair was assessed based on various statistical parameters obtained in the kinetic studies. The model was further confirmed using the characteristic profile/shape of Eadie-Hofstee plots. The rate of formation of β-estradiol-3-β-D-glucuronide was assessed to determine the rate constant and maximal reaction velocity for the metabolism of β-estradiol by UGT1A1, while the rate of formation of chenodeoxycholic acid-24-Acyl-β-D-glucuronide was analysed to determine the rate constant and maximal reaction velocity for the metabolism of CDCA by UGT1A3. The concentrations of the glucuronide metabolites formed during both the metabolic reactions were analysed using LC-MS/MS method described above.

The glucuronidation conjugation reaction of β-Estradiol by UGT1A1 in all the three enzyme systems (HLM, HIM and rUGT1A1) was found to follow AS kinetics. This atypical kinetic profile was further supported by the Eadie-Hofstee plots, which showed a bow-shaped array for the data obtained in the study. The kinetic profiles and model parameters (V_{max} and S_{50}values) of glucuronidation conjugation reaction of β-Estradiol by UGT1A1 in all the three enzyme systems are presented in Figure 2.2a and Table 2.2, respectively.

The glucuronidation conjugation reaction of CDCA by UGT1A3 in HLM was found to follow MM kinetics which was confirmed by the linear Eadie-Hofstee plot for the data obtained in the study. In HIM and rUGT1A3 enzyme systems, glucuronidation conjugation reaction of CDCA by UGT1A3 followed SI kinetics where the rate of metabolism did not reach a plateau instead, decreased with an increase in the concentration of substrate. This pattern also further confirmed from the curve shape observed in the Eadie-Hofstee plot at higher substrate concentrations, which is a characteristic of the SI kinetics model. The results obtained from the glucuronidation conjugation reaction of CDCA by UGT1A3 in each enzyme system are presented in Figure 2.2b and Table 2.3, respectively.

2.4.2 Enzyme inhibition studies for determining the IC_{50} values of inhibitors

Atazanavir potential to inhibit the formation of β-estradiol-3-β-D-glucuronide during the metabolism of β-Estradiol by UGT1A1 was determined in all three enzyme systems. In HLM and rUGT1A1 enzyme systems, at β-estradiol concentrations corresponding to it's S_{50}value of the corresponding enzyme system, atazanavir exhibited potent inhibitory activity against UGT1A1 mediated glucuronidation of β-estradiol with the IC_{50} values of 0.54 µM and 0.16 µM in HLM and rUGT1A1, respectively. Although atazanavir was found to be a potent inhibitor of UGT1A1 isoform in HLM and rUGT1A1 enzyme systems, it did not show inhibitory activity on the metabolism of β-Estradiol by UGT1A1 isoform in HIM up to the highest tested concentration of 20 µM (data not shown). However, zafirlukast, a potent inhibitor of UGT1A family isoforms, could show moderate inhibition activity on the metabolism of β-estradiol in HIM. At the half-maximal substrate concentration obtained for β-estradiol in HIM, the IC_{50} value of zafirlukast was 16.7 µM.

Lithocholic acid is known to be an inhibitor of UGT1A3 activity in HLM, HIM and rUGT1A3. The inhibitory activity of lithocholic acid on the UGT1A3 isoform was evaluated using CDCA as a substrate. The enzyme inhibition studies were performed using the K_m values corresponding to the metabolic kinetics of CDCA by UGT1A3 in HLM, HIM and rUGT1A3. Lithocholic acid inhibited the production of CDCA-24-Acyl-β-D-glucuronide in HLM, HIM and rUGT1A3 with half-maximal inhibitory concentration (IC_{50}) values of 1.68, 1.84 and 12.42 µM, respectively. Figure 2.3 illustrates the inhibition profiles of atazanavir, zafirlukast on UGT1A1 and, lithocholic acid on UGT1A3 in different enzyme systems.

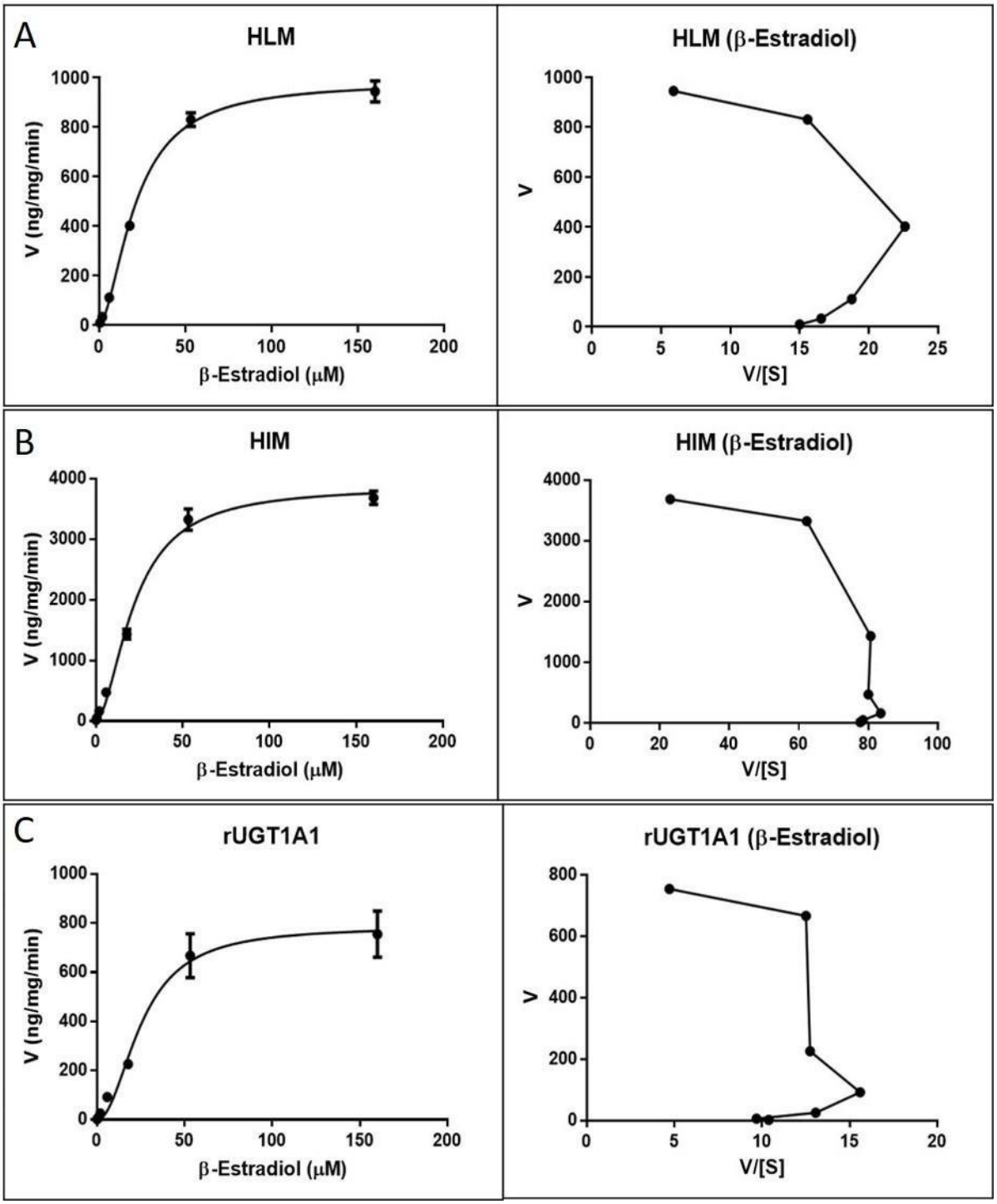

Figure 2.2a Enzyme kinetics of β-estradiol-UGT1A1 in (A) HLM, (B) HIM and (C) rUGT1A1 enzyme systems. Left hand side panel show enzyme kinetics and right hand side panel show Eadie-Hofstee plots. V – Velocity of reaction and V/[S] – Velocity of reaction over substrate concentration. Each data point in the plots presented on the left hand side panel represent the mean ± SD of three (n=3) independent incubations.

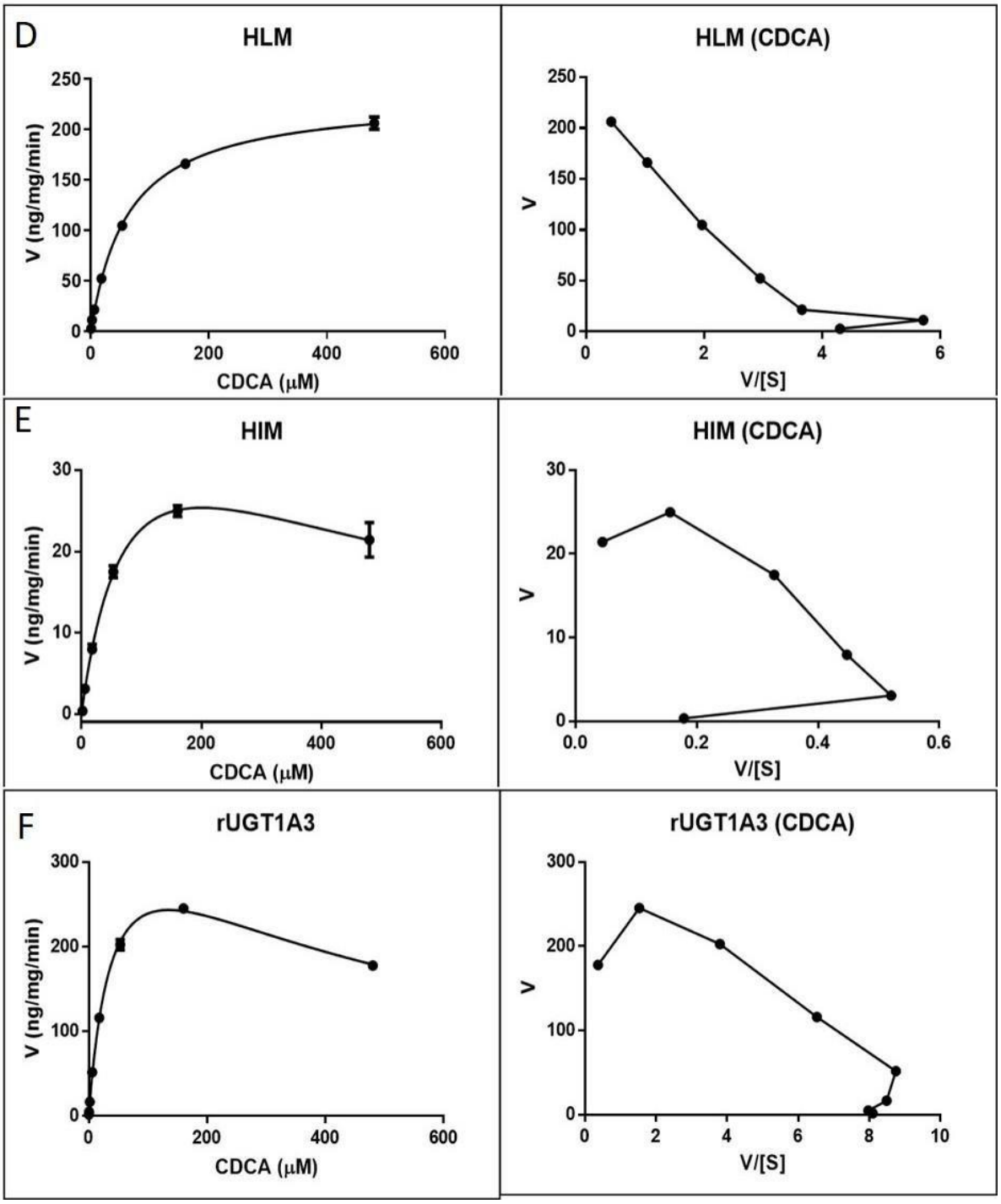

Figure 2.2b Enzyme kinetics of Chenodeoxycholic acid (CDCA)-UGT1A3 in (D) HLM, (E) HIM and (F) rUGT1A3 enzyme systems. Left hand side panel show enzyme kinetics and right hand side panel show Eadie-Hofstee plots. V – Velocity of reaction and V/[S] – Velocity of reaction over substrate concentration. Each data point in the plots presented on the left hand side panel represent the mean ± SD of three (n=3) independent incubations.

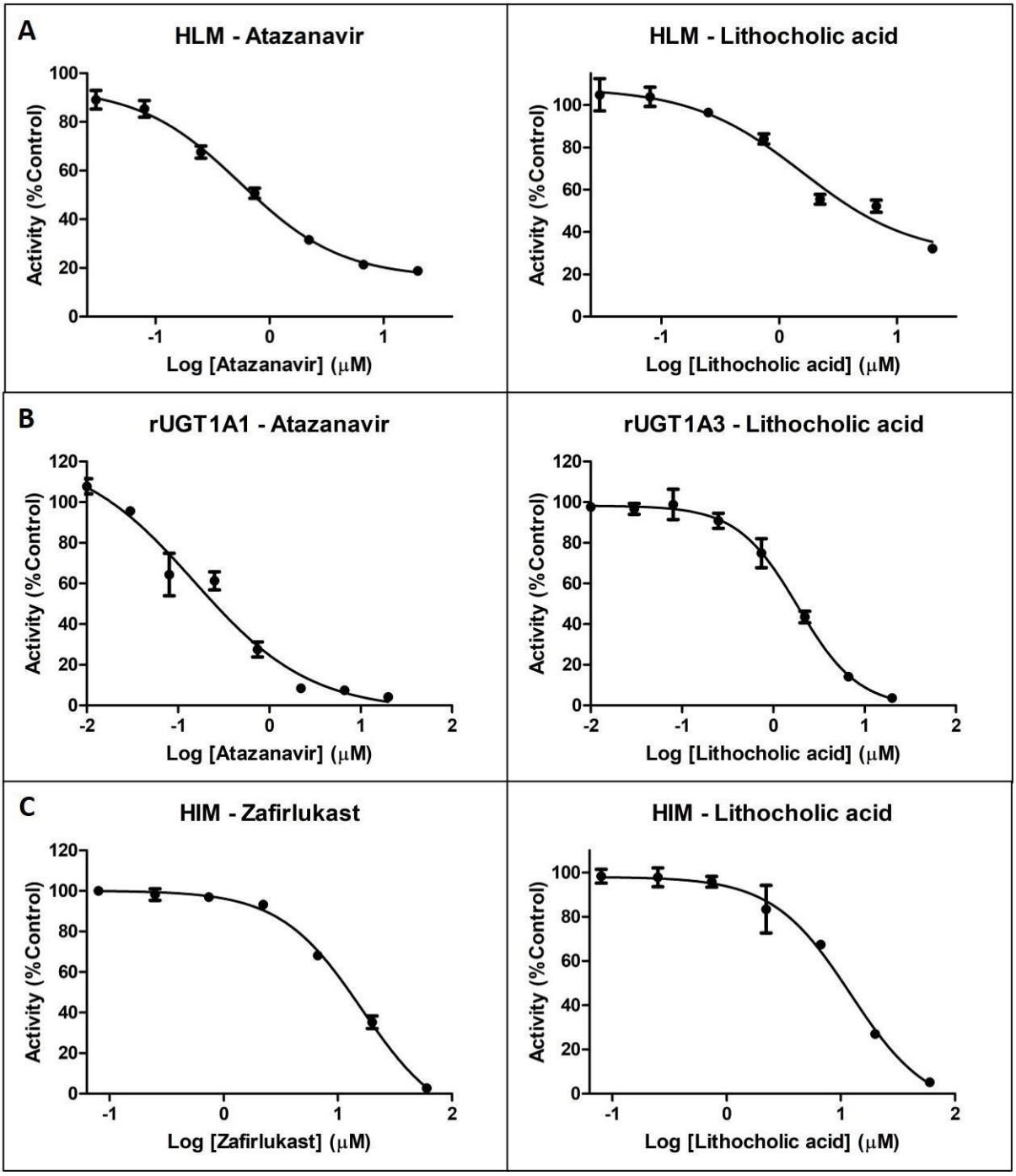

Figure 2.3. Inhibitory potentials of atazanavir (UGT1A1), zafirlukast (UGT1A1), lithocholic acid (UGT1A3) in; (A) HLM, (B) rUGT, (C) HIM. Each data point in all the plots represent the mean ± SD of three (n=3) independent incubations.

Table 2.2 Enzyme kinetics data in HLM, HIM and recombinant systems (Mean ± SD) (n=3).

	substrate	K_m/S_{50}(μM)			V_{max} (ng/mg/min)			K_i (μM)		Cl $_{int}$ (μL/min/mg)		
		HLM	rUGT	HIM	HLM	rUGT	HIM	rUGT	HIM	HLM	rUGT	HIM
UGT1A1	β-estradiol	21.3± 0.5	25.8± 1.7	22.3± 0.6	983.9± 47.2	789.7± 83.6	3870.7± 99.1			46.2± 1.3	30.7± 2.6	173.9± 9.3
UGT1A3	CDCA	63.2± 3.0	43.3± 3.1	88.6± 18.7	232.7± 6.4	400.3± 20.8	48.1± 6.4	424.2± 61.1	500.1± 234.3	3.7± 0.08	9.3± 0.2	0.5± 0.05

Table 2.3 Inhibitory potentials in HLM, rUGT and HIM (Mean ± SD) (n=3).

UGT Isoforms	Reaction	Inhibitors	IC_{50} (μM)		
			HLM	rUGT	HIM
UGT 1A1	β-Estradiol 3-β-D-glucuronide	Atazanavir	0.54±0.07	0.16±0.09	-
UGT 1A1	β-Estradiol 3-β-D-glucuronide	Zafirlukast	-	-	16.70±3.64
UGT 1A3	CDCA 24-Acyl-β-D-glucuronide	Lithocholic acid	1.68±0.56	1.84±0.15	12.42±1.47

Table 2.4 Statistical parameters indicating goodness of fit of enzyme kinetics model β-estradiol (UGT 1A1).

Substrate	β-estradiol (UGT1A1)								
Enzyme system	rUGT			HLM			HIM		
Kinetic Model	MM	AS	SI	MM	AS	SI	MM	AS	SI
R^2	0.9394	0.9651	0.9531	0.9775	0.9966	0.9961	0.9703	0.9935	0.9856
Adjusted R^2	0.9807	0.9617	0.9844	0.993	0.9961	0.9987	0.9905	0.9978	0.9952
Absolute Sum of Squares	160669	92687	124446	57554	8706	9956	1769000	386594	855249
$S_{y.x}$	85.46	66.44	76.98	59.98	24.09	25.76	283.6	135.7	201.8
AICc	68.86	208.3	67.11	47.3	122.3	37.1	88.05	76.18	82.53

MM, Michaelis-Menten kinetics; AS, Allosteric Sigmoidal kinetics; SI, Substrate Inhibition kinetics, $S_{y.x}$, Standard Error of Estimate; AICc, Akaike's Information Criterion, corrected

Table 2.5 Statistical parameters indicating goodness of fit of enzyme kinetics model for CDCA (UGT1A3).

Substrate	CDCA (UGT1A3)								
Enzyme system	rUGT			HLM			HIM		
Kinetic Model	MM	AS	SI	MM	AS	SI	MM	AS	SI
R^2	0.936	0.9552	0.9988	0.9986	0.9990	0.9986	0.9435	0.9689	0.9908
Adjusted R^2	0.9796	0.9851	0.9987	0.9985	0.9997	0.9995	0.9824	0.9896	0.9896
Absolute Sum of Squares	12637	8855	241.4	168.7	121.4	168.7	88.26	48.68	14.35
$S_{y.x}$	23.97	20.53	3.391	2.98	2.597	3.061	2.349	1.801	0.978
AICc	48.52	45.97	65.51	51.17	11.22	13.52	8.417	5.176	6.996

CDCA, Chenodeoxycholic acid; MM, Michaelis-Menten kinetics; AS, Allosteric Sigmoidal kinetics; SI, Substrate Inhibition kinetics, $S_{y.x}$, Standard Error of Estimate; AICc, Akaike's Information Criterion, corrected

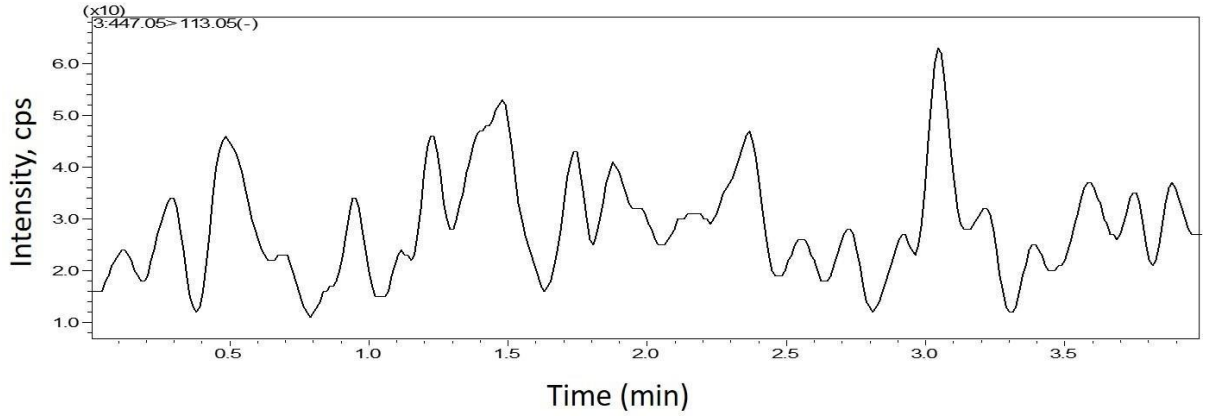

Figure 2.4a Chromatogram of β-estradiol 3-β-D-glucuronide blank sample

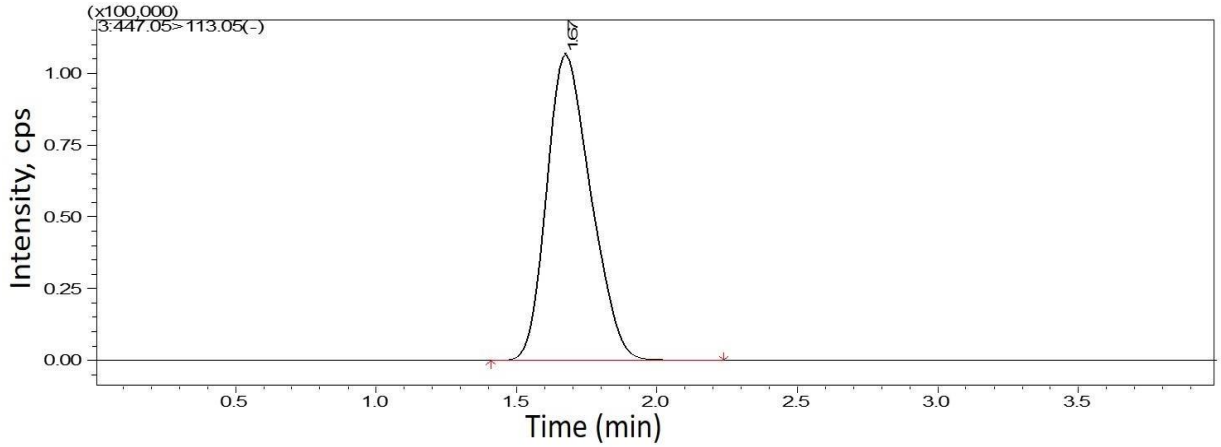

Figure 2.4b Chromatogram of β-estradiol 3-β-D-glucuronide standard obtained from calibration curve at 4000 ng/mL

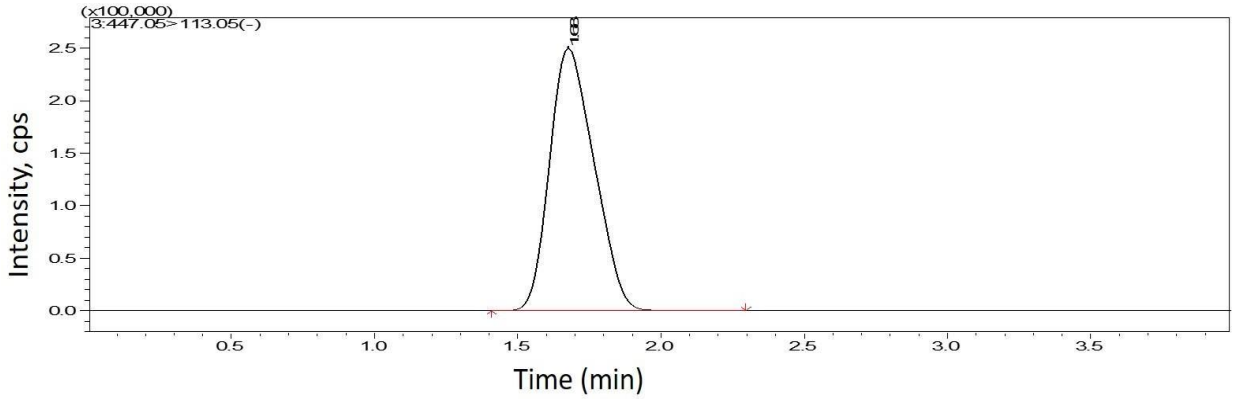

Figure 2.4c Chromatogram of β-estradiol 3-β-D-glucuronide metabolite formed in the reaction mixture

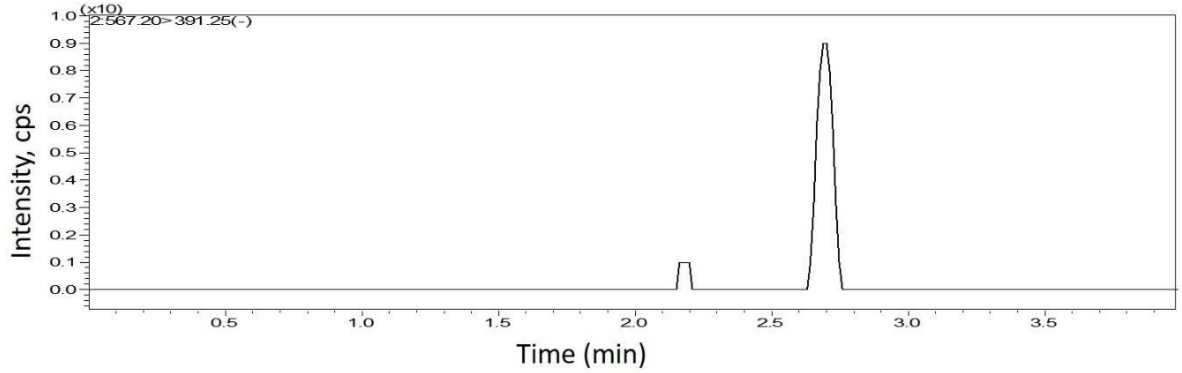

Figure 2.4d Chromatogram of CDCA 24-Acyl-β-D-glucuronide blank sample

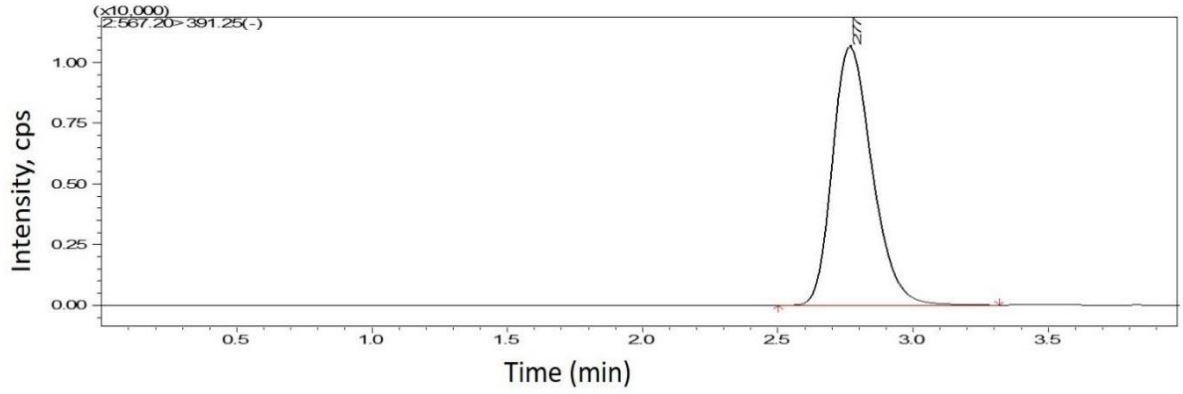

Figure 2.4e Chromatogram of CDCA 24-Acyl-β-D-glucuronide standard obtained from calibration curve at 5000 ng/mL

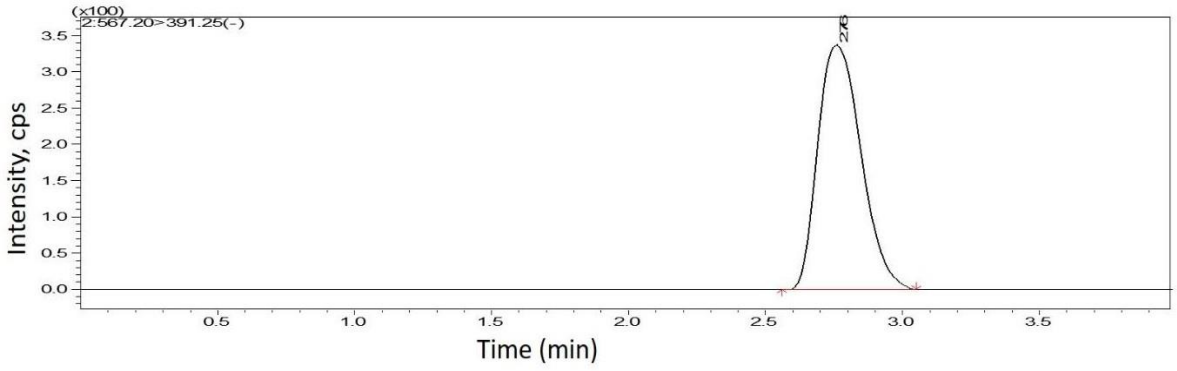

Figure 2.4f Chromatogram of CDCA 24-Acyl-β-D-glucuronide metabolite formed in the reaction mixture

2.5 Discussion

In recent years, significant progress has been made in understanding the role of UGT enzymes in drug metabolism and drug-drug interactions both *in vitro* and *in vivo* [14]. Glucuronidation is the primary phase II metabolic pathway for clearance of xenobiotics and endobiotics. According to the regulatory guidance for DDI studies, it is recommended to conduct *in vitro* DDI studies if an enzyme contributes more than 25% to the drug's metabolism [18]. Though several drugs are metabolized by Phase II metabolism pathways, defining the relative contribution of the sub-type of phase II metabolism routes is still challenging.

The involvement of UGT enzymes in the physiologic and clinical implications of several drugs highlights the importance of reaction-phenotyping using isoform selective substrates and inhibitors [110]. Although many UGT isoforms are involved in the metabolism of drugs, UGT1A1 and UGT1A3 are the crucial isoforms as they also regulate the homeostasis of endogenous biomarkers such as bilirubin and bile acids. Inhibition of these two isoforms could result in hyperbilirubinemia and bile acid induced hepatotoxicity and other bile related toxicities [103, 107, 108, 119, 120]. Therefore, we have selected these two isoforms in this report to study the enzyme kinetics and inhibition parameters.

Human liver microsomes were widely used in most of the studies to determine the UGT mediated metabolism of drugs but a very few studies used human intestinal microsomes to assess the glucuronidation metabolism. Since, intestinal UGT metabolism also contributes to the total UGT mediated clearance of drugs it is highly recommended to consider intestinal enzymes in drug metabolism and drug-drug interaction studies. [18, 110]. The major isoforms of the UGT1A sub-family present in the intestine are UGT1A1, UGT1A8 and UGT1A10 [110]. Due to high similarities in the amino acid sequence of these isoforms, there is an overlap of a majority of substrates and inhibitors for these isoforms [95]. Though UGT1A3 is expressed in small amounts in the intestines, its inhibition by chemical compounds can leads to potential

clinical outcomes through disturbance in bile acids homeostasis. UGT1A3 is the crucial enzyme in the glucuronidation of essential bile acids such as chenodeoxycholic acid [102, 121]. In the *in vitro* experiments, use of human recombinant UGT1A1 and UGT1A3 Supersomes™ can be appropriate to differentiate the isoform specific activity or inhibition for selective substrates or inhibitors. The isoform specific catalytic activity depends on the protein levels of relevant UGT isoform in the Supersomes™. Fallon et al determined the recombinant protein concentrations of Supersomes™. The mean with standard deviation values of UGT1A1 and UGT1A3 proteins were reported to be 1209.8±249.1 and 473.2±75.9 pmol/mg protein, respectively [101]. In addition, the enzyme activity depends on the active fraction of the total isoform protein, as in some circumstances there can be some amount of UGT isoform protein in the inactive state. In the present study we have used the same protein concentration of Supersomes™ as HLM or HIM in the reaction mixture. This may represent a feasible approach in conducting enzyme kinetics and inhibition studies when using different enzyme sources.

Bilirubin can be an excellent substrate for conducting *in vitro* enzyme kinetic studies with UGT1A1. However, bilirubin is reported to have high membrane/protein binding, and its glucuronide metabolites are chemically unstable [122]. β-estradiol is the substrate of choice for UGT1A1 since it is highly conjugated to form estradiol-3-glucuronide by UGT1A1 in the liver. Also, estradiol-3-glucuronidation shows a high correlation with the bilirubin glucuronidation in HLM, further supporting the use of β-estradiol-3-glucuronidation as a surrogate for bilirubin glucuronidation [89]. Atazanavir is an anti-retroviral protease inhibitor that causes hyperbilirubinemia with jaundice by preventing the glucuronidation and elimination of bilirubin via inhibition of UGT1A1. The selective UGT1A1 inhibition potential of atazanavir was further confirmed by the rapid reversible hyperbilirubinemia conditions associated with it [120]. Clinical Pharmacogenetics Implementation Consortium (CPIC) had recommended guidelines for atazanavir prescription in the context of UGT1A1 genotype [123]. Hepatic

impairment is the major problem that occurs when toxic bile acids (end products of cholesterol metabolism) accumulate in hepatocytes in disease conditions like cholestasis [124]. CDCA is an important bile acid that is exclusively metabolized by UGT1A3 to acyl-CDCA-24-glucuronide. Lithocholic acid, also a secondary bile acid, was reported to be a potent and selective inhibitor of UGT1A3 [116].

In the present research work, enzyme kinetics and inhibition studies for UGT1A1 and UGT1A3 isoforms were conducted under similar assay conditions in HLM, HIM and rUGTs and correlated the data across the enzyme systems. The product formation measurement approach was followed in the enzyme kinetic and inhibition studies as it is cost-effective and sensitive for low clearance compounds [18]. We have employed the same protein concentration, incubation time and substrate concentration range in enzyme kinetics studies to minimize the effect of variables in estimating clearance or inhibition.

In the enzyme kinetic studies involving β-estradiol as UGT1A1 substrate, the R^2 and adjusted R^2 values were consistently higher for AS model with smaller SS, $S_{y.x}$ and AICc values across all the three enzyme systems considered (Table 2.4). The same was confirmed with the Eadie-Hofstee plots showing the characteristic bow-shaped profile for the allosteric sigmoidal model (Figure 2.2a). Hence, AS was selected as the best fit model to explain the kinetics of all the three enzyme systems in the presence of β-estradiol as the substrate. At concentrations starting from 0.65 to 53.3 µM, the velocity was concentration-dependently increased, and from 160 µM, the velocity reached a plateau. The S_{50} values were found to be the same across all three enzyme systems. The V_{max} values in HLM and rUGT1A1 were found to be the same, but in HIM, the V_{max} values were 4 to 5-fold higher than HLM/rUGT1A1. The results indicate the involvement of isoforms other than UGT1A1 in the glucuronidation of β-estradiol in the intestinal microsomes. The intrinsic clearance of β-estradiol in HIM is also 3.8 times higher than in HLM.

In the enzyme kinetic studies of CDCA with rUGT1A3 and HIM, the data showed a better fit with the SI model based on the statistical parameters (Table 2.5) and the Eadie-Hofstee plot (Figure 2.2b). In the case of HLM, the data was found to fit well in all the three models with high adjusted R^2 values (> 0.999) and similar SS, $S_{y.x}$ and AICc values (Table 2.5) for all the three models. Hence, the fit of the model was confirmed based on the Eadie-Hofstee plot. The data showed a straight-line profile that is characteristic of MM enzyme kinetics (Figure 2.2b). Hence, the MM model was chosen for HLM. CDCA exhibited MM kinetics in HLM up to 480 µM concentration and mild substrate inhibition kinetics in HIM and recombinant UGT1A3 system. In HIM and rUGT, CDCA followed MM kinetics up to 160 µM concentrations, but the inclusion of 480 µM resulted in inhibition with higher K_i values. V_{max} in HIM was found to be 4.9 and 8.5 times lower as compared to HLM and recombinant isoform, respectively. The activity in HLM is 6.7-fold higher than in HIM. This is due to the lower expression of UGT1A3 in HIM. Even though the contribution is less by HIM (approximately 15% of HLM activity), it is crucial in the enterohepatic clearance of bile acids. K_m or S_{50} values in all systems were similar for β-estradiol and within 2-fold for CDCA.

The K_m or S_{50} values obtained from the enzyme kinetics studies of β-estradiol and CDCA were used as substrate concentrations in the respective inhibition assays. Atazanavir was a potent inhibitor of UGT1A1 in HLM and rUGT but failed to show an inhibitory effect in HIM. This may be due to the relatively high glucuronidation of β-estradiol in HIM compared to HLM and rUGT, which was further confirmed by the 5-fold increase in V_{max} values in HIM. β-estradiol is reported to be extensively glucuronidated by intestinal specific UGT1A8 and UGT1A10 isoforms. In addition, glucuronidation of β-estradiol by UGT1A10 was said to be ten times higher than UGT1A1 [125]. Therefore, the relative contribution of UGT1A1 in the cumulative metabolic activity of various isoforms in HIM may be less. This explains why atazanavir could not show any inhibitory effect on the metabolism of β-estradiol by UGT1A1. To confirm the

possible role of UGT isoforms like UGT1A8 and UGT1A10 in the metabolism of β-estradiol, Zafirlukast, a potent inhibitor of UGT1A8 and UGT1A10, was used to inhibit the β-estradiol glucuronidation in HIM [110]. Zafirlukast inhibited the production of β-estradiol 3-β-D-glucuronide in HIM. Based on the results obtained, we can infer that atazanavir can be employed to inhibit UGT1A1 in conducting enzyme inhibition studies. However, if the test compound is a substrate for multiple UGT isozymes (UGT1A8 and UGT1A10), including UGT1A1 isozyme, zafirlukast is the ideal choice to inhibit pan UGT activity.

In the recent literature, lithocholic acid was used as a selective inhibitor of UGT1A3 [116]. In the present report, it showed concentration-dependent inhibition in HLM, HIM and recombinant systems. It was also further confirmed by the higher inhibitory potency in the recombinant system than in HLM at the same doses. Although the UGT1A3 activity is low in HIM, the inhibitory profile of lithocholic acid followed a similar pattern as in HLM.

The activity of UGT1A3 was low in HIM compared to HLM due to the differences in levels of enzymes expressed in intestine and liver and also due to the tissue specific regulation of the UGT1A3 enzymes at the post-translational level affecting the substrate binding and turnover of the enzyme [111, 126, 127].

Based on the results obtained from these studies, we can suggest that atazanavir can be used as a potent inhibitor of the UGT1A1 enzyme, while zafirlukast can be used as a pan UGT1A isozymes inhibitor in the *in vitro* metabolic studies in HLM, HIM and rUGT enzyme systems. Lithocholic acid can be used as a potent to a moderate inhibitor of UGT1A3 in the *in vitro* metabolic studies in HLM, HIM and rUGT enzyme systems. The major advantage of this report is to identify the isoform selective (UGT1A1 or UGT1A3) substrates or inhibitors for substrate phenotyping and drug-drug interaction evaluations in *in vitro* at early screening stage.

2.6 Conclusion

The current chapter details the use of robust *in vitro* methodology to derive the enzyme kinetics and inhibition parameters using suitable probe substrates and inhibitors of UGT1A1 and UGT1A3. The kinetic parameters for β-estradiol and CDCA were determined based on the enzyme kinetic studies. Inhibitory potential of atazanavir and zafirlukast towards UGT1A1 and lithocholic acid towards UGT1A3 was evaluated. The research findings obtained in the current study can be advantageous in estimating the clearance of drugs, either new or existing if they are substrates of UGT1A1 and UGT1A3. This research can also help in identifying the potential DDIs mediated through UGT1A1 or UGT1A3 enzymes.

3

In vivo UGT1A1 and UGT1A3 mediated drug-drug interaction study in rat model using selective victim and perpetrator drugs

3.1 Introduction

Drug-drug interactions (DDIs) occur when two or more drugs are administered concurrently which leads to changes in their pharmacokinetics or pharmacodynamics profiles. The DDIs can arise due to changes in the process of absorption, distribution, metabolism and excretion of one drug caused by the drug. The increased or reduced exposure of one drug due to other drug may cause undesirable consequences to the patients under the therapy. If the concentrations of a drug decrease due to the DDI with the other drug, it can result in sub-therapeutic response of the drug. On the other hand, if the concentrations of a drug increase due to the DDI with the other drug, it can result in exceeding the maximum safe concentrations of a drug and cause adverse drug reactions. Two different kinds of DDIs are possible when two drugs are administered concomitantly. In the first, the pharmacokinetics of both the drugs are altered (each drug affects the pharmacokinetics of the other drug) due to the DDI while in the other, the pharmacokinetics of only one drug is altered. In such DDIs, the drug whose pharmacokinetic properties are altered is called the victim and the drug which causes the alteration is called the perpetrator [128].

In the drug discovery, the novel chemical entity may act as either victim or perpetrator and it should be evaluated for possible drug-drug interaction potential at the preclinical stage. Majority of the DDIs arise by metabolic enzymes mediated and by transporter mediated interactions by inhibition or induction mechanisms. Metabolism based DDIs are the most commonly reported than absorption, distribution and excretion mediated DDIs. Hence metabolic drug interactions should be studied using *in vitro* methods and possible DDIs are confirmed before conducting the *in vivo* studies in animals or humans [128-130]. For this purpose, *in vitro* DDI studies are being conducted to eliminate possible molecules having the potential to cause drug interactions at drug discovery phase itself. Otherwise, this can result in late-stage toxicities or withdrawals of drugs at developmental and post marketing stages [131].

Once the DDIs are confirmed from the *in vitro* studies, it is imperative to conduct the *in vivo* DDI studies in relevant animal species to prove *in vitro* results. This is because, the static, simplified and isolated experimental conditions used in the *in vitro* experiments cannot entirely reflect the complex, integrated and dynamic conditions present in the *in vivo* models.

UGTs are known to play a significant role in the oral bioavailability and/or clearance of several xenobiotics, pharmaceutical drugs, nutraceuticals and endogenous compounds. Modulation of UGT enzymes may lead to potential drug-drug interactions linked to UGT-mediated metabolism [100]. Several drugs are reported to inhibit UGT enzymes based on the *in vitro* metabolic studies but majority of them are not evaluated using suitable animal models to prove the *in vitro* results as well as to quantify their impact of inhibiting the UGTs [132]. It is very vital to determine the effective inhibitory concentration of the molecules from the *in vitro* metabolic studies. Further, dose finding (oral dose) studies have to be conducted for such drugs to determine the dose required to achieve similar inhibitory concentrations (as obtained from the *in vitro* studies) in the plasma. Following the oral administration, the concentrations achieved in the blood/plasma for a drug can be highly influenced by first pass metabolism including intestinal and hepatic metabolism and protein/tissue binding in the *in vivo* studies [133, 134].

Unlike measuring the glucuronide metabolites as mentioned in the *in vitro* product formation strategy, measurement of substrate remaining is a routine choice for *in vivo* conditions subjecting to the limitations such as quantity, stability, distribution and excretion of glucuronide metabolites formed in the body. And possibilities may exist for erroneous results for slowly metabolizing drugs or weak inhibitors. Nevertheless, quantification of specific glucuronidated metabolites is worthwhile to distinguish non-specific metabolism. *In vivo* benchmarking of known probe substrates and inhibitors employing specified concentrations against specific UGT isoforms will be of great advantageous to investigate other novel

chemical entities for their *in vivo* UGT inhibitory potential. A highly sensitive and validated LC-MS/MS method for the quantification of probe substrates is required to warrant the results. Thus, it helps in the *in vitro-in vivo* extrapolation and in accurate DDI measurements.

Among all various isoforms of UGTs, UGT1A1 and UGT1A3 enzymes play vital role in the glucuronidation of bilirubin and bile acids, respectively. Inhibition of UGT1A1 and UGT1A3 enzymes can result in decrease in the glucuronidation of bilirubin and bile acids and thereby results in hyperbilirubinemia and bile acid accumulation in the body [11, 135, 136]. Therefore, the inhibitory potential of existing drugs as well as novel chemical entities towards UGT1A1/1A3 should be carefully evaluated using optimized *in vitro* metabolism studies. The *in vitro* methodology presented in the Chapter 2 describes the use of selective probe substrates and inhibitors of UGT1A1 and UGT1A3 isoforms using human liver microsomes, human intestinal microsomes and human recombinant Supersomes®. This methodology can be used for rapid and high throughput DDI evaluations at the initial stages of drug discovery. Further, detailed *in vivo* studies can be conducted in suitable animal model (rat model) using putative UGT1A1 and UGT1A3 inhibitors to verify the DDI of the molecules.

Zafirlukast, a cysteinyl leukotriene type 1 receptor antagonist used to treat mild to moderate asthma, was identified as a pan-UGT inhibitor from the *in vitro* screening assays described in Chapter 2. Zafirlukast was found to inhibit hepatic and intestinal specific UGTs. It exhibited potent and moderate inhibition towards UGT1As and UGT2Bs, respectively [137]. Thus, zafirlukast can be employed as a perpetrator drug in studying hepatic and intestinal glucuronidation of either endogenous or exogenous UGT substrates. Ezetimibe is an adjuvant therapeutic agent used in the treatment of hyperlipidaemia or hypercholesterolaemia. It inhibits intestinal uptake of dietary and biliary cholesterol by targeting polytopic transmembrane cholesterol transport protein, Niemann-Pick C1-like 1 (NPC1L1). Following the oral administration, ezetimibe undergoes rapid absorption from the gastro-intestinal membranes.

However, it is extensively metabolized in the intestine and liver by glucuronidation. A phenolic ezetimibe-glucuronide (SCH 60663) is formed as the primary metabolite majorly by UGT1A1, UGT1A3 and minorly by UGT2B15 which is confirmed with human recombinant UGT enzyme systems. Both ezetimibe and its primary metabolite (phenolic ezetimibe-glucuronide) are pharmacologically active and undergo enterohepatic recycling [43, 138-140]. Since ezetimibe undergoes elimination primarily by metabolic clearance involving UGTs, the disposition of ezetimibe can be significantly affected by concomitant administration of the drug with UGT inhibitors. Although it has a favourable DDI profile with the drugs that are being used in the treatment of hypercholesterolaemia, there are no reports on metabolic DDIs of ezetimibe with other are potential UGT inhibitors (specifically UGT1A1 and UGT13 inhibitors). Therefore, it is important to first conduct the DDI studies of ezetimibe with UGT inhibitors in the preclinical setup to determine the impact on pharmacokinetics of ezetimibe before considering the clinical studies to evaluate such DDI studies.

In the *in vivo* DDI studies (either pre-clinical or clinical) involving glucuronidation conjugation, measurement of substrates (either victim or both victim and perpetrator) remaining in the blood/plasma is the preferred method to evaluate the interaction between molecules unlike measuring the metabolites in the case of the *in vitro* metabolism studies. This is due to the limitations such as quantity, stability, distribution and excretion of glucuronide metabolites formed in the body. Quantification of specific glucuronide metabolites is essential while determining the specific metabolism of the molecule involved in DDI study. Therefore, a highly selective and sensitive UHPLC-MS/MS method is required for the simultaneous quantification of both the molecules (victim and perpetrator drugs) involved in the DDI to achieve accurate and reliable results as well as to perform *in vitro-in vivo* extrapolation of the data.

At this juncture, considering the inhibition potential of zafirlukast (perpetrator) and metabolic clearance of ezetimibe (victim) by the UGTs present in the liver as well as the intestine, especially UGT1A1 and UGT1A3 enzymes, there is an opportunity to investigate the possible UGT-mediated metabolic DDIs for these two drugs. In the current chapter, we aimed to examine the inhibitory potential of zafirlukast (perpetrator) on the glucuronidation of ezetimibe (victim) using the previously described *in vitro* methods (Section 2.2, 2.3 and 2.4 in Chapter 2) [141] with some modifications. Further, the two drugs were co-administered through oral route in male Sprague Dawley rats to verify the data obtained from the *in vitro* studies.

3.2 Materials and methods

3.2.1 Materials

Zafirlukast, ezetimibe and telmisartan (used as internal standard in the LC-MS/MS method) were purchased from TCI Chemicals, India. Tris-hydrochloride, magnesium chloride ($MgCl_2$), polysorbate 80, dimethyl sulfoxide (DMSO), dipotassium ethylenediamine tetraacetate (K_2EDTA) were purchased from Sisco Research Laboratories Private Limited, Hyderabad, India. Alamethicin and uridine diphosphate glucuronic acid (UDPGA) were obtained from Sigma Aldrich (Merck) Chemicals Private Limited, Bangalore, India. LC-MS grade methanol, acetonitrile, water and formic acid were purchased from Biosolve India Limited, Hyderabad, India. Pooled human liver microsomes were purchased from GIBCO, Thermo Scientific (MA, USA). Male Sprague-Dawley (SD) rats were procured from Hylasco Biotechnology Private Limited, Hyderabad, India.

3.2.2 Preparation of reagents

Tris-HCl 50 mM (pH 7.4) was prepared in ultrapure Milli-Q water. Aqueous solutions of $MgCl_2$ and UDPGA were prepared at 100 mM concentrations, separately, using 50 mM Tris-HCl (pH 7.4) as the diluent/solvent. Alamethicin of 5 mg/mL concentration was prepared using

ethanol as the solvent. For the *in vitro* studies, different concentrations of zafirlukast and ezetimibe were prepared using DMSO as solvent.

3.2.3 Enzyme kinetics studies for determining the K_m (substrates) and IC_{50} (Inhibitor)

In vitro enzyme kinetic studies were conducted for ezetimibe using pooled human liver microsomes (HLM) to determine the reaction rate constant ($K_m/S_{50}/K_i$) and the maximum reaction velocity (V_{max}) based on the rate of formation of ezetimibe-glucuronide (primary metabolite of ezetimibe formed by the UGTs). The incubation time and protein concentrations were optimized and the following conditions were employed in the *in vitro* kinetic studies. The final incubation mixture consisted of 50 mM Tris-HCl buffer (pH 7.4), 5 mM $MgCl_2$, 10 µg/mL alamethicin, 0.25 mg/mL HLM, 5 mM UDPGA and different concentrations of ezetimibe (0.073 – 53.33 µM) in a total reaction volume of 100 µL. Briefly, a master mix sufficient for triplicate reactions was prepared with Tris-HCl buffer, $MgCl_2$, HLM and alamethicin and incubated on ice bath for 15 min. Then 94 µL of this mixture was transferred to each well of 96-well plate and 1 µL of different concentrations of ezetimibe (0.073 – 53.33 µM) was added, gently mixed and incubated at 37 ° C for 5 min. Finally, 5 µL of pre-warmed UDPGA (warmed to 37 ^{o} C) was added to each well and incubated at 37 ° C for 10 min. Reaction was terminated by adding 300 µL of ice-cold acetonitrile containing the internal standard (telmisartan). The 96-well plate was centrifuged at 4000 rpm for 20 min and the supernatant was analyzed using UHPLC-MS/MS to quantify ezetimibe glucuronide in the samples. The data obtained from the enzyme kinetics data was analyzed using GraphPad Prism 6 (GraphPad Software Inc., CA, USA). Kinetic behavior was determined by fitting the data into Michaelis-Menten (MM), substrate inhibition (SI) and allosteric sigmoidal (AS) equations to determine the most appropriate model based on the goodness of fit and the various statistical parameters. The reaction rate constant ($K_m/S_{50}/K_i$) and maximum reaction velocity (V_{max}) were determined from

the identified kinetic model. The study was performed in triplicates and the values are reported as mean ± standard deviation of three independent measurements.

The inhibitory potential of zafirlukast on the glucuronidation of ezetimibe mediated by UGT enzymes was evaluated in pooled human liver microsomes (HLM) to determine its half-maximal inhibitory concentration (IC_{50}). The final incubation mixture in the enzyme inhibition studies consisted of 50 mM Tris-HCl (pH 7.4) buffer, 5 mM of $MgCl_2$, 10 µg/mL of alamethicin, substrate (1 µM), different concentrations (0.247-540 µM) of inhibitor, HLM at 0.25 mg/mL concentration and 5 mM UDPGA in a total incubation volume of 100 µL. All the reactions were conducted in 96-deep well plate. Sufficient amount of master mix consisting of Tris-HCl buffer, $MgCl_2$, HLM, alamethicin was prepared and kept on ice for 15 min. Then, substrate was added to the master mix solution to yield final concentration of 1 µM and mixed gently. 94.5 µL of this mixture was transferred to each well of incubation plate and 0.5 µL of different concentrations of inhibitor was added to corresponding labelled wells. The plate was preincubated for 5 min at 37 °C in a shaking water bath. Then 5 µL of UDPGA solution (prewarmed to 37 °C) to each well of the incubation plate and incubated for 10 min at 37 °C in shaking water bath. After 10 min of incubation, the reaction was stopped by adding 300 µL of ice-cold acetonitrile containing internal standard (telmisartan, at a concentration of 100 ng/mL) and the plate was kept on an orbital shaker for 10 min with shaking at 250 rpm at room temperature. Then the plate was centrifuged at 4000 rpm for 20 min and the supernatant was analyzed by UHPLC-MS/MS. DMSO was used as a vehicle control. One well in each replicate without cofactor was used to represent the total substrate concentration at the end of incubation which was used in the calculation of percentage substrate remaining at each inhibitor concentration. Inhibition data was analyzed using GraphPad Prism 6 (GraphPad Software Inc., CA, USA) by applying non-linear regression using Hill equation. The IC_{50} values were reported as the mean ± standard deviation of triplicate measurements.

3.2.4 *In vivo* experiments

In vivo studies were conducted in male SD rats to assess the inhibitory potential of zafirlukast on the UGT-mediated metabolic clearance of ezetimibe. Prior approval was obtained from institutional animal ethical committee (BITS/IAEC/2022/38) for the *in vivo* study protocol and the study was conducted according to the guidelines prescribed by CCSEA, India. Male SD rats (7-8 weeks of age) weighing between 200-250 g were procured and immediately quarantined for 7 days in our institute animal house facility under standard laboratory conditions (air conditioned with adequate air supply). The rats were housed in standard polypropylene cages (3 rats per cage), with stainless top grill having facilities for pelleted food and drinking water *ad libitum*. The temperature and relative humidity were maintained at 22 ± 1 ° C and 50 ± 10 %, with approximately 12 h light and 12 h dark cycle in the animal house facility. Rats were kept for fasting for at least 8 h before the administration of treatments used in the study.

3.2.4.1 Study design

Animals were divided into three groups viz., Ezetimibe, Zafirlukast and Ezetimibe + Zafirlukast, three animals per each group. The Ezetimibe animals were administered ezetimibe (substrate) only, zafirlukast animals received zafirlukast (inhibitor) only, while Ezetimibe + Zafirlukast animals were co-administered ezetimibe with zafirlukast (substrate + inhibitor). Formulations of drugs for oral dosing were freshly prepared in 2% DMSO, 2% polysorbate 80 and 96% purified water on the day of dosing. Both the substrate and inhibitor were given at a dose of 10 mg/kg and a dose volume of 5 mL/kg by oral gavage. Blood samples were collected by retro orbital plexus method under slight isoflurane anesthesia at predose, 0.25, 0.5, 1, 2, 4, 6, 8 and 24 h post dosing from each animal into an anticoagulant (200 mM K_2EDTA at 2% concentration in blood) containing centrifuge tubes and kept on ice bath until processing.

Plasma was harvested by centrifuging the blood samples at 10000 rpm for 10 min at 4 °C. The supernatant plasma was collected, labelled, and stored at -80 °C until LC-MS/MS analysis.

3.2.5 Bioanalysis

An ultra-high performance liquid chromatography (Nexera 40D-XS, Shimadzu Corporation, Kyoto, Japan) coupled with tandem mass spectrometry (SCIEX QTRAP® 4500, Sciex, MA, USA) was used for the quantification of ezetimibe, ezetimibe-glucuronide and zafirlukast from *in vitro* and *in vivo* plasma samples. Acquisition and integration of the chromatograms was performed using Analyst software (Version 1.7). Protein precipitation method was used as the sample preparation method for *in vitro* and *in vivo* samples. Negative electrospray ionization was applied during analysis. Calibration curve was constructed in the range of 0.25 - 2000 ng/mL (0.25, 0.5, 1, 2, 10, 50, 200, 550, 800, 1600, 2000 ng/mL) for ezetimibe, 2-8000 ng/mL (2, 10, 50, 200, 500, 800, 900, 1000, 2000, 4000, 8000 ng/mL) for ezetimibe-glucuronide and 1-1000 ng/mL (1, 2, 10, 50, 200, 500, 800, 900, 1000 ng/mL) for zafirlukast and, linearity of the method was assessed by performing the least-square linear regression analysis of observed concentrations versus the nominal concentrations of the analyte for the calibration curve samples with $1/x^2$ weighting factor. The chromatographic separation of ezetimibe and ezetimibe glucuronide was achieved on Kinetex polar C18 column (4.6 × 50 mm, 2.6 µm) (Phenomenex, Hyderabad, India). The chromatography of zafirlukast was developed using Cortecs C8 column (2.1 × 50 mm, 2.7µm) (Waters India Private Limited, Bangalore, India). The mobile phase composed of 10 mM ammonium formate in water (mobile phase A) and acetonitrile with 0.1% formic acid (mobile phase B) was pumped at a flow rate was 0.6 mL/min using the following gradient program: 0.00 min – 10% B, 0.80 min – 90% B, 1.60 min – 90%B, 1.61 min – 10% B, 3.00 min – 10% B. and 2 µL of final sample was injected into the instrument (extracted plasma samples of zafirlukast was diluted to 50-folds and submitted for analysis).

Autosampler and column oven were maintained at 15 °C and 40 °C, respectively. UHPLC-MS/MS details of ezetimibe, ezetimibe-glucuronide and IS were given in Table 3.1 and their respective chromatograms were shown in Figure 3.1a-e.

3.2.6 Pharmacokinetic analysis

Phoenix WinNonlin® software (Version 8.3) was used to calculate the pharmacokinetic parameters using non-compartmental model analysis. The area under the plasma concentration-time curve (AUC_{0-t}) was calculated by the linear trapezoidal rule from time zero to the time of last quantifiable concentration. The $AUC_{0-\infty}$ was obtained by adding AUC_{0-t} and the extrapolated area determined using the ratio of C_{last}/K_{el} (provided the elimination phase is well-defined). Peak plasma concentration (C_{max}) and time for the peak plasma concentration (T_{max}) were the observed values. The elimination rate constant (K_{el}) was calculated by log-linear regression of concentration data during the elimination phase with a correlation coefficient of >0.8.

Table 3.1 Optimized mass spectrometer conditions used in the analysis of ezetimibe, ezetimibe-glucuronide and zafirlukast and telmisartan (IS)

Mass Spectrometer Parameter	**Value**
Curtain gas flow rate	35 L/h
Collision gas flow rate	Medium
Ion spray voltage	(-)4500 volts
Ion source temperature	500 ºC
Nebulizer gas	50 psi
Drying gas	45 psi

MRM conditions used in the optimized method

Analyte	**Q1 Mass (Da)**	**Q3 Mass (Da)**	**Dwell time (msec)**	**DP (V)**	**CE (V)**	**CXP (V)**	**Rt (min)**
Ezetimibe	408.0	271.1	200	-70	-22	-8	2.1
Ezetimibe-Glucuronide	584.5	271.1	200	-84	-35	-13	1.9
Zafirlukast	574.1	462.3	200	-81	-45	-10	1.6
Telmisartan (IS)	513.2	287.2	200	-82	-10	-10	2.1

DP – Declustering potential; EP – Entrance potential; CE– Collision energy; CXP – Collision cell exit potential; Rt – Retention time and IS – Internal standard; V – volts

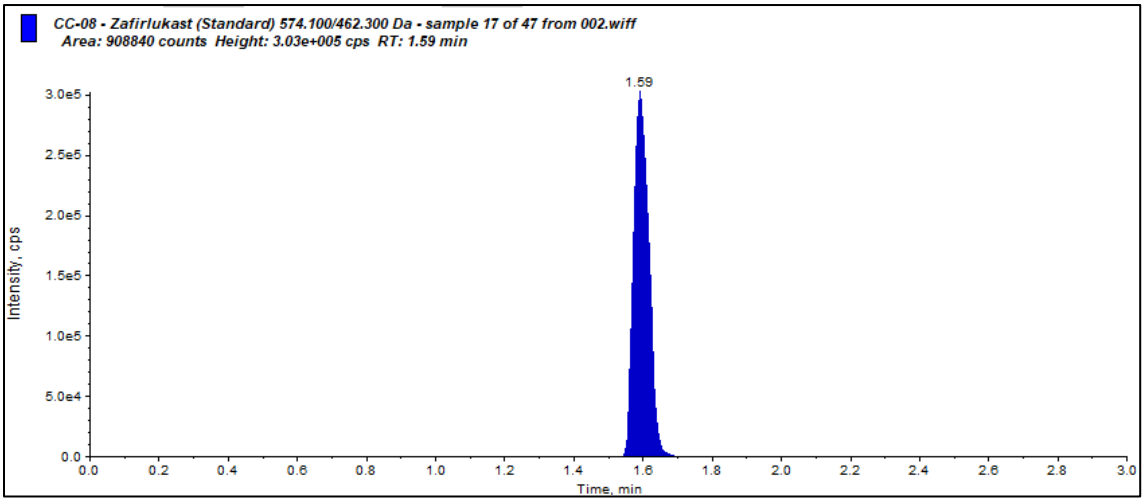

Figure 3.1a Chromatogram of zafirlukast from calibration curve standard (900 ng/mL)

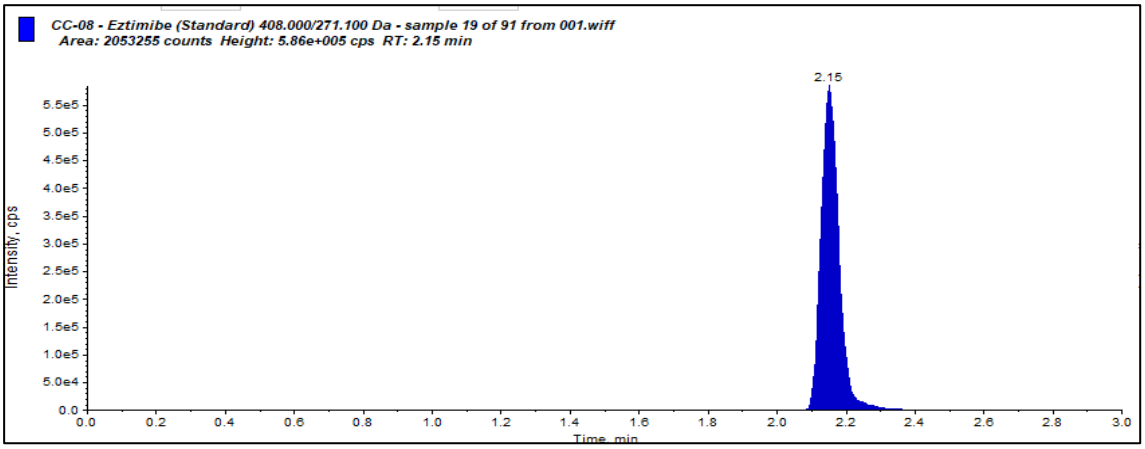

Figure 3.1b Chromatogram of ezetimibe from calibration curve standard (550 ng/mL)

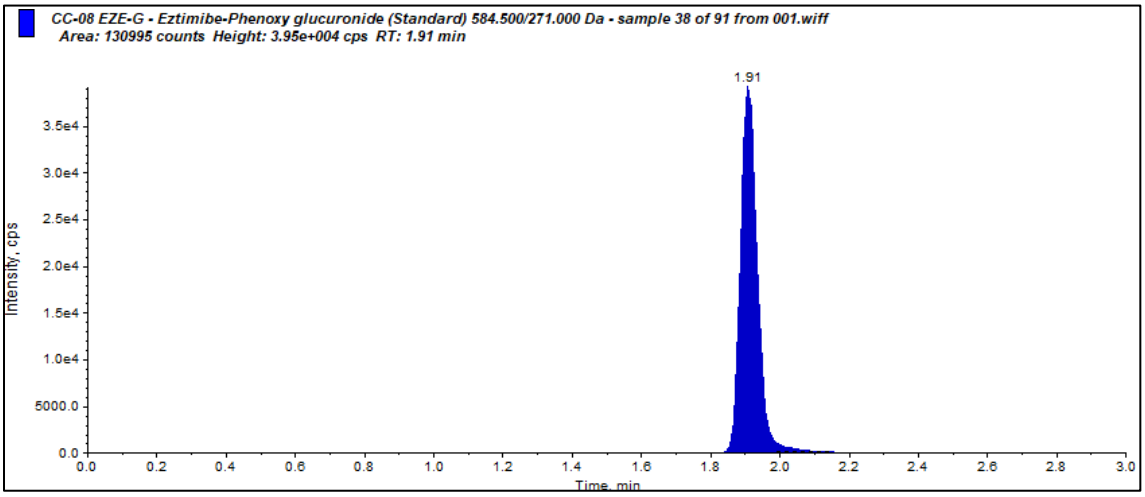

Figure 3.1c Chromatogram of ezetimibe-β-D-glucuronide from calibration curve standard (1000 ng/mL)

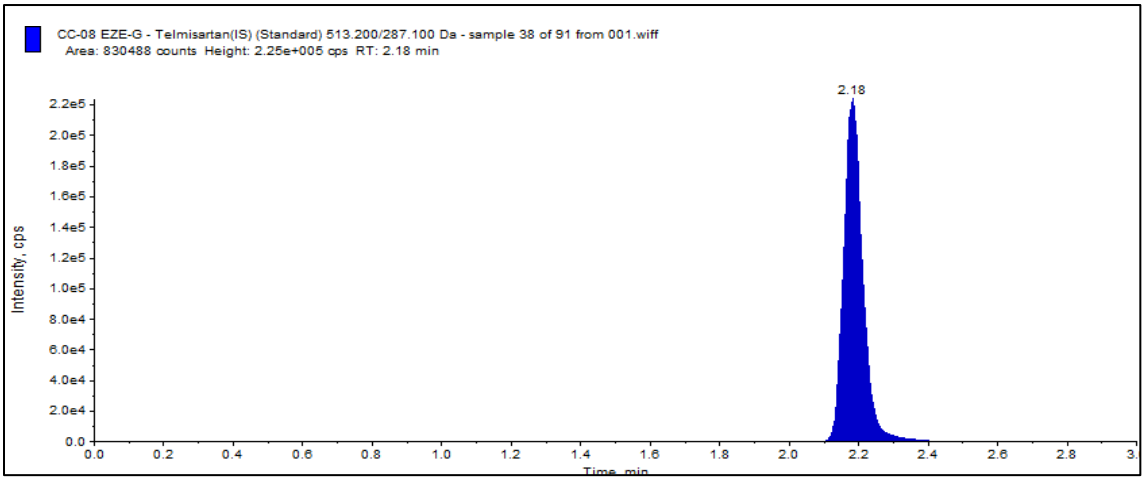

Figure 3.1d Chromatogram of telmisartan (IS) at a concentration of 100 ng/mL

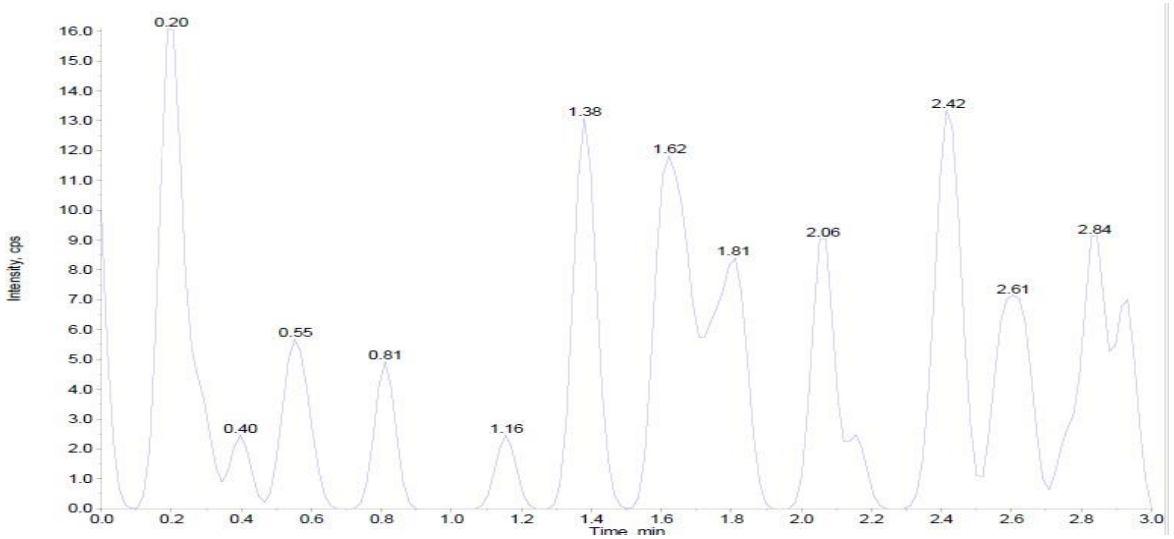

Figure 3.1e Chromatogram of blank sample

3.3 Results

In the enzyme kinetic studies, reaction rate constant (K_m/ S_{50} / K_i) and maximal reaction velocity (V_{max}) for substrates were determined based on the rate of formation of glucuronide metabolite in the metabolic reactions. The goodness of fit of various models (MM, SI and AS) for enzyme-substrate was assessed based on various statistical parameters obtained in the kinetic studies. The model was further confirmed using the characteristic profile/shape of Eadie-Hofstee plots. The rate of formation of ezetimibe-β-D-glucuronide was assessed to determine the rate constant and maximal reaction velocity for the metabolism of ezetimibe by

UGT1A1/UGT1A3. The concentrations of the glucuronide metabolite formed during the metabolic reaction was analysed using the UHPLC-MS/MS method described above.

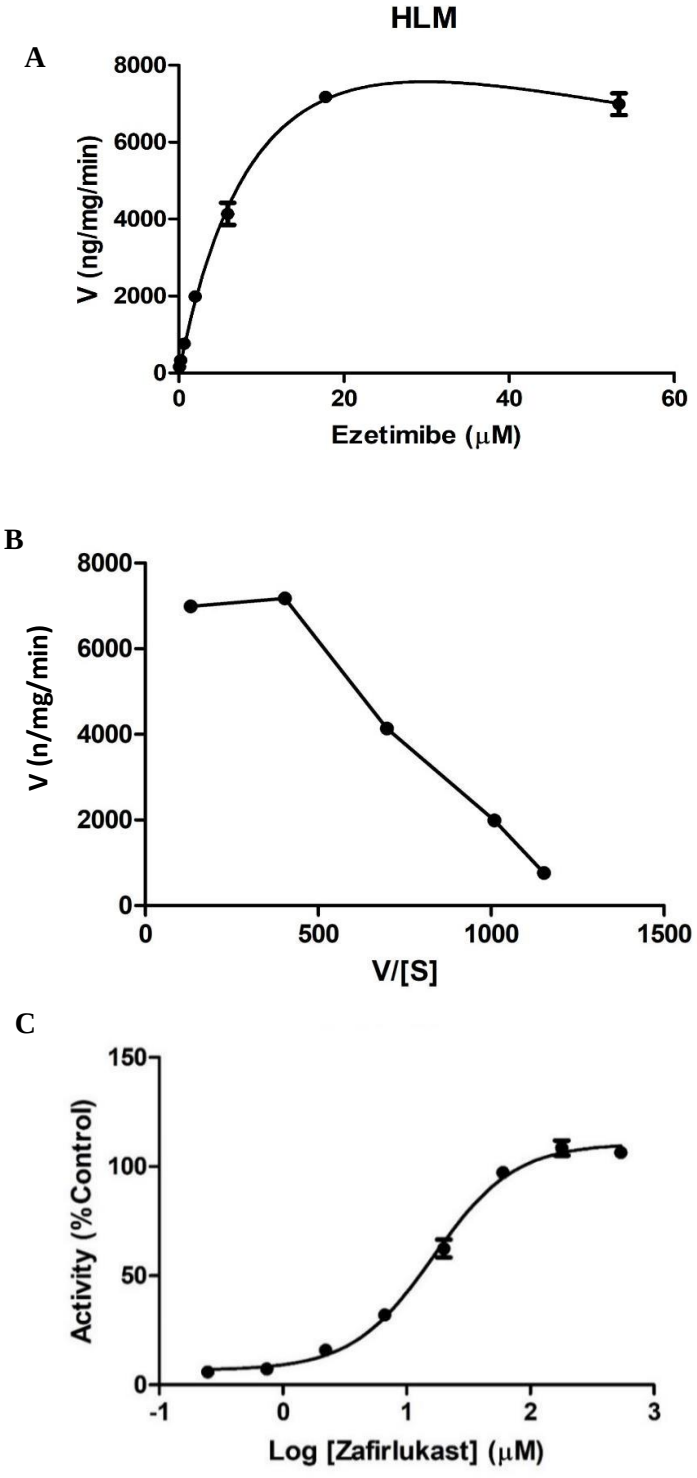

Figure 3.2 UGT mediated enzyme kinetics profile of ezetimibe (A) and respective Eadie-Hofstee plot (B); and UGT inhibition potential of zafirlukast on ezetimibe glucuronidation (C) in HLM. Each data point values are mean ± SD of 3 independent incubations.

The glucuronidation conjugation reaction of ezetimibe by UGT1A1/UGT1A3 in HLM was found to follow substrate inhibition (SI) kinetics, where the rate of metabolism did not reach a plateau at higher concentrations of the substrate. Instead at higher substrate concentrations, the rate of metabolism decreased with an increase in the concentration of substrate. The kinetic model was further confirmed from the curve shape observed in the Eadie-Hofstee plot at higher substrate concentrations, which is a characteristic of the SI kinetics model. The kinetic profiles of glucuronidation conjugation reaction obtained in the study are presented in Figure 3.2. The K_m and V_{max} values were found to be 13.23±2.37 µM and 14275±1633 ng/min/mg protein, respectively. Since ezetimibe followed SI kinetics, the inhibition constant (K_i) was calculated and the value of 'K_i' was found to be 67.49±17.56 µM. Zafirlukast potential to inhibit the formation of ezetimibe-β-D-glucuronide during the metabolism of ezetimibe by UGT1A1/UGT1A3 was determined in HLM. In the enzyme inhibitions studies, with ezetimibe at concentrations corresponding to less than 5-folds below to it's $K_m$value, zafirlukast exhibited inhibitory activity against UGT1A1/UGT1A3 mediated glucuronidation of ezetimibe with the IC_{50} values of 16.41±3.65 µM.

The mean plasma concentration-time profiles of ezetimibe following single dose administration of ezetimibe alone (10 mg/kg) and co-administration of ezetimibe (10 mg/kg) and zafirlukast (10 mg/kg) through oral route are illustrated in Figure 3.3. The pharmacokinetic parameters of ezetimibe, such as T_{max}, C_{max}, $AUC_{0\text{-}last}$ and $AUC_{0\text{-}\infty}$, for both the treatment groups are reported in Table 3.2. Ezetimibe was found to absorbed rapidly with T_{max} of 0.25 h in both the treatment groups. The C_{max} of ezetimibe increased by 3.48-folds while the $AUC_{0\text{-}last}$ increased by 2.34-folds in the treatment group which received ezetimibe + zafirlukast compared to the treatment group which received ezetimibe alone.

The mean plasma concentration-time profiles of zafirlukast following single dose administration of zafirlukast alone (10 mg/kg) and co-administration of ezetimibe (10 mg/kg)

and zafirlukast (10 mg/kg) through oral route are illustrated in Figure 3.4. Statistically no significant differences were oobserved in the pharmacokinetics profiles of zafirlukast when given alone and in co-administration with ezetimibe. The pharmacokinetic parameters of zafirlukast are reported in Table 3.3. Zafirlukast reached the maximum concentration within 0.5 h in both cases. The C_{max} and $AUC_{0\text{-}last}$ values of zafirlukast were similar in both the treatment groups.

Table 3.2 Pharmacokinetic parameters of ezetimibe obtained following oral administration of ezetimibe and co-administration of ezetimibe (10 mg/kg) and zafirlukast (10 mg/kg) in male SD rats (n=3)

Matrix	Pharmacokinetic Parameter	Ezetimibe	Ezetimibe + Zafirlukast
Plasma	**T_{max}** (h)[a]	0.25	0.25
	C_{max} (ng/mL)[b]	3.28 ± 0.97	11.43 ± 2.67
	$AUC_{0\text{-}tlast}$ (ng×h/mL)[b]	11.33 ± 2.43	26.49 ± 4.13
	$AUC_{0\text{-}\infty}$ (ng×h/mL)[b]	14.12 ± 0.92	29.34 ± 7.02

[a]T_{max} is represented as median of three independent (n=3) observations. [b]Data are represented as Mean ± SD of three independent (n=3) observations.

Table 3.3 Pharmacokinetic parameters of zafirlukast following oral administration of zafirlukast and co-administration of zafirlukast (10 mg/kg) and ezetimibe (10 mg/kg) in male SD rats (n=3)

Matrix	Pharmacokinetic Parameter	Zafirlukast	Zafirlukast + Ezetimibe
Plasma	**T_{max}** (h)[a]	0.5	0.5
	C_{max} (ng/mL)[b]	7903.99 ± 101.23	8353.53 ± 122.67
	$AUC_{0\text{-}tlast}$ (ng×h/mL)[b]	63796.54 ± 1547.32	58764.50 ± 3024.74
	$AUC_{0\text{-}\infty}$ (ng×h/mL)[b]	63800.36 ± 1250.25	59746.77 ± 4106.15

[a]T_{max} is represented as median of three independent (n=3) observations. [b]Data are represented as Mean ± SD of three independent (n=3) observations.

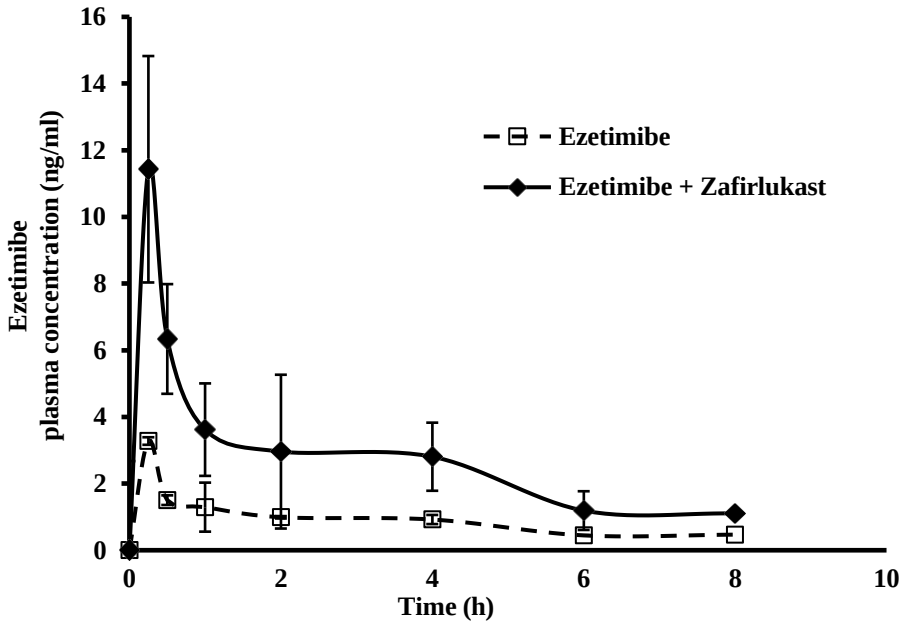

Figure 3.3 Plasma concentration-time curves of ezetimibe (10 mg/kg) obtained following the administration of ezetimibe alone and ezetimibe in combination with zafirlukast (10 mg/kg) in male SD rats (n=3).

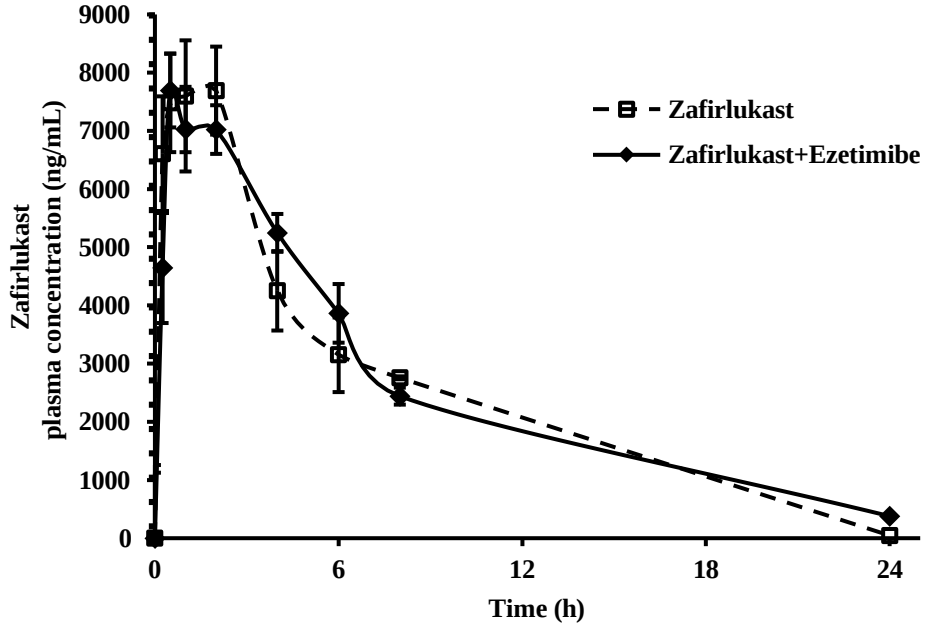

Figure 3.4 Plasma concentration-time curves of zafirlukast (10 mg/kg) obtained following the administration of zafirlukast alone and zafirlukast in combination with ezetimibe (10 mg/kg) in male SD rats (n=3).

3.4 Discussion

Glucuronidation is an important phase-II metabolic pathway that conjugates glucuronic acids to many endogenous and exogenous compounds and involves in the detoxification process. Assessment of potential UGT mediated DDIs is important for drugs that are metabolized majorly by these enzymes when concurrently administered with potent UGT inhibitors [16]. As mentioned in the introduction section, endogenous moieties such as bilirubin and bile acids are mainly metabolized by UGT1A1 and UGT1A3 isoforms in the liver and intestine, inhibition of these isoforms leads to the toxic buildup of bilirubin and bile acids that eventually result in hyperbilirubinemia and cholestasis. In Chapter 2, we found that atazanavir (a potent UGT1A1 inhibitor), inhibited the glucuronidation of β-estradiol in HLM but did not show inhibition in HIM due to the presence of other UGT enzymes present in the intestine responsible for its metabolism. This phenomenon may be attributed to the substrate overlapping across multiple UGTs. Moreover, the maximum velocity (V_{max}) of its glucuronidation in HIM was greater than in HLM [128]. Hence it is suggested to incorporate intestinal UGT metabolism while assessing the total clearance of compounds. Although β-estradiol and chenodeoxycholic acid are routinely used in the screening of UGT1A1 and UGT1A3 inhibitors, respectively, in the *in vitro* methodologies [18, 128], but their use in *in vivo* DDI studies is restricted as they are endogenous molecules. Therefore, accurate and reliable DDI assessment with such endogenous molecules is not possible as their systemic levels are effected by many factors like food, stress, medication, and pathophysiological conditions etc. Hence an exogenous substrate is required to address this issue. Extensive literature search revealed that ezetimibe undergoes rapid and extensive glucuronidation, majorly by UGT1A1 and 1A3 isoforms, in the liver and intestine [43]. Moreover, ezetimibe undergoes enterohepatic recycling similar to the bile acids. Therefore, ezetimibe was considered as an ideal victim drug to investigate potential interactions of UGT isoforms in the gut and liver. Shingo et al., identified zafirlukast as a common inhibitor

of different hepatic and intestine specific UGT enzymes [129]. Based on this literature data, the possibility of UGT-mediated metabolic DDIs of zafirlukast (as perpetrator) and ezetimibe (as victim) was assessed by *in vitro* and *in vivo* methods in the current study.

Enzyme kinetics profile of ezetimibe exhibited substrate inhibition behavior with K_i values of 67.49 µM. The reaction velocity was measured by product formation approach. Though, Ghosal et al. have reported the enzyme kinetic studies of ezetimibe, they did not clearly demonstrate the type of enzyme kinetics involved in the study. In addition, longer incubation times of 120 min were used in the study due to the lower protein concentration of 0.05 mg/mL [130]. The enzyme concentration and incubation times were not optimized in reported study. In the current study, we optimized the protein concentration and incubation times which enabled us to perform the reactions with less incubation times (10 min). Inhibitory potential of zafirlukast on the glucuronidation of ezetimibe was preliminarily confirmed by an *in vitro* assay using HLM with an IC_{50} value of 16.41±3.65 µM.

In the oral pharmacokinetic study involving co-administration of ezetimibe and zafirlukast, the $AUC_{0\text{-last}}$ of ezetimibe increased by 2.34-folds compared to when ezetimibe was administered alone, indicating that zafirlukast is a moderate inhibitor according to the Food and Drugs Administration (FDA) specified classification of metabolic enzyme inhibitors [131]. However, zafirlukast was identified as a potent UGT1A inhibitor when tested in human recombinant systems, the moderate inhibition in rats may be due to reasons such as substrate-dependent inhibition (nature of ezetimibe interaction with enzymes), species differences, UGT expression levels, effective inhibitor concentration at the site etc. Similar results were observed in terms of effect of inhibitors in different species. The V_{max} of bisphenol A glucuronidation in male rat intestinal microsome was nearly 30-fold higher than that of mixed-gender HIM [132].

The involvement of intestinal and/or hepatic transporters such as p-glycoprotein (p-gp, ABCB1) and multidrug resistance-associated protein-2 (MRP2, ABCC2) in the uptake and secretion of ezetimibe also affect its disposition. The increased maximum serum concentrations and decreased fecal excretion of ezetimibe when co-administered with rifampin (a modulator of p-gp and MRP2) was a possible outcome of transporter inhibition [133]. The effectiveness of zafirlukast on the inhibition of these transporters is not evident. Nonetheless, the mild increase in the sensitivity of anticancer activity of paclitaxel in ABCB1 overexpressing HEK cells was observed with higher concentration (100 μM) of zafirlukast in MTT assay. But the transporter inhibition assays were not conducted to prove this p-gp inhibition and also other possibilities such as effect on some proteins or protein-protein cross talk by zafirlukast should also be explored to confirm p-gp inhibitory potential [134]. A molecular docking study comparing the affinity and binding energies of zafirlukast towards both UGTs and ABCB1 will be useful to assess their impact on disposition. The increased exposure in terms of C_{max} and AUC of ezetimibe in presence of zafirlukast was assumed to be UGT related as supported by the *in vitro* results. Our results also correlated with the outcome of a clinical interaction study in healthy volunteers to study the impact of efavirenz on the pharmacokinetics of ezetimibe. This study reported that inhibition of UGT1A1-mediated glucuronidation of ezetimibe with single or multi-dose of efavirenz resulted in the increased exposure of ezetimibe and decreased exposure of ezetimibe-glucuronide while highlighting the intestinal UGT metabolism [135].

In vitro methodology described in the present report can be utilized to screen UGT1A1 and UGT1A3 inhibitors employing ezetimibe as substrate and, to estimate the fraction metabolized (f_m) by important UGTs employing zafirlukast as common inhibitor. Further, UGT mediated *in vivo* DDIs in rat can be evaluated by employing ezetimibe as victim and zafirlukast as perpetrator drugs.

3.5 Conclusion

The *in vitro* enzyme kinetic studies indicate that UGT1A1/UGT1A3-mediated glucuronidation of ezetimibe follows substrate inhibition kinetics in HLM. The glucuronidation conjugation of ezetimibe by UGTs was inhibited by zafirlukast with an IC_{50} value of 16.41±3.65 µM. In the *in vivo* DDI study, zafirlukast increased the C_{max} (3.48-folds) and $AUC_{0\text{-}last}$ (2.34-folds) of ezetimibe. These results confirm that zafirlukast was capable of inhibiting UGT1A1/UGT1A3 enzymes *in vivo* and can be used as a research tool in further applications where UGT inhibition is required to explore key mechanisms in xenobiotic metabolism or disease conditions.

4

UHPLC-MS/MS method development and validation for quantification of seven selected bile acids in rat plasma

4.1 Introduction

Bile acids (BAs) are synthesized from cholesterol and then conjugated to glycine or taurine to form bile salts. These BAs are secreted into the bile duct and stored in gall bladder. Bile is released into the small intestine based on the stimuli received from food intake or other factors. The oral absorption of lipids, fat-soluble vitamins and other lipophilic nutrients present in the food is facilitated by the bile constituents, primarily by the bile salts. Most of the BAs are reabsorbed into the systemic circulation from the terminal ileum. Some BAs are converted to secondary BAs in the intestine by gut microbiota, some are excreted in the feces and some are metabolized to their respective sulfates and glucuronides and excreted in urine. All BAs that are reabsorbed into the systemic circulation enter into the liver and involve in the enterohepatic circulation [52, 81, 136]. BA homeostasis is maintained by various nuclear receptors and signaling pathways [137]. Bile acid synthesis and their homeostasis is disrupted in diseases like primary biliary cholangitis, liver cirrhosis and non-alcoholic fatty liver disease. Altered total BA composition is observed in the inflammatory bowel syndrome, Chron's disease and ulcerative colitis. BAs, at higher concentrations, are reported to exhibit toxicity due to their surfactant like property and can contribute to hepatobiliary as well as intestinal disorders [138].

Farnesoid X receptor (FXR) is the crucial nuclear receptor expressed mainly in the liver and intestine which involves in the homeostasis and enterohepatic circulation of bile acids. FXR also involves in the homeostasis of lipid and glucose and has become a promising target in the management of hyperlipidemia, diabetes, non-alcoholic fatty liver disease, cholestasis, primary biliary cholangitis and chronic inflammatory diseases of the liver and intestine [139-143]. Recently, the differential tissue expression and the tissue specific functionalities of FXR is attracting more attention in exploring various ligands for its agonistic and/or antagonistic activities [144-146] .

Ivermectin (IVM) is a broad spectrum antiparasitic drug and had been identified as a highly selective FXR ligand. IVM was first categorized as a partial FXR agonist and later some *in vitro* studies reported its antagonistic activity to FXR. However, the FXR antagonistic activity of IVM was not well characterized *in vivo* [147-150]. It reduces serum cholesterol and glucose while increasing the insulin sensitivity by stimulating FXR in mice which causes reduction in body weight as well as hepatic lipid accumulation in diabetic mice. Since FXR is a BA-activated nuclear receptor and regulates BA homeostasis, it would be clinically important to study the *in vivo* effect of IVM in the regulation of BA homeostasis and quantitative measurement of important BAs in rats including primary BAs cholic acid (CA), chenodeoxycholic acid (CDCA), secondary BAs deoxycholic acid (DCA) and its glyco/tauro-conjugates (G/T-DCA), murine specific tauro-α-muricholic acid (Tα-MCA) and tauro-β-muricholic acid (Tβ-MCA). Moreover, BAs such as DCA and GDCA were reported to be endogenous etiologic agents in gastrointestinal cancer [151]. Further, GDCA and TDCA were significantly increased in NASH patients with fibrosis and fibrosis mouse models[152]. Therefore, specific and accurate estimation of these BAs can be highly advantageous in studying the effect of drugs like IVM on BA pool, in the diagnosis and detection of drug induced liver injury (DILI) as well as to predict BA related disorders [108, 153, 154]. Though BAs are majorly present in bile, it is important to estimate the bile acids in plasma as they are reabsorbed into the systemic circulation due to enterohepatic circulation [155].

The development of an LC-MS/MS method of BAs is of great interest in the liver diseases and other metabolic diseases research area. Due to the structural similarities in some of the BAs, separation and quantification of isobaric BAs is challenging. Several LC-MS/MS based methods have been developed for detection, separation and quantification of different BAs in the recent years. Many research papers in the literature developed methods for human specific BAs, while few publications report both human and rodent specific BAs. But they included

many BAs in their list which increased run time. There is a need to develop a method to draw crucial conclusions by incorporation of important human and rodent specific BAs in a simultaneous method for mechanistic understanding of BA homeostasis in rats and human.

Many reported methods included the quantification of primary, secondary and/or their conjugated BAs but lacked the quantification of murine specific BAs, especially, Tα-MCA and Tβ-MCA [156-170]. Some reports employed complex sample preparation methods such as solid phase extraction or liquid-liquid extraction [157, 158, 161, 171-173]. Higher injection volumes were used to achieve better sensitivity for few BAs in some of the reported methods [157, 160, 174-176]. Moreover, most of the reported methods were developed with longer sample analysis run times [160, 169, 171-186]. Few methods reported relative quantification of the BAs rather than their absolute quantification which raises questions on their reliability or reproducibility [169, 187-190]. The baseline separation of isobaric BAs such as CDCA/DCA and Tα-MCA/Tβ-MCA was not achieved in some of the reported methods [178, 184, 185, 191]. More importantly, some of the reports lack complete method validation as per the regulatory guidelines.

Detailed analysis of the currently reported literature methods reveals either one or more of the issues such as complex sample preparation methods, longer runtimes, separation of isobaric bile acids, use of charcoal stripped surrogate matrix, higher injection volumes, relative quantification instead of absolute quantification, lack of deuterated internal standards, and paucity of method validation of all parameters for human and murine specific BAs in rat plasma. Therefore, the current LC-MS/MS method was developed and validated to simultaneously quantify seven bile acids (CA, CDCA, GDCA, TDCA, Tα-MCA, Tβ-MCA and DCA). Further, the developed method was used to evaluate the effect of IVM on these BA

profiles in rat plasma. To our knowledge this is the first paper to study the effect of IVM on BA levels in rats which may lead to further exploration of IVM as an FXR modulator.

4.2 Experimental Methods

4.2.1 Materials

Cholic acid (CA) and chenodeoxycholic acid (CDCA) were purchased from TCI Chemicals (India) Private Limited, Hyderabad, India. Deoxycholic acid (DCA), glycodeoxycholic acid (GDCA), taurodeoxycholic acid (TDCA) and dimethyl sulfoxide (DMSO) were purchased from Sigma Aldrich (Merck) Chemicals Private Limited, Bangalore, India. Tauro-α-muricholic acid (Tα-MCA), tauro-β-muricholic acid (Tβ-MCA), cholic acid-d4, deoxycholic acid-d4, glycodeoxycholic acid-d4, taurodeoxycholic acid-d4, taurocholic acid-d4 were purchased from Cayman Chemical Company, MI, USA. IVM and dipotassium EDTA were purchased from Sisco Research Laboratories Private Limited, Hyderabad, India. LC-MS grade methanol, acetonitrile, water and formic acid were purchased from Biosolve India Limited, Hyderabad, India. Male Sprague-Dawley rats and rat pooled plasma were procured from Hylasco Biotechnology Private Limited, Hyderabad, India.

4.2.2 Instrumentation

An Ultra-High Performance Liquid Chromatographic system (Nexera 40D-XS, Shimadzu Corporation, Kyoto, Japan) coupled with a SCIEX QTRAP® 4500 mass analyser attached with Turbo V™ and electron-spray ionization probe (Sciex, MA, USA) was used in the analysis. Acquisition and integration of the chromatograms was performed using Analyst software (Version 1.7). Aqueous mobile phase was filtered through a 0.22 µm Millipore® (MA, USA) filtration membrane using a vacuum pump. The samples were prepared using calibrated micropipettes (Eppendorf, Chennai, India). Vortex mixer (Tarsons India Private Limited) and

refrigerated centrifuge (Eppendorf 5810R, Eppendorf, Hamburg, Germany) were used for sample processing while deep freezer (Panasonic, Osaka, Japan) was used for storing the samples during method development, validation and *in vivo* studies.

4.2.3 Preparation of charcoal stripped plasma

Dextran-coated charcoal (C6241, Sigma Aldrich, 0.025% w/w or 10:1) was vortex mixed at 4 °C for 16 h in 50 mL preparation buffer (0.25 M sucrose, 1.5 mM MgCl2, 10 mM HEPES, pH 7.4) at a concentration of 0.25% (w/v). 40 mL of this mixture was centrifuged at 2000 rpm for 10 min to pellet down the charcoal. The supernatant was decanted and 40 mL of blank plasma was added to the charcoal pellet and vortex mixed at 4 ºC for 16 h. The mixture was centrifuged at 2000 rpm for 10 min and the supernatant was collected into a fresh centrifuge tube and repeated the centrifugation one more time. Following the centrifugation, the supernatant was separated and passed through 0.2 µm filter to get clear stripped plasma. The stripped plasma was aliquoted and stored at -80 °C.

4.2.4 Stock solutions, calibration standards and quality control samples preparation

Primary stock solutions of each of the seven bile acids and their respective deuterated internal standards (IS) were prepared, separately, at a concentration of 1 mg/mL using DMSO as the solvent. These primary stock solutions were divided into 0.25 mL aliquots and stored at -80 °C to avoid repeated freezing and thawing. From each of the primary stock solutions of the seven bile acids, 25 µL was drawn and added into a fresh centrifuge tube and diluted with 825 µL of diluent (methanol: water (1:1)) to yield a pooled stock solution containing each bile acid at concentration of 25000 ng/mL. The pooled stock solution was used to prepare further working stock solutions to spike the charcoal stripped plasma to construct nine-point calibration curve for each of the seven bile acids. The working stock solutions were prepared in the range of

25.03-25000 ng/mL (25.03, 50.06, 250.31, 1251.56, 5006.25, 12515.63, 20025, 22500 and 25000 ng/mL) with the same diluent used in the preparation of pooled stock solution. The calibration curve range and calibration points values were set same for all the seven bile acids. Each calibration curve standard, in the calibration curve range, was prepared separately by spiking 2 µL of appropriate working stock solution to 48 µL of charcoal stripped blank plasma. The calibration curve was developed in the range of 1- 1000 ng/mL using nine calibration standards (1, 2, 10.01, 50.06, 200.25, 500.63, 801, 900 and 1000 ng/mL) for each of the bile acids. The lower quality control (LQC), medium quality control (MQC) and higher quality control (HQC) standards were set at 3 ng/mL, 500 ng/mL and 840 ng/mL, respectively. The pooled internal standard working solution (2500 ng/mL) was prepared by aliquoting 2.5 µL of each of the internal standard primary stock solutions (2.5 µL × 5 = 12.5 µL) to a fresh centrifuge tube and diluting with 987.5µL of diluent (1:1 mixture of methanol and water). All stocks were stored at -20 °C until use.

4.2.5 Collection of rat plasma

Under light isoflurane anesthesia, 200 µL of blood was collected from retro-orbital plexus using rat bleeding capillary tubes. The blood was collected into fresh microcentrifuge tubes containing anticoagulant solution (200 mM K_2EDTA in normal saline) at a concentration of 2% v/v (in the blood collected). The blood samples were kept in the wet ice until centrifugation. The blood samples were centrifuged in a cooling centrifuge at 10000 rpm for 10 min at 4 °C and the supernatant plasma was collected carefully, labelled and stored at -80 °C until LC-MS/MS analysis.

4.2.6 Sample preparation

A simple and convenient protein precipitation method was utilized for plasma sample preparation. Ice-cold acetonitrile containing 100 ng/mL of each of the internal standards was used to precipitate the proteins. The protein precipitating solvent was prepared just before to use by adding 5 µL of each of the internal standard primary stock solutions (1 mg/mL) (5 µL × 5 = 25 µL) into 49.975 mL of ice-cold acetonitrile. The plasma sample preparation was done as followed. 50 µL of plasma was added to a fresh 0.5 mL centrifuge tube and 200 µL of ice-cold acetonitrile containing internal standards was added to precipitate proteins. The tube was vortexed for 2 min and then centrifuged at 10000 rpm for 10 min at 4 °C and the supernatant was transferred into 96-well plate for LC-MS/MS analysis. In the case of samples whose concentrations were higher than the ULOQ, the samples were diluted with acetonitrile as required and centrifuged for 5 min at 10000 rpm at 4 ^{o}C. The supernatant obtained was subjected to LC-MS/MS analysis.

4.3 Method development

Individual bile acids at 100 ng/mL concentration were introduced in to the mass spectrometer by infusion syringe pump to identify and optimize compound specific mass spectrometric parameters. The mass analyzer conditions were optimized by studying the effect of ion-source temperature, ion-spray voltage, flow rates of curtain gas, nebulizer gas and drying gas, declustering potential, collision energy, entry and exit potential etc. Pseudo-Multiple reaction monitoring (Pseudo-MRM) method was employed for quantification of the bile acids. In the preliminary chromatographic method development trials, simultaneous separation of seven bile acids and the internal standards was achieved by optimizing various LC conditions like mobile phase composition, flow rate, column chemistry and oven temperature as well as peak shape/properties, separation and intensity. Different ammonium salts including acetate,

formate, carbonate and bicarbonate we along with pH modifiers were tried as the aqueous phase component. The effect of methanol and acetonitrile as the non-aqueous phase component of the mobile phase was also studied. Further, the mobile phase gradient, flow rate and column temperature were also optimized.

4.4 Chromatographic and mass spectrometric conditions

The chromatographic separation of the seven bile salts was achieved on ACQUITY UPLC® HSS T3 column (1.8 µm, 2.1x100 mm) (Waters India Private Limited, Bangalore, India). The mobile phase consisted of eluent A (water containing 0.1% v/v formic acid) and eluent B (100% acetonitrile). The mobile phase was pumped in a gradient elution mode as per the following program: at 0 min – 5% B, 0.5 min – 5% B, 1 min – 35% B, 2 min – 30% B, 3 min – 30% B, 4 min – 40% B, 5 min – 45% B, 6 min – 70% B, 7 min – 100% B, 8 min – 100% B, 9 min – 5% B and at 10 min – 5% B. The mobile phase flow rate was fixed at 0.45 mL/min. 2 µL of sample was injected for analysis. The column temperature and autosampler temperature were set at 40 °C and 15 °C, respectively. The column was pre-saturated with the same mobile phase gradient program and the chromatography system was stabilized for 60 min by observing the baseline prior to actual analysis. The mass spectrometer was operated with the electron spray ionization probe in negative polarity. The ion source temperature (TEM) was set to 500 °C. The curtain gas (CUR) was set at 35 L/h, collision gas (CAD) was set to medium, ion spray voltage (IS) at 4500 volts, nebulizing gas (GS1) at 50 psi and drying gas (GS2) at 45 psi. Nitrogen was used as both nebulizing as well as drying gas. Pseudo-Multiple reaction monitoring (Pseudo-MRM) was used in the method development as well as the analysis of the samples obtained from the *in vivo* studies. Peak integration was done for each bile acid and their respective internal standard at their retention times. The ratio of peak area of a specific analyte to its corresponding internal standard was calculated.

4.5 Method validation

Since bile acids are endogenous molecules, a surrogate matrix (charcoal stripped plasma) was employed in the current method for method validation. The method was validated for selectivity, specificity, carryover, sensitivity, linearity, matrix effect, recovery, accuracy and precision, dilution integrity, reinjection reproducibility and stability according to FDA Guidance for Industry-Bioanalytical Method Validation and Study Sample Analysis [192].

4.5.1 Selectivity, specificity and carryover

Selectivity of the method was established by evaluating any possible interference due to the components present in the blank matrix at the retention times of the bile acids and their respective internal standards. Specificity of the method to detect and differentiate bile acids from other or related compounds was established by comparing the chromatograms of zero samples, sample containing only the bile acids and the LLOQ samples, to check for any possible interferences at the retention time of bile acids. Chromatograms were obtained for stripped blank plasma, stripped plasma spiked bile acids and internal standards (at calibration curve standard, 500.63ng/mL) and only spiked internal standards (100 ng/mL), blank study sample (unstripped) and compared. Carryover was performed to check the analyte response (for each bile acid) in the blank samples analyzed immediately following the analysis of upper limit of quantification (ULOQ) sample. The response of each bile acid, at their respective retention times, in the blank or zero samples should not be more than 20% of lower limit of quantification (LLOQ) sample. In addition, the mean peak area of internal standard at respective retention time in blank or only analyte spiked samples should not be more than 5% of internal standard area at LLOQ concentration.

4.5.2 Linearity

To evaluate the linearity, nine calibration standards in the range of 1.0-1000 ng/mL (1, 2, 10.01, 50.06, 200.25, 500.63, 801, 900 and 1000 ng/mL) were prepared independently and assayed in triplicate. Specified amounts of standard stock solutions were added to charcoal stripped plasma for the preparation of nine calibration points. The samples were prepared as discussed in sample preparation section above. Three calibration curves were constructed by plotting the peak-area ratios of the bile acids to their ISs against the nominal concentrations. Linearity of the method for each bile acid was assessed by performing the least-square regression analysis of observed concentrations versus the nominal concentration of the analyte for the calibration curve samples. Least-square linear regression analysis was performed without and with different weighting factors to determine equations (for each bile acid) with higher adjusted R^2 and R^2_{PRESS} values and with lower standard error of estimate values. The mean calibration curve was constructed based on the data obtained from triplicates (n=3). Method sensitivity was determined by considering peak shape and background noise threshold at the LLOQ concentration for each bile acid. The mean accuracy of the back calculated concentration should be within ±20% and ±15% for LLOQ and other calibration standards respectively.

4.5.3 Accuracy and precision

Accuracy was reported as the percentage bias (%bias) of the back calculated concentration of the QC samples using the calibration equation. Precision was reported as the percent coefficient of variation (%CV) within the replicate samples at all QC samples. Intra-day and inter-day precision and accuracy assessment was done by analysis of LLOQ and QC samples (LQC, MQC, HQC) in replicates (n=6). For intra-day precision, two batches were analyzed on same while for inter-day precision, one batch was analyzed each day for three consecutive days.

4.5.4 Extraction recovery and matrix effect

The extraction recovery of bile acids from charcoal stripped plasma was determined by analyzing the QC samples (LQC, MQC, HQC) and internal standards at 100 ng/mL in replicates (n=6) by comparing the peak areas from extracted samples to which analytes or internal standards were added prior to the acetonitrile extraction (pre-extraction) with those of post-extracted samples to which analytes or internal standards were added after extraction with acetonitrile. Extraction recoveries of internal standards were used to calculate the internal standards normalized recoveries of bile acids. More than at least 50% recovery was expected for the required sensitivity. To determine the matrix effect, LQC and HQC samples were spiked into stripped plasma (n=6) and compared the effect of matrix by the mean concentration of neat standard samples without matrix at the same nominal concentration. Similarly, matrix effect for internal standards also evaluated at 100 ng/mL concentration. The accuracy and precision should be ±15% and ≤15% respectively.

4.5.5 Stability, reinjection reproducibility and dilution integrity

Stability of the samples was assessed by subjecting LQC, HQC samples (n=6) to different conditions viz., auto-sampler/injector stability (up to 24 h at 15 °C), bench-top stability, freeze-thaw stability (5 cycles) and long-term stability at -20 °C and -80 °C. The percentage deviation was determined by comparing the concentrations observed from zero time and stability samples. Auto-sampler/injector stability was assessed by storing the QC samples in autosampler and analysing the samples after a period of 24 h. Freeze thaw cycles were repeated for five consecutive days and one set of samples which completed fifth cycle were analysed for freeze thaw stability. The QC samples were stored at -20 °C and -80 °C for a period of 18 days and were analyzed for assessing the long-term stability. A calibration curve was constructed using freshly prepared calibration curve standards to quantify the analytes in the

stability samples. Stock solution and working stock stabilities were assessed at LQC and HQC levels in diluent (methanol: water (1:1)) at room temperature for 24 h in replicates (n=6) and the areas ratios were compared in both conditions. Also, working stock stability of internal standards was assessed at 100 ng/mL concentration at room temperature for 24 h in replicates (n=6) and the stability sample areas were compared with freshly prepared samples. The precision and accuracy should be within ≤15% and ±15% of their nominal concentrations respectively. A reinjection reproducibility batch consisting of quality controls at LQC, MQC and HQC levels in replicates (n=6) under a calibration curve were analyzed and the reproducibility of the method was reported in terms of precision and accuracy of reinjected QC samples. Dilution integrity was evaluated by diluting the sample (2000 ng/mL) by 5-folds and 20-folds with stripped plasma and quantified against a surrogate calibration curve. The accuracy and precision of the diluted samples should be within ±15% and <15% of their nominal concentrations respectively.

4.6 Effect of multi-dose administration of IVM on plasma concentration of bile acids

The protocol for animal experiments was reviewed and approved by our institutional animal ethics committee (BITS-IAEC-2023-17) prior to the study. Male Sprague Dawley (SD) rats of 6-8 weeks' age having 220-250 gm body weight were procured and quarantined for 5 days in our institute's animal house. The rats were acclimatized to the conditions in the animal house where the temperature and relative humidity were maintained at 22±1 °C and 50±10 %, respectively, with 12 h dark-light cycle. The rats were provided free access to regular rat chow diet and water. IVM formulation was prepared by dissolving the drug in a solvent containing the mixture of 2% DMSO, 2% tween 80 and 96% purified water. Following the quarantine period, IVM formulation was administered to rats (n=6) through oral route using gavage, at a dose of 5 mg/kg and dose volume of 5 mL/kg body weight. Rats were fasted for at least 4 h

prior to the dosing of IVM formulation on each day of dosing. The animals were administered with IVM formulation once a day at a fixed time (11:00 AM on every day) for 14 consecutive days. Blood samples were collected by retro orbital plexus method at predose (1 h before administering the first dose) and at 2 h after dosing on the day-14. The blood samples were processed immediately after collection and the plasma samples were labelled properly and stored at -80 °C until LC-MS/MS analysis.

4.7 Statistical analysis

Least-square simple linear regression analysis was employed to determine the calibration equation. The difference in the bile acid concentrations in the samples collected at predose and day-14 was analyzed by using a paired t-test (two-sided) at 5% significance level (α=0.05).

4.8 Results

4.8.1 Method development

Mass spectrometric conditions were optimized for each of the bile acids and all the internal standards in negative ESI mode. Nebulizer gas, heat block temperature and desolvation gases were optimized simultaneously. For each of the bile acids and internal standards, Q1 masses were detected and the DPs were optimized. Pseudo-MRM was applied in the method for quantification of individual bile acids. In the chromatography trials, better separation was achieved with aqueous phase containing 0.1% v/v formic acid in water. The peak intensity of most of the bile acids and internal standards was better with acetonitrile as the organic phase compared to methanol. The mobile phase composition containing water with 0.1% v/v formic acid as the aqueous phase (eluent A) and acetonitrile as the organic phase (eluent B) in a gradient program resulted in better peak properties, separation and peak intensity for the analytes compared to any other mobile phase composition. Considering detector sensitivity and

reproducibility, the injection volume was set as 2 µL. The specific identification of isobaric compounds such as CDCA/DCA and Tα-MCA/Tβ-MCA were confirmed by comparing their retention times in mixture and individual bile acid injections with the same method conditions. The optimized mass spectrometer conditions and MRM details of bile acids and internal standards are presented in Table 4.1.

4.8.2 Method validation

The developed method was validated as per the FDA guidelines for its intended purpose to quantitatively determine bile acids in rat plasma. Charcoal stripped blank rat plasma was used as a surrogate matrix in the current LC-MS/MS method to avoid the possible effect of endogenous bile acids in the analysis. The complete stripping of the bile acids from the plasma was confirmed by the absence of selected bile acids at their specific retention times in the chromatogram of stripped blank plasma.

4.8.2.1 Selectivity, specificity and carryover

Pseudo multiple reaction monitoring (Pseudo-MRM) transitions and efficient chromatographic separation enabled the highly selective and specific analysis of bile acids in plasma. Typical chromatograms obtained from four scenarios as mentioned in methods were analyzed and no significant interferences were observed either for analytes or for internal standards at the specified concentration levels at their respective retention times. Differentiation of isobaric compounds like CDCA-DCA, TαMCA-TβMCA was achieved by separating them at different retention times. However, some other isobaric compounds containing identical molecular weights to that of selected bile acids were observed in the unstripped blank plasma at different retention times. No interference of these compounds observed during analysis. Accordingly, no analyte response was observed in the subsequent blank samples after the ULOQ injections in the carryover studies. Chromatograms of stripped blank plasma, internal standards spiked in

stripped blank plasma (100 ng/mL), a calibration curve standard and, unstripped blank plasma are presented in Figures 4.1a-b, 4.2, 4.4 and 4.4, respectively.

4.8.2.2 Linearity

The least-square linear regression equations constructed using '$1/x^2$' as the weighting factor yielded higher adjusted R^2 (>0.9965) and R^2_{PRESS} (>0.9936) values compared to unweighted or any other weighting factors (1/x or 1/y or $1/y^2$). The slope and intercept values of the calibration equations, obtained from the least-square linear regression analysis with '$1/x^2$' as the weighting factor, of all the seven bile acids are presented in Table 4.2. All the seven bile acids showed a linear response in the calibration range of 1 to 1000 ng/mL. Higher adjusted R^2 (>0.9965) and R^2_{PRESS} (>0.9936) and low standard error of estimates (<23.57) for the calibration equations of all the seven bile acids indicate the ability of the regression equations to predict the concentrations of unknown samples as close as possible to the actual concentrations. The samples which exceed the calibration range were reanalyzed by diluting them to five folds with diluent.

4.8.2.3 Accuracy and precision

The results obtained from accuracy and precision studies of the developed method are presented in Table 4.3a and 4.3b. The accuracy values, expressed in terms of %bias, for all the bile acids across all the samples (LLOQ, LQC, MQC and HQC) were between -8.77% to 13.5%, suggesting that the method is accurate for quantification of the seven bile acids in plasma. The intra-day precision, expressed in terms of percent coefficient of variation (%CV), for all the bile acids across all the samples (LLOQ, LQC, MQC and HQC) was between 3.04% to 14.23%, while the intra-day precision was between 3.14% to 12.47%. The %CV values for the intra-day and inter-day precision studies were well within the acceptable limit of <15%, indicating that the developed method is precise for quantification of the seven bile acids.

4.8.2.4 Extraction recovery and matrix effect

The extraction recoveries of bile acids following the protein precipitation from the striped plasma samples at three different QC levels (LQC, MQC and HQC levels) and internal standards at 100 ng/mL are presented in Table 4.4. The mean recovery values of the seven bile acids varied between 74.14% (for DCA at LQC level) to 87.86% (for Tα-MCA at HQC level) with %CV of not more than 13.25% for any of the bile acids at any QC level. The mean recovery values of internal standards varied between 81.22% (for d_4-DCA) to 92.98% (for d_4-TCA) with %CV of not more than 4.72% for any of the internal standards.

The overall accuracy and precision of the matrix effect on the analysis of the seven bile acids at two QC levels is presented in Table 4.5. The highest %bias (accuracy) was 13.86% (for TDCA) and the precision (%CV) was not more than 11.39% for the matrix effect on any of the bile acids, at any of the two QC levels. For each of the seven bile acids, at two different QC levels, no significant suppression or enhancement was observed in the response. Therefore, it can be inferred that there is no matrix effect on the analysis of the seven bile acids. Similarly, no significant matrix effect was also observed in the analysis of internal standards. The highest %bias for the matrix effect on any of the internal standards was -13.55% (for d4-DCA) and the precision (%CV) was not more than 13.81% for any of the internal standards (Table 4.5). These results suggest that the method exhibited no significant matrix effect.

4.8.2.5 Stability, reinjection reproducibility and dilution integrity

Table 4.6 presents the results obtained from the stability studies of the seven bile acids evaluated using three QC standards (LQC, MQC and HQC) when subjected to different stress conditions. All the seven bile acids were stable in the stripped plasma when subjected to five cycles of freeze-thaw (-20 °C to room temperature) on five consecutive days and long-term stability for a period of 18 days when stored at -20 ^{o}C as well as -80 ^{o}C. No significant

degradation was observed in the processed samples when placed on bench top at room temperature (25±2 ^{o}C) or in the autosampler racks (15±0.5 ^{o}C) for a period of 24 h. The primary stock solutions and the working standard solution of the bile acids and the working standard solutions of internal standards were stable for 24 h when stored at room temperature (25±2 ^{o}C). The %deviation was within the acceptable limits of ±15% for the stock solutions of bile acids and internal standards used in the study. Stabilities of bile acids at different conditions and stock solution stabilities were reported in Table 4.6 and Table 4.7 respectively.

The mean accuracy and precision values of the reinjected QC standards (LQC, MQC and HQC) are given in Table 4.8. The accuracy was ranging from -4.70% (for DCA at MQC) to 5.39% (for Tβ-MCA at LQC) and precision was less than 8.5% across all QC levels for all bile acids. The accuracy and precision values of the dilution integrity samples (5-folds and 20-folds dilution) were within the specifications of ±15% and <15% of the nominal concentration. The results obtained from dilution integrity studies are presented Table 4.9.

4.8.2.6 Effect of multi-dose administration of IVM on plasma concentrations of bile acids

In the *in vivo* study, effect of oral administration of IVM in a multi-dose regimen (at 5 mg/kg body weight, once daily for 14 days) on the plasma concentrations of seven bile acids was studied. A comparison of plasma concentrations of the seven bile acids before and after IVM treatment is shown in Figure 4.5. The plasma concentrations of CA were significantly (P=0.003) lesser in the day-14 samples compared to the predose samples. There was no significant (P=0.352) difference in the CDCA concentrations before and after treatment of IVM. However, a statistically (P=0.0324) significant reduction was observed in the DCA concentrations from predose to day-14. Statistically no significant difference was observed in the concentrations of GDCA and TDCA at predose and day-14 of IVM treatment. Interestingly, in contrast to the CA or DCA results where the concentrations decreased at day-14, there was

a significant increase in the concentrations of Tα-MCA (P=0.02) and Tβ-MCA (P=0.045) at day-14 compared to predose. Overall, multi-dose administration of IVM (once daily for 14 days) resulted in significant reduction in CA and DCA levels; significant increase in the Tα-MCA and Tβ-MCA levels and no significant change in the CDCA levels.

Table 4.1 Optimized mass spectrometer conditions used in the analysis of bile acids and their respective internal standards

Mass Spectrometer Parameter	**Value**
Curtain gas flow rate	35 L/h
Collision gas flow rate	Medium
Ion spray voltage	(-)4500 volts
Ion source temperature	500 ºC
Nebulizer gas flow rate	50 psi
Drying gas flow rate	45 psi

MRM conditions used in the optimized method

Analyte	**Q1 Mass (Da)**	**Q3 Mass (Da)**	**Dwell time (msec)**	**DP (V)**	**EP (V)**	**CE (V)**	**CXP (V)**	**Rt (min)**	**IS used**
CA	407.2	407.2	50	-100	-10	-16	-10	7.08	d_4-CA
CDCA	391.3	391.3	50	-100	-10	-26	-10	7.73	d_4-DCA
DCA	391.2	391.2	50	-100	-10	-26	-10	7.81	d_4-DCA
GDCA	448.3	448.3	50	-100	-10	-23	-10	7.24	d_4-GDCA
TDCA	498.2	498.2	50	-100	-10	-33	-10	6.99	d_4-TDCA
Tα-MCA	514.1	514.1	50	-100	-10	-36	-10	4.11	d_4-TCA
Tβ-MCA	514.2	514.2	50	-100	-10	-20	-10	4.27	d_4-TCA
d_4-CA	411.3	411.3	50	-100	-10	-23	-10	7.07	
d_4-DCA	395.2	395.2	50	-100	-10	-28	-10	7.80	
d_4-GDCA	452.3	452.3	50	-100	-10	-28	-10	7.23	
d_4-TDCA	502.3	502.3	50	-100	-10	-25	-10	6.98	
d_4-TCA	518.3	518.3	50	-100	-10	-21	-10	5.71	

DP – Declustering potential; EP – Entrance potential; CE– Collision energy; CXP – Collision cell exit potential; Rt – Retention time and IS – Internal standard; V – volts

Table 4.2 Weighted least-square linear regression analysis of the calibration curves of seven bile acids (n = 3)

Analyte	**Linearity range (ng/mL)**	**Intercept**	**Slope**	**R^2**	**Adjusted R^2**	**R^2_{PRESS}**	**SEE**
CA	1-1000	6.136±3.895	0.952±0.017	0.9980	0.9977	0.9956	19.21
CDCA		7.157±3.736	0.950±0.024	0.9984	0.9981	0.9970	17.27
DCA		8.838±3.306	0.9499±0.017	0.9970	0.9965	0.9936	23.57
GDCA		7.2089±5.106	0.9525±0.018	0.9975	0.9971	0.9946	21.48
TDCA		7.6692±5.126	0.9518±0.014	0.9976	0.9972	0.9948	21.09
Tα-MCA		5.1845±3.690	0.9441±0.019	0.9985	0.9983	0.9969	16.46
Tβ-MCA		5.2467±3.352	0.9550±0.014	0.9990	0.9989	0.9981	13.29

Table 4.3a Inter-day accuracy and precision studies of the developed method

Analyte		LLOQ (1 ng/mL)	LQC (3 ng/mL)	MQC (500 ng/mL)	HQC (840 ng/mL)
Inter-day accuracy and precision studies (n=18)					
CA	Accuracy (%bias)	6.50	0.70	-6.79	-3.49
	Precision (%CV)	9.85	9.57	3.65	4.25
CDCA	Accuracy (%bias)	-2.46	-4.43	-7.10	-3.32
	Precision (%CV)	12.86	9.25	5.31	4.48
DCA	Accuracy (%bias)	9.20	4.60	-5.63	-1.92
	Precision (%CV)	8.68	6.70	5.11	3.04
GDCA	Accuracy (%bias)	7.40	4.60	-7.27	-2.10
	Precision (%CV)	12.62	7.74	4.36	3.85
TDCA	Accuracy (%bias)	0.20	-4.13	-5.40	-3.22
	Precision (%CV)	13.07	8.44	5.07	3.24
Tα-MCA	Accuracy (%bias)	-2.11	-1.36	-8.77	-5.88
	Precision (%CV)	14.23	8.12	4.84	3.63
Tβ-MCA	Accuracy (%bias)	4.00	-3.37	-8.66	-4.20
	Precision (%CV)	11.62	10.48	4.72	3.35

LLOQ: Lower Limit of Quantification, LQC: Lower Quality Control, MQC: Middle Quality Control, HQC: Higher Quality Control

Table 4.3b Intra-day accuracy and precision studies of the developed method

Analyte		LLOQ (1 ng/mL)	LQC (3 ng/mL)	MQC (500 ng/mL)	HQC (840 ng/mL)
	Intra-day accuracy and precision studies (n=12)				
CA	Accuracy (%bias)	1.40	6.30	-6.49	-3.25
	Precision (%CV)	10.42	10.16	5.73	4.60
CDCA	Accuracy (%bias)	1.20	-5.21	-7.88	-5.47
	Precision (%CV)	12.47	8.43	6.93	4.18
DCA	Accuracy (%bias)	5.20	7.10	-5.87	-5.07
	Precision (%CV)	11.60	9.32	4.69	6.56
GDCA	Accuracy (%bias)	13.5	8.60	-7.22	-3.29
	Precision (%CV)	5.69	4.53	6.56	5.70
TDCA	Accuracy (%bias)	-5.45	-5.58	-5.79	-4.29
	Precision (%CV)	12.25	6.94	5.28	3.14
Tα-MCA	Accuracy (%bias)	-0.91	-3.05	-7.02	-4.13
	Precision (%CV)	11.30	6.48	5.52	4.10
Tβ-MCA	Accuracy (%bias)	6.50	-1.83	-8.29	-4.33
	Precision (%CV)	10.68	7.48	5.59	3.89

LLOQ: Lower Limit of Quantification, LQC: Lower Quality Control, MQC: Middle Quality Control, HQC: Higher Quality Control

Table 4.4 Extraction recoveries of bile acids and their respective internal standards in the developed method (n = 6)

Analytes		%Recovery							
		Analyte at QC Levels			IS used	IS (100 ng/mL)	IS Normalized		
		LQC	MQC	HQC			LQC	MQC	HQC
CA	Mean (%)	81.72	76.40	79.37	d_4-CA	91.78	89.03	93.24	86.47
	%CV	12.08	3.74	11.47		2.50	12.08	3.74	11.47
CDCA	Mean (%)	87.22	79.84	80.45	d_4-DCA	81.22	107.38	98.30	99.05
	%CV	13.25	5.16	10.36			13.25	5.16	10.36
DCA	Mean (%)	74.14	80.60	86.98		3.21	91.28	99.23	107.09
	%CV	6.38	6.37	12.17			6.38	6.37	12.17
GDCA	Mean (%)	76.61	75.29	78.78	d_4-GDCA	88.33	86.73	85.23	89.18
	%CV	11.64	3.74	11.58		2.06	11.64	3.74	11.58
TDCA	Mean (%)	76.61	84.74	87.09	d_4-TDCA	86.14	88.93	98.37	101.10
	%CV	10.49	3.28	9.92		3.44	10.49	3.28	9.92
Tα-MCA	Mean (%)	79.08	80.06	87.86	d_4-TCA	92.98	85.05	86.10	94.49
	%CV	10.05	11.74	11.22			10.05	11.74	11.22
Tβ-MCA	Mean (%)	76.61	83.49	87.71		4.72	82.39	89.79	94.51
	%CV	11.76	4.87	11.45			11.76	4.87	11.45

Table 4.5 Accuracy and precision of LQC and HQC to study the matrix effect of bile acids and internal standards (n = 6)

Analytes		Mean value		IS (100 ng/mL)		Mean value
		LQC	HQC			
CA	Accuracy (%bias)	9.43	12.66	d_4-CA	Accuracy (%bias)	-10.34
	Precision (%CV)	4.10	3.05		Precision (%CV)	6.74
CDCA	Accuracy (%bias)	9.41	8.60	d_4-DCA	Accuracy (%bias)	-13.55
	Precision (%CV)	9.88	4.87		Precision (%CV)	11.81
DCA	Accuracy (%bias)	12.77	-12.85			
	Precision (%CV)	10.14	4.31			
GDCA	Accuracy (%bias)	13.05	12.09	d_4-GDCA	Accuracy (%bias)	-4.42
	Precision (%CV)	10.59	3.08		Precision (%CV)	7.51
TDCA	Accuracy (%bias)	12.37	13.86	d_4-TDCA	Accuracy (%bias)	-8.18
	Precision (%CV)	7.74	3.61		Precision (%CV)	9.36
Tα-MCA	Accuracy (%bias)	7.60	10.76	d_4-TCA	Accuracy (%bias)	-11.36
	Precision (%CV)	6.80	7.42		Precision (%CV)	11.70
Tβ-MCA	Accuracy (%bias)	6.25	12.65			
	Precision (%CV)	11.91	3.97			

Table 4.6 % Deviation of stability samples of bile acids under different stress conditions (n = 6)

Analytes		ASS		BTS		FTS		LTS at -20 °C		LTS at -80 °C	
		LQC	HQC	LQC	HQC	LQC	HQC	LQC	HQC	LQC	HQC
CA	%Deviation*	1.60	3.70	-5.26	1.80	0.93	2.21	-7.73	3.10	-1.87	0.30
	%CV	7.87	2.05	11.05	2.46	14.57	1.28	5.74	1.50	12.99	6.06
CDCA	%Deviation	10.50	-13.96	7.60	-14.00	-14.28	-12.42	-13.18	-13.88	-12.02	-14.02
	%CV	4.97	0.79	6.83	0.88	0.56	1.97	1.25	0.65	7.05	2.44
DCA	%Deviation	8.30	6.20	12.80	3.50	12.70	3.30	3.10	5.70	3.20	1.70
	%CV	2.92	3.43	1.33	2.86	0.91	1.23	0.91	3.03	3.91	4.38
GDCA	%Deviation	11.40	2.30	9.90	0.40	10.60	-0.40	13.40	2.53	13.00	-1.73
	%CV	1.80	2.77	3.91	2.69	2.35	2.63	6.52	1.02	1.45	7.34
TDCA	%Deviation	7.60	5.20	8.50	3.50	11.20	3.20	9.40	3.70	10.87	2.90
	%CV	4.38	2.06	5.63	2.27	2.89	0.92	3.17	2.08	6.98	4.45
Tα-MCA	%Deviation	10.90	6.20	12.70	3.10	12.60	4.00	9.00	5.20	13.40	3.20
	%CV	3.30	2.39	1.34	3.26	4.31	1.44	11.06	2.93	2.03	5.51
Tβ-MCA	%Deviation	8.80	5.70	3.20	2.60	9.70	3.70	8.10	5.30	5.80	2.80
	%CV	4.66	2.15	8.18	3.40	3.60	1.99	5.66	2.80	5.85	4.92

%Deviation* = [(Observed concentration at time t – Nominal concentration at time 0) / Nominal concentration at time 0] ×100
(ASS-autosampler stability; BTS-bench top stability; FTS- freeze thaw stability; LTS-long term stability)

Table 4.7 Stability of primary stock and working standard solutions of the bile acids and working standard solutions of internal standards (n = 6)

Analytes		SSS		WSS		IS		WSS of IS
		LQC	HQC	LQC	HQC			
CA	%Deviation*	6.92	1.58	1.42	2.06	d_4-CA	%Deviation	-3.68
	%CV	8.41	4.36	2.17	3.19		%CV	2.67
CDCA	%Deviation	3.89	1.71	6.67	1.07	d_4-DCA	%Deviation	-3.06
	%CV	13.52	5.32	13.83	6.32		%CV	4.13
DCA	%Deviation	2.45	-0.22	-7.21	0.73			
	%CV	13.38	5.18	8.08	3.14			
GDCA	%Deviation	-11.46	0.83	-3.56	1.90	d_4-GDCA	%Deviation	-1.72
	%CV	4.43	4.06	8.24	5.75		%CV	3.58
TDCA	%Deviation	2.56	0.42	0.09	1.40	d_4-TDCA	%Deviation	-2.98
	%CV	3.87	5.19	4.69	6.38		%CV	2.06
Tα-MCA	%Deviation	-5.69	1.24	-5.16	3.10	d_4-TCA	%Deviation	-0.90
	%CV	14.89	5.75	5.87	3.26		%CV	3.04
Tβ-MCA	%Deviation	8.80	5.70	3.20	2.60			
	%CV	4.66	2.15	8.18	3.40			

%Deviation* = [(Observed concentration at time t – Nominal concentration at time 0) / Nominal concentration at time 0] ×100
(SSS-stock solution stability; WSS-working solution stability; IS-internal standard)

Table 4.8 Accuracy and precision of reinjection reproducibility of quality control samples of bile acids (n = 6)

Analyte		LQC (3 ng/mL)	MQC (500 ng/mL)	HQC (840 ng/mL)
CA	Accuracy (%bias)	4.59	-1.22	1.47
	Precision (%CV)	6.12	4.75	5.12
CDCA	Accuracy (%bias)	2.51	-1.84	0.35
	Precision (%CV)	8.50	5.50	1.21
DCA	Accuracy (%bias)	5.39	-4.70	-0.04
	Precision (%CV)	7.31	5.69	0.94
GDCA	Accuracy (%bias)	0.67	-3.64	1.66
	Precision (%CV)	2.88	1.76	4.26
TDCA	Accuracy (%bias)	-1.49	-1.68	-0.33
	Precision (%CV)	4.67	4.12	1.02
Tα-MCA	Accuracy (%bias)	0.42	0.87	-0.12
	Precision (%CV)	1.88	4.88	0.88
Tβ-MCA	Accuracy (%bias)	5.97	-1.79	-0.09
	Precision (%CV)	6.83	7.66	0.96

Table 4.9 Accuracy and precision of dilution integrity samples of bile acids (n = 6)

Analytes		5-folds dilution of 2000 ng/mL	20-folds dilution of 2000 ng/mL
CA	Accuracy (%bias)	-12.51	-11.15
	Precision (%CV)	1.61	2.46
CDCA	Accuracy (%bias)	-12.92	-13.65
	Precision (%CV)	1.62	1.11
DCA	Accuracy (%bias)	-11.67	-11.08
	Precision (%CV)	2.17	1.05
GDCA	Accuracy (%bias)	-9.87	-10.60
	Precision (%CV)	2.52	3.83
TDCA	Accuracy (%bias)	-9.96	-10.01
	Precision (%CV)	1.23	1.46
Tα-MCA	Accuracy (%bias)	-11.94	-11.08
	Precision (%CV)	2.15	2.65
Tβ-MCA	Accuracy (%bias)	-10.61	-10.21
	Precision (%CV)	3.73	3.72

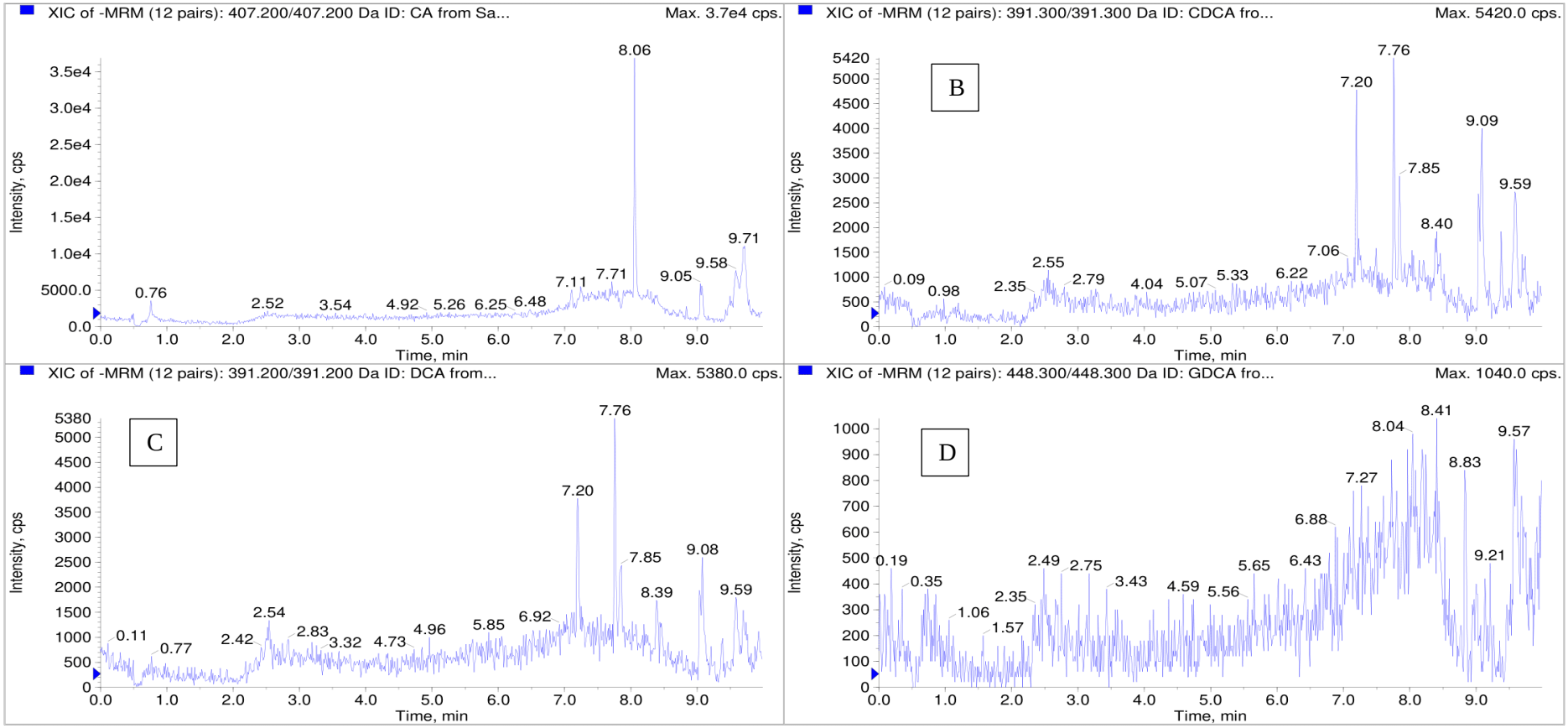

Figure 4.1a Chromatogram of charcoal stripped rat blank plasma representing respective pseudo-MRM transitions of: (A) Cholic acid (407.20/407.20), (B) Chenodeoxycholic acid (391.20/391.20), (C) Deoxycholic acid (391.3/391.3), (D) Glycodeoxycholic acid (448.30/448.30).

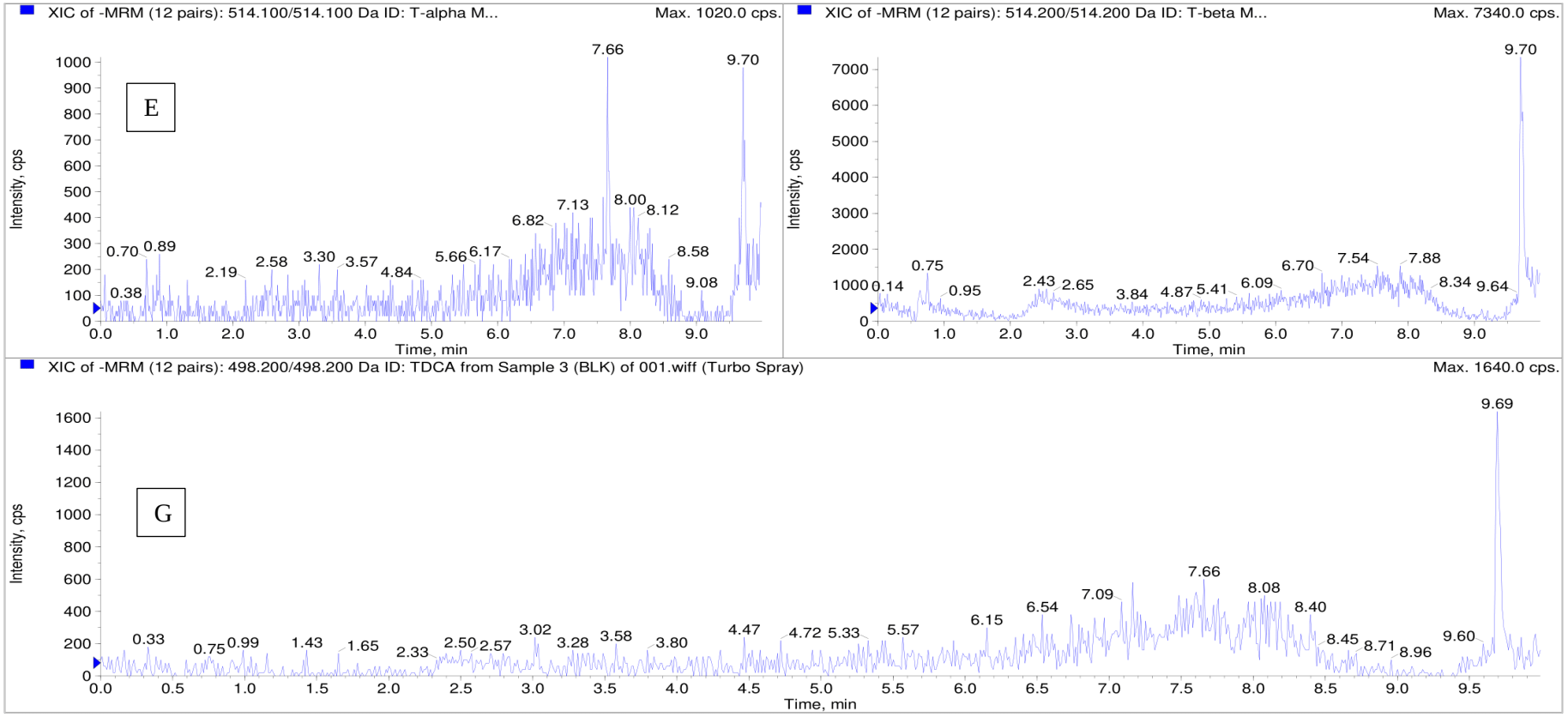

Figure 4.1b Chromatogram of charcoal stripped rat blank plasma representing respective pseudo-MRM transitions of: E-Taurodeoxycholic acid (498.20/498.20), F-Tauro-α-muricholic acid (514.10/514.10), G-Tauro-β-muricholic acid (514.20/514.20).

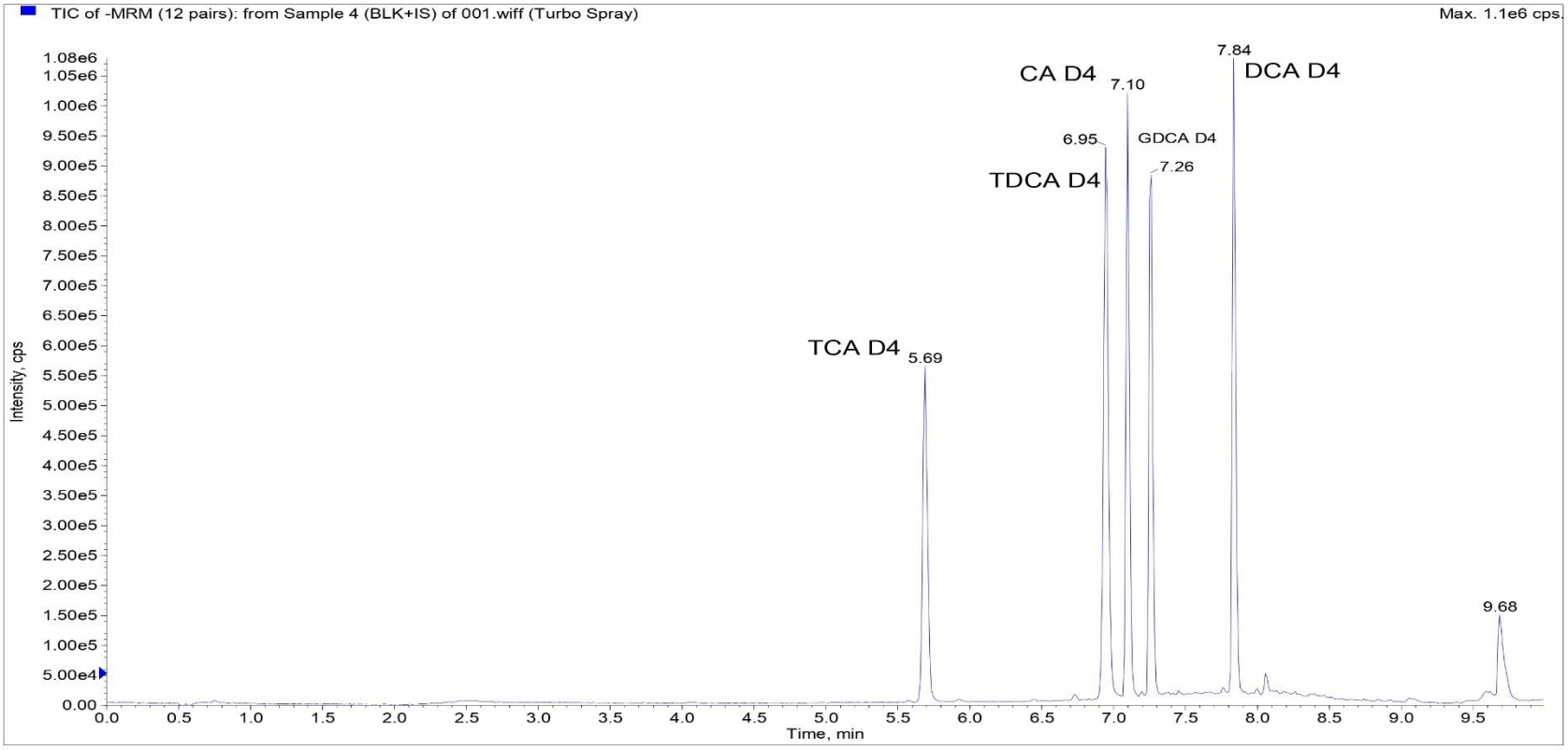

Figure 4.2 Chromatogram of deuterated bile acid internal standards spiked in stripped blank plasma.

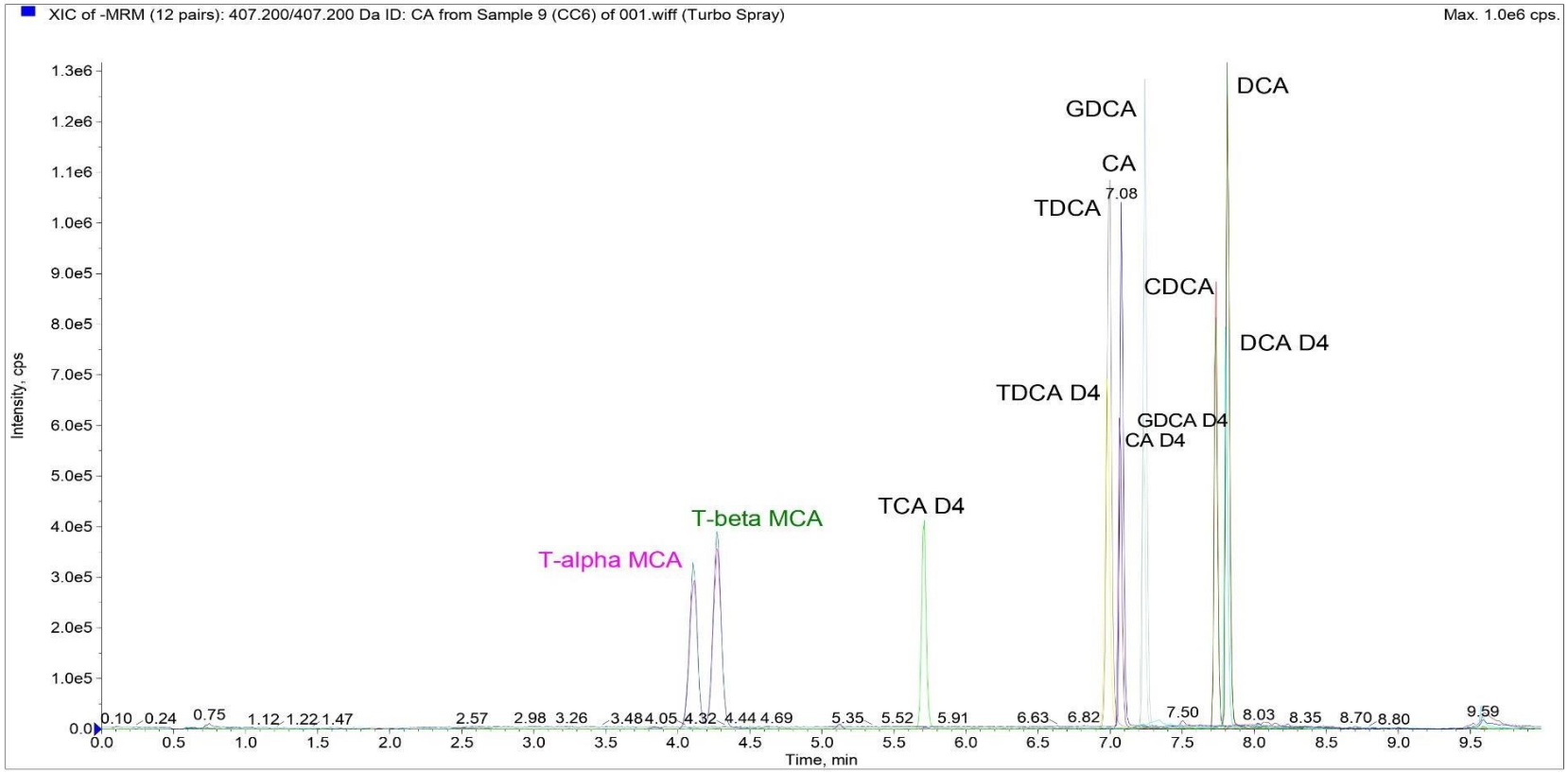

Figure 4.3 Chromatogram of seven bile acids (500 ng/mL) and internal standards (100 ng/mL) in stripped plasma.

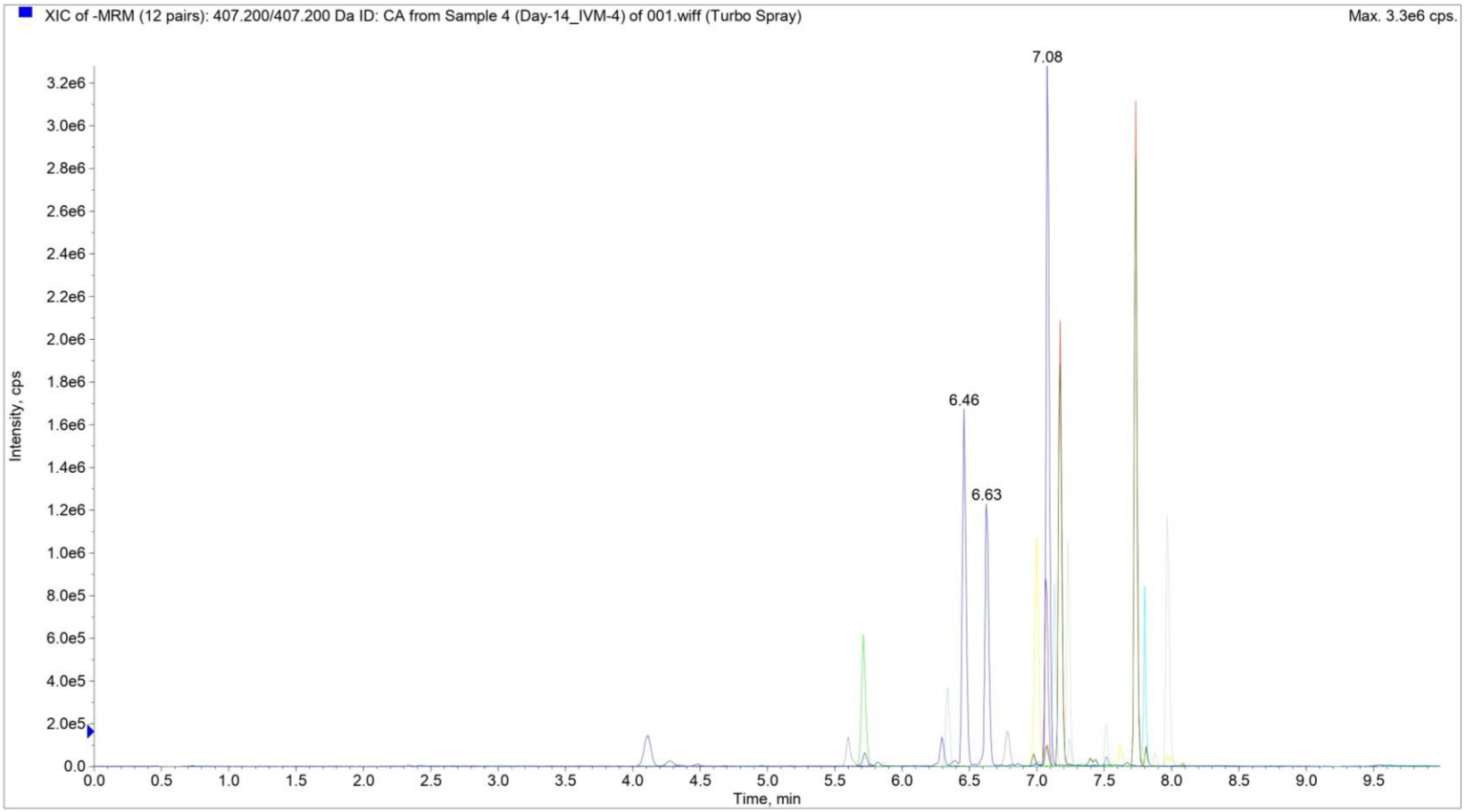

Figure 4.4 Chromatogram of all endogenous bile acids corresponding the MRM transitions of the method in rat plasma.

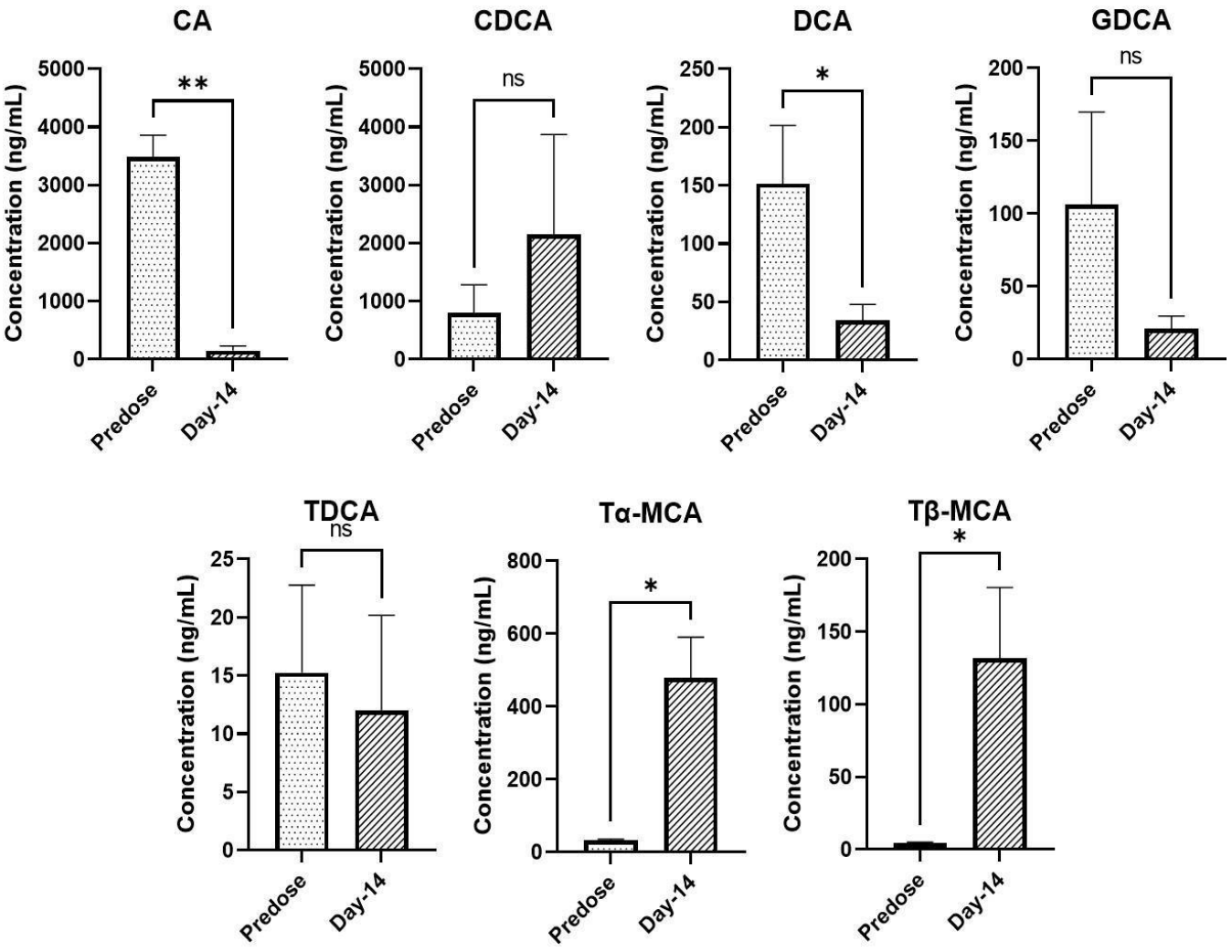

Figure 4.5 Plasma concentrations of seven bile acids before and after multidose oral treatment of IVM (5 mg/kg once a day for 14-days; n=6) (ns=not significant (P>0.05), *=significant (0.01<P<0.05), **=very significant (0.001<P<0.01).

4.9 Discussion

The LC-MS/MS based methods, reported in the literature, for detection, separation and quantification of bile acids in the recent years lack validated method for this specific set of human and murine specific major bile acids provoked us to develop and validate a simultaneous LC-MS/MS method which can be advantageous to the research community for studying metabolic disease mechanisms in relation to bile acid accumulation or in regulation of bile acids homeostasis. Development and validation of LC-MS/MS method for simultaneous estimation of bile acids is challenging due to structural similarities and presence of isobaric bile acids. The cross talk between the isobaric bile acids is a major challenge in their absolute quantification.

Several method development trials were conducted to achieve separation and intensity for the bile acids. 10 mM ammonium acetate and 10 mM ammonium formate (both with and without 0.1% formic acid) as mobile phase A (aqueous phase) and methanol or acetonitrile as mobile phase B (organic phase) were tried initially using Kinetex C18 column (2.6 µm, 100×3 mm). Different gradient programmes starting with 15% organic mobile phase to 100% with different runtimes ranging 5-25 min were tried. The isobaric pairs of Tα-MCA/Tβ-MCA and CDCA/DCA were found to be either merged or partially resolved. Changing the buffer concentration and incorporation of additives like formic acid and acetic acid in the aqueous phase did not result in the separation of these isobaric pairs. Further, increased sensitivity was observed with reducing the buffer concentration. 10 mM ammonium hydrogen carbonate with methanol/acetonitrile as mobile phase using Agilent InfinityLab Poroshell 120 SB-C18 column (2.6 µm, 100 × 3 mm) with 16 min of runtime resulted in separation of CDCA and DCA pair but Tα-MCA and Tβ-MCA were observed as a split peak. In another attempt, 2 mM ammonium carbonate with 0.012% v/v formic acid and methanol as mobile phases using Ascentis® Express

C18 column (2.7 µm, 150×2.1 mm) with different gradient methods were tried. Tα-MCA, Tβ-MCA and CDCA, DCA were separated but an M-shape like peak was observed for Tα-MCA and Tβ-MCA with 25 min run time. Finally, an aqueous mobile phase of 0.1% formic acid in water and an organic mobile phase of acetonitrile, Acquity UPLC® HSS T3 column (1.8 µm, 100×2.1 mm) and the optimized gradient method resulted the current method.

In the current method, charcoal stripped plasma was used instead of normal plasma to avoid the interference of endogenous bile acids. Further, the use of stable isotopic labelled internal standards enhances the reliability of the method for accurate and precise quantification of analytes. The developed method offers the advantage of uniform calibration curve range (1-1000 ng/mL) having same calibration points for all the seven bile acids. In addition, the developed method employs a simple, cost and time saving approach of protein precipitation for the sample preparation instead of solid phase extraction or liquid-liquid extraction methods. The method offers higher sensitivity with the LLOQ values of 1 ng/mL with baseline separation of isobaric bile acids with short run time of 10 min without any equilibration of column between the runs. Due to the high sensitivity of the developed method even with a small injection volume of 2 µL, the current method would avoid unnecessary deposition of the sample in the mass analyzer which improves the life of the instrument. The developed method was validated for all the parameters as per the regulatory guidelines which was found missing in many of the reported methods.

The synthesis of bile acids in humans and murine happen via two pathways, the classical pathway and alternative pathway. Classical pathway produces two major bile acids, CA and CDCA, while alternative pathway produces only CDCA. In murine, CDCA is further converted into α-MCA and β-MCA, which upon conjugation with taurine produces Tα-MCA and Tβ-MCA as the major bile acids. CA and CDCA are conjugated to glycine or taurine in hepatocytes

by BACS/BAAT enzymes while deconjugation occurs in the intestine by gut microbiota and are further dehydroxylated to DCA and LCA, respectively, as secondary bile acids. These secondary bile acids are passively absorbed from colon and returned to liver where they are conjugated with taurine/glycine. GDCA and TDCA enter enterohepatic circulation while LCA further undergo sulfation at C-3 position and in contrast to other bile acids, the sulphated taurine/glycine conjugated LCA is not efficiently absorbed from the intestine and promptly eliminated from the body. Therefore, it accounts for only less than 5% of the total bile acid pool while CA, CDCA and DCA represent the major biliary bile acid composition. Meanwhile, CDCA, DCA and CA are the natural FXR agonists with order of potency of CDCA>DCA>CA, whereas Tα-MCA and Tβ-MCA were identified as natural FXR antagonists [193, 194]. Therefore, we have developed a LC-MS/MS method for quantification of seven major human and murine specific bile acids, namely, CA, CDCA, DCA, GDCA, TDCA, Tα-MCA and Tβ-MCA and studied the effect of multi-dose administration of IVM, a highly selective FXR ligand, on the haemostasis of the above seven bile acids.

Multi-dose administration of IVM reduced the plasma concentration of CA and DCA while it increased the plasma concentrations of Tα-MCA and Tβ-MCA. Based on the FXR negative feedback mechanism [195, 196], we assume that IVM, could be acting as an FXR agonist, inhibiting CYP7A1 enzyme (rate limiting enzyme in classical bile acid synthesis) and thereby reducing CA synthesis in the classical pathway. As DCA is the secondary metabolite derived from CA, the levels of DCA were also reduced in line with the CA levels. Multi-dose administration of IVM did not cause a significant change in the concentration of CDCA. This could be possibly be due to the balancing out effect of IVM on two different pathways. On one hand IVM may be acting as FXR agonist which causes the inhibition of CYP7A1/CYP8B1 enzyme (and thereby the classical pathway) and reduction in the synthesis of CDCA while on the other hand IVM may be activating the CYP27A1/CYP7B1 enzymes involved in the

synthesis of CDCA by alternative pathway. The increase in concentrations of Tα-MCA and Tβ-MCA could be due to the possible activation of CYP2C70 enzyme which is responsible for the conversion of CDCA (produced from either classical or alternative pathway) into α/β-MCA and the eventual formation of their taurine conjugates. The above results indicate that IVM has an opposite effect on classical and alternative bile acid synthesis pathways by inhibition and activation, respectively, and result in significant changes in the bile acid haemostasis. However, further studies are required to elucidate the exact mechanism involved in inhibition of the classical pathway and activation of the alternative pathway of bile acids synthesis by IVM.

4.10 Conclusion

A simple, sensitive, reliable and reproducible LC-MS/MS method was developed and validated for the quantitative analysis of seven important bile acids in charcoal stripped rat plasma. The developed method had a uniform calibration curve range of 1-1000 ng/mL for all the bile acids. The isobaric bile acids pairs of Tα-MCA/Tβ-MCA and CDCA/DCA were well resolved for their accurate and precise quantification. The method was successfully applied to study the effect of multi-dose administration of IVM on the plasma concentration of the seven bile acids. The results obtained suggest that IVM significantly affect the plasma concentration of the seven major bile acids by acting both on the classical pathway and alternate pathway of bile acid synthesis. Further, this study provides useful insights regarding the FXR modulation in relation to bile acid homeostasis in rats upon treatment with IVM. The described LC-MS/MS method can be further employed in the future preclinical studies to discover the detailed mechanisms of IVM or any other molecule of interest on bile acid homeostasis in rats.

5

Drug-endobiotic interaction effect of UGT enzymes inhibition on systemic bile acids in rat model

5.1 Introduction

Drug metabolizing enzymes and drug transporters are known to be the key players in the metabolism and excretion of xenobiotics. These enzymes and transporters also play an important role in the metabolism and transportation of endobiotics and maintain their homeostasis in the body [197-199]. In particular, some of the drug metabolizing enzymes and drug transporters are specifically involved in the synthesis, metabolism and transportation of endogenous bile acids [81]. Xenobiotic receptors, such as Pregnane X receptor (PXR), constitutive androstane receptor (CAR), and aryl hydrocarbon receptor (AHR), regulate the expression of drug metabolizing enzymes and drug transporters. Modulation (either activation or inhibition) of the xenobiotic receptors can affect the gene expression of drug metabolizing enzymes and drug transporters which can in turn affect the pharmacokinetic properties of xenobiotics and endobiotics that are substrates for such enzymes/transporters. The xenobiotic receptors are modulated by a variety of endogenous, exogenous ligands and environmental chemicals [200].

Uridine 5′-diphospho-glucuronosyltransferases (UGTs) are a class of phase-II metabolising enzymes that catalyse the transfer of glucuronic acid from uridine 5′-diphospho-glucuronic acid to the substrates. UGTs are responsible for the elimination of majority of xenobiotics and endobiotics by the glucuronidation pathway. The endobiotics glucuronidated by different UGTs include catecholamines such as serotonin, dopamine; steroidal hormones like estradiol, progesterone, testosterone, androsterone, aldosterone, estrone, estriol; corticosteroids like cortisol; retinoids and bile acids [93, 201-203]. The modulation of UGTs (either inhibition or induction of the UGTs) by any drug can significantly affect the haemostasis of endobiotics which are eliminated by glucuronidation pathways. This can potentially lead to drug-endobiotic pharmacokinetic or pharmacodynamic interactions. Some of these interactions can be detrimental to the safety of the patient receiving the drug. A classic example of this type of

drug-endobiotic interaction is between atazanavir and bilirubin. In this case, atazanavir inhibits UGT1A1, an enzyme responsible for the glucuronidation of bilirubin, thereby increasing the concentration of unconjugated bilirubin in the blood and eventually leading to hyperbilirubinemia in patients receiving atazanavir [204]. A second example is of the interaction between phenytoin and thyroxine. Thyroxine is an important hormone that plays a vital role in the brain development. It is metabolized by glucuronidation reaction by UGT1A1 isoform along with UGT1A3, 1A8 and 1A10. Phenytoin is an anticonvulsant drug used in the management and treatment of generalized tonic-clonic seizures, complex partial seizures, and status epilepticus. Phenytoin is reported to cause induction of UGT1A1 enzymes. It was reported that administration of phenytoin in children suffering from seizures/epilepsy showed increased risk of developing neurotoxicity due to the decreased levels of thyroxine. This is due to the rapid metabolism of thyroxine by the UGT1A1 enzymes, induced by phenytoin, causing a significant decrease in thyroxine levels and thereby neurotoxicity [205, 206]. Therefore, the inhibition or induction of UGTs can accordingly result in decrease or increase in the plasma concentration of endobiotics which are metabolised by the UGTs. However, the impact of change in the plasma concentration of an endobiotic due to the modulation of UGTs (involved in the metabolism of the endobiotic) is dependent on the physiological role played that endobiotic. Hence, a case-by-case analysis should be done to understand and evaluate such drug-endobiotic interactions. Prior to the clinical evaluation of drug-endobiotic interactions, preclinical assessment in laboratory animals can provide critical decisive information on such interactions.

Though glucuronidation of bile acids is one of the major pathways for the clearance of unconjugated bile acids, more importantly mediated by UGT1A3 isoform in the intestine and liver, the effect of inhibition of UGT on the clearance of bile acids is not yet studied [12, 81, 207]. Since, bile acids regulate their own metabolism and transport and also maintain metabolic

homeostasis via binding to certain nuclear receptors, disruption of bile acids homeostasis can contribute to a wide range of gastrointestinal and liver diseases such as cholestasis, non-alcoholic fatty liver disease (NAFLD), hepatocellular carcinoma, irritable bowel syndrome etc [208, 209]. Interestingly, the current use of bile acids (CDCA and UDCA) as therapeutic agents in the management of liver diseases further rises the importance of their functional role in the pathophysiological and disease modifying roles [210].

In order to contribute to this field of research, we aimed to investigate the hitherto unexplored effect of inhibition of UGT-mediated clearance pathway of bile acids on the homeostasis of bile acids in rat model. In the Chapter 3, we evaluated zafirlukast as a common UGT inhibitor and confirmed its inhibitory potential in rats by studying the change in disposition of ezetimibe, a UGT1A1 and UGT1A3 substrate. In the current chapter, we studied the effect of zafirlukast, a common UGT inhibitor of UGT1A1 and UGT1A3 enzymes, on the plasma levels of bile acids and bilirubin in rats within the context of understanding the drug-endobiotic interactions.

5.2 Materials

Zafirlukast, cholic acid (CA) and chenodeoxycholic acid (CDCA) were purchased from TCI Chemicals (India) Private Limited, Hyderabad, India. Deoxycholic acid (DCA), glycodeoxycholic acid (GDCA), taurodeoxycholic acid (TDCA) and dimethyl sulfoxide (DMSO) were purchased from Sigma Aldrich (Merck) Chemicals Private Limited, Bangalore, India. Tauro-α-muricholic acid (Tα-MCA), tauro-β-muricholic acid (Tβ-MCA), cholic acid-d4, deoxycholic acid-d4, glycodeoxycholic acid-d4, taurodeoxycholic acid-d4, taurocholic acid-d4 were purchased from Cayman Chemical Company, MI, USA. Polysorbate 80 and dipotassium ethylenediamine tetraacetate (K_2EDTA) were purchased from Sisco Research Laboratories Private Limited, Hyderabad, India. LC-MS grade methanol, acetonitrile, water and formic acid were purchased from Biosolve India Limited, Hyderabad, India. Male Sprague-

Dawley (SD) rats and rat pooled plasma were procured from Hylasco Biotechnology Private Limited, Hyderabad, India.

5.3 *In vivo* experiments

The effect of UGT inhibition by zafirlukast on the plasma levels of bile acids was assessed in male SD rats. Prior approval for the *in vivo* study protocol was obtained from institutional animal ethics committee (IAEC) of BITS Pilani-Hyderabad (Approval number: BITS-IAEC-2023-17) and in accordance with CCSEA, India. Male SD rats (7-8 weeks of age) weighing between 200-250 g were procured and immediately quarantined for 7 days in our institute animal house facility under standard laboratory conditions. The rats were housed in standard polypropylene cages (3 rats per cage), with stainless top grill having facilities for pelleted food and drinking water ad libitum. The temperature and relative humidity were maintained at 22±1 °C and 50±10%, respectively, with approximately 12 h light and 12 h dark cycle in the animal house facility. Rats were kept for fasting for at least 8 h before the administration of treatments used in the study.

5.3.1 Study design

In the *in vivo* study, an aqueous solution of zafirlukast (0.2% w/v) was administered through oral route in six rats (n=6). Aqueous solution of zafirlukast (0.2% w/v) was freshly prepared by dissolving the drug in a solvent mixture consisting of 2% DMSO, 2% polysorbate 80 and 96% purified water. The drug (zafirlukast) was administered at a dose of 10 mg/kg and a dosing volume of 5 mL/kg in each of the rats using oral gavage. The oral dose of zafirlukast required to achieve an average concentration at steady state ($\bar{C_{ss}}$) equivalent to the IC_{50} (from the enzyme inhibition studies) was determined using the following equation (Eq. 1).

$$X_o = \frac{\bar{C_{ss}} \times Cl_s \times \tau}{F} \qquad \text{Eq. 1.}$$

Where, 'X_o' is the dose of zafirlukast administered through oral route at dosing interval of 'τ' (where, τ = 24 h); '$\bar{C_s}_s$' is the average concentration at steady state achieved by administering the drug every 24 h (where '$\bar{C_s}_s$' is set equivalent to the IC_{50} value of zafirlukast); 'Cl_s' is the systemic clearance of the drug in rat (extrapolated by allometric scaling from human systemic clearance value) and the oral bioavailability 'F' (reported to be 50%) of the drug.

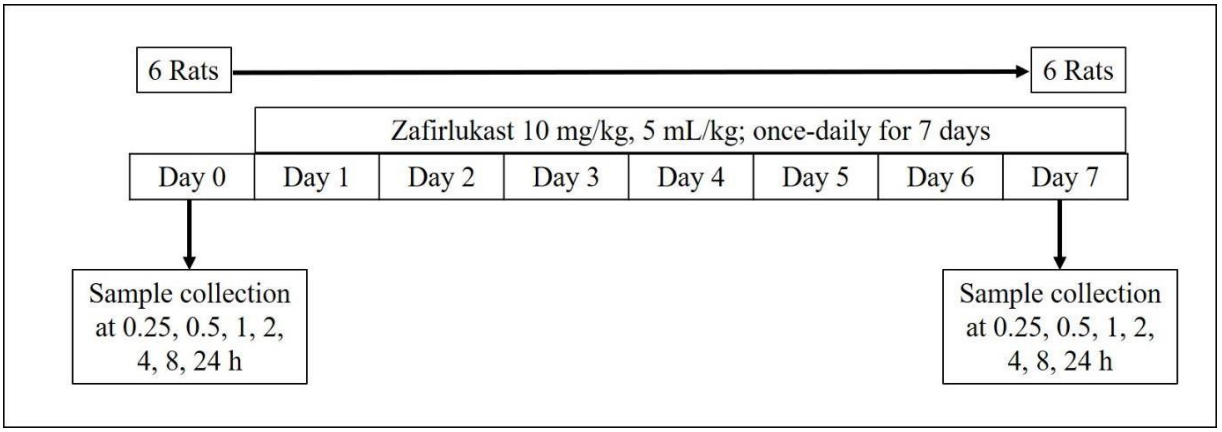

Figure 5.1 *In vivo* study design for zafirlukast dosing in male SD rats.

The *in vivo* study plan is shown in Figure 5.1. Following the administration of the aqueous solution of zafirlukast in the rats, blood samples were collected by retro orbital plexus method under slight isoflurane anesthesia at 0.25, 0.5, 1, 2, 4, 8, 24 h on day-0 (before administering the 1st dose) and at 0.25, 0.5, 1, 2, 4, 8, 24 h on day-7 (after administering the 7th dose) from each animal into centrifuge tubes containing an anticoagulant (200 mM K_2EDTA at 2% v/v concentration in blood) The centrifuge tubes containing the blood samples were immediately kept on ice bath until further processing. Plasma was harvested by centrifuging the blood samples at 10,000 rpm for 10 min at 4 °C. The supernatant plasma was collected, labelled and stored at -80 °C until UHPLC-MS/MS analysis.

5.4 Bioanalysis

An ultra-performance liquid chromatography (Nexera 40D-XS, Shimadzu Corporation, Kyoto, Japan) coupled with tandem mass spectrometry (UHPLC-MS/MS) (SCIEX QTRAP® 4500, Sciex, MA, USA) was used for the quantification of bile acids in the plasma samples. Protein precipitation method was used to extract plasma bile acids. Calibration curve was constructed in the range of 1 - 1000 ng/mL and linearity of the method was assessed by performing the least-square regression analysis of observed concentrations versus the nominal concentration of the analyte for the calibration curve samples with $1/x^2$ weighting factor. The complete details of the sample preparation (Section 4.2), method development (Section 4.3), chromatographic and mass spectrometric conditions (Section 4.4) and method validation (Section 4.5) with the results (Section 4.8) are discussed in Chapter 4. The above validated UHPLC-MS/MS method was employed to quantify each of the bile acids in plasma samples collected in the *in vivo* study. The bilirubin levels were measured by collecting the blood samples at 0.5 h on day-0 and 0.5 h on day-7 of the study. The bilirubin content was measured in the serum samples using the biochemical analysis. Bilirubin glucuronide directly reacts with sulphodiazonium salt and forms coloured azobilirubin that is measured by semi-automatic Erba Chem 5X Biochemistry analyser (Erba Lachema, Czech Republic). Serum total and direct bilirubin was measured by using Erba®Mannheim kit (BLT00011) and the assay was performed as per the instructions provided by the manufacturer. The serum and assay reagents were mixed and incubated at 37 °C for 5 min and the absorbance was measured at 546 nm. Indirect bilirubin was calculated by subtracting direct bilirubin from total bilirubin and the results are presented in Table 5.1.

5.5 Pharmacokinetic analysis

Phoenix WinNonlin® software (Version 8.3) was used to calculate the pharmacokinetic parameters using non-compartmental model analysis. The area under the plasma concentration-time curve between time 't=0' to time 't=24 h' ($AUC_{0\text{-}24h}$) was calculated by the linear trapezoidal rule.

5.6 Statistical analysis

The $AUC_{0\text{-}24h}$ values of each bile acid obtained in the pharmacokinetic study were expressed as mean ± standard deviation of three independent determinations. The effect of zafirlukast on the plasma levels of the seven bile acids was assessed by comparing the mean $AUC_{0\text{-}24h}$ of plasma time course profile of each bile acid obtained before dosing and after dosing zafirlukast for seven days. A paired t-test, at 5% level of significance, was used to analyse the statistical difference in the '$AUC_{0\text{-}24h}$' of plasma time course profile of each bile acid before and after zafirlukast exposure. Statistical analysis was performed using GraphPad Prism software.

5.7 Results

A statistically significant reduction was observed in the plasma exposure (expressed in terms of $AUC_{0\text{-}24h}$) of CA, CDCA and DCA by 73.59% (P=0.023), 88.50% (P=0.026), 56.50% (P=0.044), respectively, in the day-7 samples compared to day-0 samples. Statistically no difference (P>0.05) was observed in the plasma exposure of GDCA, Tα-MCA and Tβ- in the day-7 samples compared to day-0 samples. Interestingly, the plasma exposure of TDCA increased significantly by 223.10% (P=0.040) after seven days' exposure with zafirlukast. The systemic levels of bilirubin were unaffected following the multi-dose administration of zafirlukast. Figure 5.2 illustrates the effect of multi-dose administration of zafirlukast on plasma exposure of the seven bile acids and bilirubin.

Table 5.1 Serum concentrations of bilirubin and area under curve of seven bile acids before and after 7-days oral dosing of zafirlukast in male SD rats (n=6)

Analyte	PK Parameter	Before zafirlukast exposure	After zafirlukast exposure
Bilirubin	$C_{0.5h}$ (mg/dL)	0.164±0.06	$0.194±0.10^{ns}$
CA	AUC_{0-24h} (ng×h/mL)	54221.27±8582.77	14316.56±6969.72*
CDCA		35353.47±13730.40	4062.42±1715.57*
DCA		3540.76±294.46	1540.10±804.22*
GDCA		1686.24±296.84	$975.32±659.48^{ns}$
TDCA		315.87±148.60	1020.58±303.46*
Tα-MCA		2122.88±652.58	$2662.69±663.37^{ns}$
Tβ-MCA		358.026±17.67	$541.63±162.91^{ns}$

$C_{0.5h}$ – Concentration of bilirubin in samples collected at 0.5 h on day-0 and day-7. AUC_{0-24h} – Area under the plasma time course profile of a bile acid (either for plasma samples collected on day-0 or day-7 of zafirlukast dosing). Data presented is mean ± standard deviation of three independent observations (n=3). ns – Statistically no significant difference between before and after treatment values (P>0.05); * – Statistically significant difference between before and after treatment values (0.01<P<0.05).

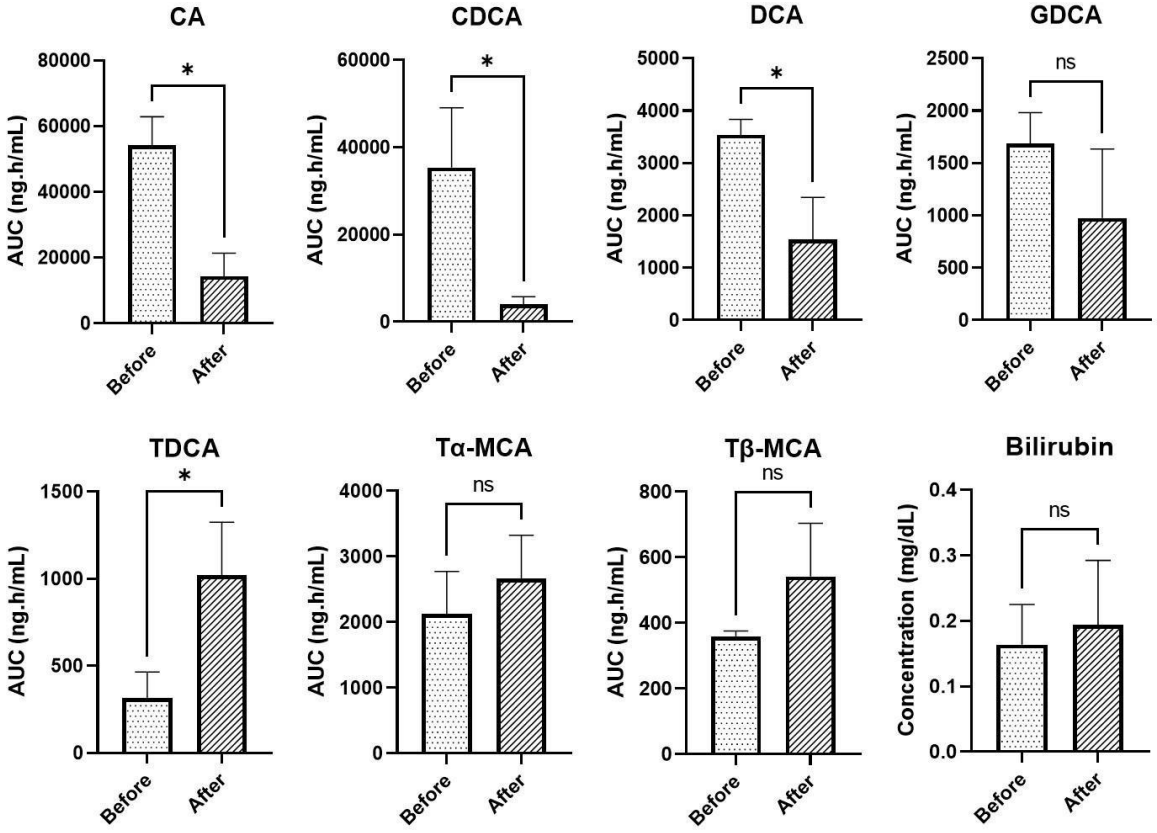

Figure 5.2 Area under the plasma concentration vs time curve of seven bile acids and serum bilirubin concentrations before and after 7-days exposure to zafirlukast in male SD rats (n=6). ns – Statistically no significant difference between before and after treatment values (P>0.05); * – Statistically significant difference between before and after treatment values (0.01<P<0.05).

5.8 Discussion

The UGT-mediated drug-endobiotic interactions are attracting more interest in the pharmaceutical industry due to their beneficial or detrimental roles in health and disease conditions [211]. Investigating such drug-endobiotic interactions help in unravelling key mechanisms in pathophysiology or to deepen the understanding of endobiotic response upon xenobiotic exposure [212]. Bile acids not only regulate their own metabolic fate but also determine the fate of other endogenous molecules which can lead to significant clinical outcomes [212]. As a result, either UGT inhibition or induction play crucial roles in the homeostasis of different endobiotics and their subsequent implications in disease modification. It is therefore essential to study the effects of xenobiotic drugs on these UGT mechanisms to ensure safety and non-specific pharmacological profiles of drugs.

Bile acids by binding to their nuclear receptors regulate lipid, glucose and energy homeostasis and involve in inflammation, cell proliferation and immunomodulatory effects. Moreover, gastrointestinal and hepatic diseases are intertwined with altered bile acid profiles [209, 213]. In spite of the clinical significance, effect of inhibition of UGT metabolism of bile acids was not yet studied. In the current research work, we studied the effect of a pan-UGT inhibitor (zafirlukast) on the plasma levels of seven bile acids following a multi-dose administration of the drug. In addition to the bile acids, bilirubin (endogenous UGT1A1 substrate) was also measured. In accordance with the theoretical principles, the concentration of a substrate should increase when its metabolic enzyme(s) are inhibited. This correlation was observed only with TDCA and complete opposite results were observed for CA, CDCA and DCA which is an interesting finding in this work. The reason for this could be the feed-forward mechanism for UGT enzymes that are involved in the glucuronidation of these selected bile acids (i.e. CA, CDCA and DCA). This assumption is further supported by the reported literature that

activation of FXR by both endogenous or exogenous agonists resulted in the induction of UGT1A3 enzyme [214]. UGT1A3 is primarily involved in the glucuronidation of bile acids such as CA, CDCA and DCA at carbon-24 position of carboxylic acid to form their respective acyl-glucuronides. Inhibition of UGT1A3 in the intestine and liver results in increase in the plasma concentration of CA, CDCA and DCA. These unconjugated bile acids are also reported to act as endogenous FXR agonists. Activation of FXR by these endogenous bile acids leads to the feedback mechanism for bile acid synthesis. Briefly, in the feedback mechanism, binding of bile acids to FXR leads to the release of FGF15 (in rat) [or FGF19 in human] in the intestine and enters the liver via portal circulation and inhibits CYP7A1 enzyme (a rate limiting enzyme in bile acid synthesis). In addition, activation of FXR in the liver results in the release of SHP which inhibits CYP7A1. This feedback mechanism inhibits the bile acid synthesis from cholesterol in the liver. Therefore, such a feedback mechanism may be responsible for the reduced bile acid levels after UGT1A3 inhibition by zafirlukast [12, 87].

Further there are literature reports which suggest that activation of FXR also leads to the induction of UGT1A enzymes. This can result in increased levels of UGT1A3 (which is part

of the UGT1A isozymes) which is involved in the metabolic clearance of CA, CDCA and DCA by glucuronidation conjugation and thereby decreasing their plasma levels. This could be a second possible reason for the overall decrease in the plasma levels of the above three unconjugated bile acids. This mechanism is called feedforward mechanism [215, 216].

Therefore, both bile acid-FXR mediated feedback mechanism (inhibition of bile acid synthesis) and feedforward mechanism (induction of UGT enzymes) may be responsible for the overall reduction in the plasma levels of CA, CDCA and DCA.

Selectivity or specificity of substrate towards any particular UGT isoform and the structural position at which glucuronidation occurs determine the substrate dependent metabolism. FXR

activation also induce the expression of UGT2B4 thereby reduces the toxic bile acid levels by increased clearance by glucuronidation metabolism [217]. In contrast, UGT2B7 expression was down regulated by lithocholic acid via FXR activation and UGT2B7 involves in the glucuronidation of bile acids at C3-hydroxy position [33, 218]. This might be one of the reasons for the increased levels of TDCA due to reduced expression of UGT2B4 and glucuronidation. This assumption is not warrant until identification specific glucuronidation of TDCA by UGT2B7. Meanwhile, GDCA also possess similar structure to that of TDCA having possibility for glucuronidation at C3-hydroxy position, but its levels were not increased. This may be due to shift towards taurine conjugation rather than glycine conjugation. This notion is supported by the findings of reported literature that FXR activation by bile acid agonists upregulated biosynthesis of taurine and its conjugation with bile acids [219]. Overall, the changes in the bile acids profiles after 7-days exposure to zafirlukast seems to be mediated by the involvement of FXR-mediated UGT expression and activity. Hence, FXR plays a major role in the regulation of bile acid homeostasis by either feedback or feedforward mechanisms.

Bilirubin is a well noted specific substrate for UGT1A1 isoform and its inhibition should lead to increased levels of bilirubin that result in hyperbilirubinemia in rats. Inhibition of UGT1A1 by zafirlukast could not alter the bilirubin levels. Similar results were also observed in the literature where multi-dose administration of zafirlukast at a dose of 80 mg/kg every 24 h for ten days in hepatic ischemia perfusion rat model did not alter the bilirubin levels [220]. Moreover, bilirubin was reported to regulate its own metabolism by induction of UGT1A1 expression [221]. FXR agonists like UDCA, obeticholic acid and GW4064 induce intestinal UGT1A1 by direct or indirect regulation [222]. In addition to FXR other nuclear receptors or nuclear factors like PXR, CAR, AhR, Nrf2, PPARα also regulate UGT1A1 transcription [223]. Direct binding of zafirlukast to these receptors or factors may also affect the expression of UGTs. Zafirlukast was found to inhibit UGT enzymes in a substrate specific manner, i.e., the

UGT inhibitory potential is dependent on the substrate being used in the reaction. This substrate specific inhibition was might be also a possible reason for the unaltered bilirubin levels after zafirlukast exposure in rats [129]. In addition, the time of zafirlukast exposure (7-days only) may not be sufficient to exert significant changes in the bilirubin levels in the rats. The inhibition or induction potential of xenobiotics on UGT1A1/UGT1A3 enzymes has to be evaluated at the preclinical stage to avoid drug-endobiotic interactions between drug molecules and bilirubin or bile acids. To our knowledge, this is the first study to examine the effect of UGT inhibition on systemic levels of bile acids in rats. Since UGTs are involved in glucuronidation of important endogenous molecules like thyroxine, oestrogen, androgens, bilirubin and bile acids, changes in their disposition due to altered metabolism by xenobiotics can cause clinically significant outcomes in the patients under their treatment. Preference should be given to such research at least for important disease modifying endobiotics homeostasis. This could preferentially predict or prevent adverse reactions mediated by drugs during clinical studies of drug development. Thus, appropriate labelling or dose adjustments can be done prior to marketing those drug products.

5.9 Conclusion

In conclusion, we examined the effect of UGT enzymes inhibition by zafirlukast (a pan-UGT inhibitor) on the systemic levels of bilirubin and seven selected bile acids in rat model. Once a day administration of zafirlukast for seven consecutive days, resulted in a significant change in the plasma concentration of some of the bile acids. The plasma levels of CA, CDCA, DCA reduced significantly while a significant increase was observed in the plasma levels of TDCA. However, the plasma levels of GDCA and Tα/β-MCA remained unaffected. Interestingly, the plasma levels of bilirubin were not affected even though zafirlukast is a potent UGT1A1 inhibitor. These results indicate that either inhibition or induction of UGTs by drug candidates

may potentially alter the disposition of bile acids which can result in outcomes with clinical significance. Therefore, it is important to evaluate such kind of drug-endobiotic interactions to the understand effect of drugs on metabolic fate and homeostasis of endogenous molecules.

6

Conclusions

Drug-drug interactions (DDIs) are the major challenges in drug disposition related toxic effects that are mediated either by drug metabolizing enzymes or drug transporters. Identification of such interactions at preclinical levels saves a potential drug candidate to be failed in the clinical trials or post-market withdrawals. Apart from the major metabolizing enzymes such as CYPs, uridine diphosphate glucuronosyl transferases (UGTs) came into lime light few decades ago and their contribution in drug metabolism is constantly increasing. Moreover, the importance of endogenous compounds that are being metabolized by UGTs increased the attention of UGT-mediated DDIs. Noteworthy point is that the research focus on the effect of drug candidates on the homeostasis of endogenous molecules became the thrust research area in the drug metabolism and pharmacokinetics (DMPK) in academia and pharmaceutical drug industry.

The research envisioned in the current thesis describes a systematic approach to identify UGT1A1 and UGT1A3 mediated DDIs arising from either substrate or inhibitor candidates. The *in vitro* methodology will be helpful in conducting high-throughput screening of isoform specific probe substrates or inhibitors in a simplified manner. Further the results obtained from this can be used to draw relative activity factors for each mentioned isoform which can be used during the *in vitro-in vivo* extrapolation and prediction of human clinical DDIs. The incorporation of both human recombinant, liver and intestinal microsomes, especially in a similar reaction condition, is advantageous in the characterization of substrates and inhibitors covering hepatic and extrahepatic first pass metabolism. β-estradiol and chenodeoxycholic acid (CDCA) were used as selective substrates for UGT1A1 and UGT1A3 enzyme kinetic studies, respectively. β-estradiol exhibited allosteric sigmoidal or cooperative binding kinetics while CDCA exhibited either Michaelis-Menten or substrate inhibition kinetics across the three enzyme systems used in the study. Due to the specific inhibition of UGT1A1 mediated glucuronidation of β-estradiol (confirmed from the results of intestinal metabolism), atazanavir

can be used to distinguish the substrate overlapping in liver or intestine even during clinical settings. Since most of the UGTs are homologous in nature, substrate overlapping is a common problem. A common-inhibitor like zafirlukast is more appropriate to account for UGT potential substrates.

The translation of *in vitro* results into *in vivo* scenario is not always a true case for all compounds due to the involvement of many factors involved in the in-life environment. Hence, it is important to characterize suitable UGT1A1 and UGT1A3 victim and perpetrator drugs in preclinical models. The evaluation of ezetimibe and zafirlukast as common substrate and inhibitor for both these UGT isoforms resulted in a reasonable strategy to study the *in vivo* DDI potential of new chemical entities in the drug discovery industry. The suitability of ezetimibe as substrate is supported in the literature by the extensive major metabolism by glucuronidation by these isoforms with almost similar reaction velocities at intestine and liver. Likewise, zafirlukast is a potent inhibitor of these isoforms in the hepatic and intestinal glucuronidation. This victim-perpetrator combination can be effectively employed in studying preclinical UGT1A1/1A3 mediated metabolic DDIs. However, co-administration of both the victim and perpetrator drugs is an important consideration to be followed in order to account for intestinal metabolism too, because effective inhibitor concentration is essential to inhibit glucuronidation of some compounds that are rapidly glucuronidated at the intestine. Nevertheless, the current *in vivo* method can be applied to screen prospective UGT1A1 and UGT1A3 substrates or inhibitors in a preclinical setting. Of note, about two-fold increase in the AUC of ezetimibe with zafirlukast co-administration was classified as moderate inhibition, the substrate specific inhibition, species differences and doses of either drugs may contribute to the overall results and hence *in silico* DDI simulations using compartmental or physiologically based pharmacokinetics (PBPK) models will be used to predict human clinical DDIs.

For most of the drug candidates or novel chemical entities the drug interaction potential is limited to few selected drugs that are concomitantly administered as polypharmacy for treating multiple ailments or for same disease targeting multiple pathways. But the interactions of these inhibitors with endogenous molecules is largely ignored. This leads to potential drug-endobiotic interactions that may cause clinically significant alterations in the homeostasis of crucial biomolecules such as bilirubin, thyroxine, androgens, oestrogens and bile acids which are majorly metabolized by glucuronidation by UGT1A1 and UGT1A3 enzymes.

To understand the effect of xenobiotics on endobiotic levels, an accurate and precise quantification methods are prerequisite and hence a UHPLC-MS/MS method for simultaneous estimation of seven major bile acids was developed and validated as per the FDA M10 bioanalytical method guidelines. The developed method was robust enough to measure cholic acid, deoxycholic acid, chenodeoxycholic acid, glyco- and tauro-deoxycholic acid and tauroα/β-murichолic acid in rat plasma. The method was validated for selectivity, specificity, carryover, matrix effect, recovery, stability, linearity, dilution integrity and reinjection reproducibility. This method can be applied not only to study the xenobiotic effects on these bile acids and also to investigate the effects of pharmacological agents on these bile acids levels in rats for mechanistic understanding of bile acid related diseases such as cholestasis, non-alcoholic fatty liver disease etc. Such an application was studied with ivermectin which is an FXR modulator drug involves in the regulation of lipids, energy metabolism. The drug induced alterations in the bile acid homeostasis was confirmed with the significant reductions of CA, CDCA, DCA and increase in Tα/β-MCA levels after 14-days exposure with ivermectin rats. Likewise, 7-days exposure with zafirlukast, a pan-UGT inhibitor, on these bile acids and bilirubin levels was also assessed in rats. The plasma concentrations of CA, CDCA and DCA, which are majorly glucuronidated at C-24 position by UGT1A3 isoform, reduced significantly due to the inhibition of UGT enzymes by zafirlukast. Surprisingly, the levels of TDCA were

increased by at least 3-folds. A small shift towards taurine conjugation may be responsible for the increased levels of taurine species in the bile acid pool. The total bilirubin levels were not affected by UGT inhibition. These results infer that endobiotic levels are differentially altered in relation to the xenobiotic mediated inhibition of their corresponding metabolic enzymes. In addition, from the literature it was assumed that the increased concentrations by inhibition of UGT clearance of these bile acids may be due to the induction of the relevant enzymes by ligand activated transcription factors or nuclear receptors. This notion was further supported by the induction of UGT1A3 expression by FXR agonists. Indeed, both CDCA, CA and DCA are endogenous FXR agonists and their increased levels (as a result of inhibition of UGT mediated clearance), can in turn induce UGT1A1/UTG1A3 enzymes by distinct FXR regulated feed forward mechanism or can reduce the biosynthesis of bile acids from cholesterol by negative feedback mechanism. Thus, an eye on the critical endobiotic homeostasis upon drug exposure that alter UGT metabolism is imperative to avoid UGT mediated metabolic drug-endobiotic interactions.

Conclusively, the current research work highlights the importance of UGT1A1 and UGT1A3 mediated metabolism and their inhibition on either co-administered drugs or endobiotics and paves the ways for successful identification of possible substrates and inhibitors of these isoforms using *in vitro* and *in vivo* methods. Further, these research findings contribute to the DMPK research area for further exploration of drugs and endobiotics relationships. Critical outcomes from such kind of UGT inhibition/induction studies may alert drug makers for their detrimental effects on health and/or may find application in identifying alternative therapeutic strategies for beneficial effects in disease conditions. The overall goal of this research work was fruitful with interesting ground breaking and thought-provoking outcomes in relation to UGT inhibition and endobiotic levels. Further research warrants the identification of distinct mechanisms of the paradox.

7

Future scope of work

In this research work, we have established *in vitro* and *in vivo* methodologies to identify selective substrates and inhibitors for UGT1A1 and UGT1A3 enzymes. A UHPLC-MS/MS method for quantitative measurement of selected major human and murine specific bile acids in rat plasma was developed to study the effect of ivermectin and zafirlukast on the plasma bile acids levels in rat model. Till date there are no published reports on the study of effect of inhibition of UGT1A1 and UGT1A3 enzymes on the plasma levels of bile acids. Although, the goal of proposed research hypothesis was achieved, further mechanistic research is needed to understand the mechanisms involved in the changes in plasma bile acids levels due to the inhibition of UGT1A1 and UGT1A3 enzymes. In addition, studies are required to know if they are any other players such as transporters or nuclear receptors involved in the changes observed in plasma bile acid levels due to the inhibition of UGT1A1 and UGT1A3 enzymes. Further investigations involving how zafirlukast mediated UGT inhibition result in the induction of UGT enzymes has to be carried out. Although, the results obtained from our studies indicate that zafirlukast could cause metabolic DDI with ezetimibe, prediction of clinical DDI between the two drugs should be evaluated using suitable PBPK modelling to make appropriate dosage adjustments in combination therapy of the two drugs. Potential application of UGT mediated inhibition or induction as a therapeutic target for certain metabolic diseases can also be explored as future scope of this current research work.

8

References

1. Miners, J.O., et al., *Evidence-based strategies for the characterisation of human drug and chemical glucuronidation in vitro and UDP-glucuronosyltransferase reaction phenotyping.* Pharmacology & Therapeutics, 2021. **218**: p. 107689.
2. Shanu-Wilson, J., et al., *Biotransformation: Impact and Application of Metabolism in Drug Discovery.* ACS Med Chem Lett, 2020. **11**(11): p. 2087-2107.
3. Ufer, M., et al., *Metabolite profiling in early clinical drug development: current status and future prospects.* Expert Opinion on Drug Metabolism & Toxicology, 2017. **13**(8): p. 803-806.
4. Zhao, M., et al., *Cytochrome P450 Enzymes and Drug Metabolism in Humans.* Int J Mol Sci, 2021. **22**(23).
5. McDonnell, A.M. and C.H. Dang, *Basic review of the cytochrome p450 system.* J Adv Pract Oncol, 2013. **4**(4): p. 263-8.
6. Stanley, L., *Drug metabolism*, in *Pharmacognosy*. 2017, Elsevier. p. 527-545.
7. Bachmann, K., *Drug metabolism*, in *Pharmacology*. 2009, Elsevier. p. 131-173.
8. Jancova, P., P. Anzenbacher, and E. Anzenbacherova, *Phase II drug metabolizing enzymes.* Biomed Pap Med Fac Univ Palacky Olomouc Czech Repub, 2010. **154**(2): p. 103-16.
9. Petra, J. and Š. Michal, *Phase II Drug Metabolism*, in *Topics on Drug Metabolism*, P. James, Editor. 2012, IntechOpen: Rijeka. p. Ch. 2.
10. Bowman, C.M. and L.Z. Benet, *In Vitro-In Vivo Extrapolation and Hepatic Clearance-Dependent Underprediction.* J Pharm Sci, 2019. **108**(7): p. 2500-2504.
11. Zhou, J., T.S. Tracy, and R.P. Remmel, *Bilirubin glucuronidation revisited: proper assay conditions to estimate enzyme kinetics with recombinant UGT1A1.* Drug Metab Dispos, 2010. **38**(11): p. 1907-11.
12. Barbier, O., et al., *Lipid-activated transcription factors control bile acid glucuronidation.* Mol Cell Biochem, 2009. **326**(1-2): p. 3-8.
13. Li, Y., et al., *Current trends in drug metabolism and pharmacokinetics.* Acta Pharm Sin B, 2019. **9**(6): p. 1113-1144.
14. Rowland, A., J.O. Miners, and P.I. Mackenzie, *The UDP-glucuronosyltransferases: their role in drug metabolism and detoxification.* Int J Biochem Cell Biol, 2013. **45**(6): p. 1121-32.
15. Hu, D.G., et al., *Transcriptional regulation of human UDP-glucuronosyltransferase genes.* Drug Metab Rev, 2014. **46**(4): p. 421-58.
16. Miners, J.O., et al., *Drug-drug interactions that alter the exposure of glucuronidated drugs: Scope, UDP-glucuronosyltransferase (UGT) enzyme selectivity, mechanisms (inhibition and induction), and clinical significance.* Pharmacol Ther, 2023. **248**: p. 108459.
17. Tukey, R.H. and C.P. Strassburg, *Human UDP-glucuronosyltransferases: metabolism, expression, and disease.* Annu Rev Pharmacol Toxicol, 2000. **40**: p. 581-616.
18. Busse, D., et al., *Industrial Approach to Determine the Relative Contribution of Seven Major UGT Isoforms to Hepatic Glucuronidation.* J Pharm Sci, 2020. **109**(7): p. 2309-2320.
19. Ladumor, M.K., et al., *A repository of protein abundance data of drug metabolizing enzymes and transporters for applications in physiologically based pharmacokinetic (PBPK) modelling and simulation.* Sci Rep, 2019. **9**(1): p. 9709.
20. Proctor, N.J., G.T. Tucker, and A. Rostami-Hodjegan, *Predicting drug clearance from recombinantly expressed CYPs: intersystem extrapolation factors.* Xenobiotica, 2004. **34**(2): p. 151-78.
21. Maruo, Y., et al., *Polymorphism of UDP-glucuronosyltransferase and drug metabolism.* Curr Drug Metab, 2005. **6**(2): p. 91-9.
22. Court, M.H., *Interindividual variability in hepatic drug glucuronidation: studies into the role of age, sex, enzyme inducers, and genetic polymorphism using the human liver bank as a model system.* Drug Metab Rev, 2010. **42**(1): p. 209-24.
23. Basit, A., et al., *Characterization of Differential Tissue Abundance of Major Non-CYP Enzymes in Human.* Molecular Pharmaceutics, 2020. **17**(11): p. 4114-4124.

24. Guillemette, C., et al., *UGT genomic diversity: beyond gene duplication.* Drug Metab Rev, 2010. **42**(1): p. 24-44.
25. Mackenzie, P.I., D.G. Hu, and D.A. Gardner-Stephen, *The regulation of UDP-glucuronosyltransferase genes by tissue-specific and ligand-activated transcription factors.* Drug Metab Rev, 2010. **42**(1): p. 99-109.
26. Gregory, P.A., et al., *Cloning and characterization of the human UDP-glucuronosyltransferase 1A8, 1A9, and 1A10 gene promoters: differential regulation through an interior-like region.* J Biol Chem, 2003. **278**(38): p. 36107-14.
27. Hu, D.G. and P.I. Mackenzie, *Estrogen receptor alpha, fos-related antigen-2, and c-Jun coordinately regulate human UDP glucuronosyltransferase 2B15 and 2B17 expression in response to 17beta-estradiol in MCF-7 cells.* Mol Pharmacol, 2009. **76**(2): p. 425-39.
28. Kaeding, J., et al., *Calcitrol (1alpha,25-dihydroxyvitamin D3) inhibits androgen glucuronidation in prostate cancer cells.* Mol Cancer Ther, 2008. **7**(2): p. 380-90.
29. Hu, D.G., et al., *A novel polymorphism in a forkhead box A1 (FOXA1) binding site of the human UDP glucuronosyltransferase 2B17 gene modulates promoter activity and is associated with altered levels of circulating androstane-3alpha,17beta-diol glucuronide.* Mol Pharmacol, 2010. **78**(4): p. 714-22.
30. Sugatani, J., et al., *The phenobarbital response enhancer module in the human bilirubin UDP-glucuronosyltransferase UGT1A1 gene and regulation by the nuclear receptor CAR.* Hepatology, 2001. **33**(5): p. 1232-8.
31. Gardner-Stephen, D., et al., *Human PXR variants and their differential effects on the regulation of human UDP-glucuronosyltransferase gene expression.* Drug Metab Dispos, 2004. **32**(3): p. 340-7.
32. Barbier, O., et al., *Peroxisome proliferator-activated receptor alpha induces hepatic expression of the human bile acid glucuronidating UDP-glucuronosyltransferase 2B4 enzyme.* J Biol Chem, 2003. **278**(35): p. 32852-60.
33. Lu, Y., et al., *Lithocholic acid decreases expression of UGT2B7 in Caco-2 cells: a potential role for a negative farnesoid X receptor response element.* Drug Metab Dispos, 2005. **33**(7): p. 937-46.
34. Verreault, M., et al., *The liver X-receptor alpha controls hepatic expression of the human bile acid-glucuronidating UGT1A3 enzyme in human cells and transgenic mice.* Hepatology, 2006. **44**(2): p. 368-78.
35. Senekeo-Effenberger, K., et al., *Expression of the human UGT1 locus in transgenic mice by 4-chloro-6-(2,3-xylidino)-2-pyrimidinylthioacetic acid (WY-14643) and implications on drug metabolism through peroxisome proliferator-activated receptor alpha activation.* Drug Metab Dispos, 2007. **35**(3): p. 419-27.
36. Sugatani, J., et al., *The induction of human UDP-glucuronosyltransferase 1A1 mediated through a distal enhancer module by flavonoids and xenobiotics.* Biochem Pharmacol, 2004. **67**(5): p. 989-1000.
37. Lankisch, T.O., et al., *Aryl hydrocarbon receptor-mediated regulation of the human estrogen and bile acid UDP-glucuronosyltransferase 1A3 gene.* Arch Toxicol, 2008. **82**(9): p. 573-82.
38. Bock, K.W. and B.S. Bock-Hennig, *UDP-glucuronosyltransferases (UGTs): from purification of Ah-receptor-inducible UGT1A6 to coordinate regulation of subsets of CYPs, UGTs, and ABC transporters by nuclear receptors.* Drug Metab Rev, 2010. **42**(1): p. 6-13.
39. Yueh, M.F. and R.H. Tukey, *Nrf2-Keap1 signaling pathway regulates human UGT1A1 expression in vitro and in transgenic UGT1 mice.* J Biol Chem, 2007. **282**(12): p. 8749-58.
40. Beckers, M., N. Fechner, and N. Stiefl, *25 Years of Small-Molecule Optimization at Novartis: A Retrospective Analysis of Chemical Series Evolution.* Journal of Chemical Information and Modeling, 2022. **62**(23): p. 6002-6021.
41. Leeson, P.D. and A.M. Davis, *Time-Related Differences in the Physical Property Profiles of Oral Drugs.* Journal of Medicinal Chemistry, 2004. **47**(25): p. 6338-6348.

42. Yang, G., et al., *Glucuronidation: driving factors and their impact on glucuronide disposition.* Drug Metab Rev, 2017. **49**(2): p. 105-138.
43. Kosoglou, T., et al., *Ezetimibe: a review of its metabolism, pharmacokinetics and drug interactions.* Clin Pharmacokinet, 2005. **44**(5): p. 467-94.
44. Christrup, L.L., *Morphine metabolites.* Acta Anaesthesiol Scand, 1997. **41**(1 Pt 2): p. 116-22.
45. Ebner, T., K. Wagner, and W. Wienen, *Dabigatran acylglucuronide, the major human metabolite of dabigatran: in vitro formation, stability, and pharmacological activity.* Drug Metab Dispos, 2010. **38**(9): p. 1567-75.
46. Shah, M.B., *Inhibition of CYP2C8 by Acyl Glucuronides of Gemfibrozil and Clopidogrel: Pharmacological Significance, Progress and Challenges.* Biomolecules, 2022. **12**(9).
47. Asha, S. and M. Vidyavathi, *Role of human liver microsomes in in vitro metabolism of drugs—a review.* Applied biochemistry and biotechnology, 2010. **160**: p. 1699-1722.
48. Li, A.P., *Human hepatocytes: isolation, cryopreservation and applications in drug development.* Chemico-biological interactions, 2007. **168**(1): p. 16-29.
49. Boulenc, X., W. Schmider, and O. Barberan, *In Vitro/In Vivo Correlation for Drug–Drug Interactions*, in *Drug Discovery and Evaluation: Methods in Clinical Pharmacology*, H.G. Vogel, J. Maas, and A. Gebauer, Editors. 2011, Springer Berlin Heidelberg: Berlin, Heidelberg. p. 133-160.
50. Lu, Y., S. Kim, and K. Park, *In vitro-in vivo correlation: perspectives on model development.* Int J Pharm, 2011. **418**(1): p. 142-8.
51. Miners, J.O., et al., *In vitro-in vivo correlation for drugs and other compounds eliminated by glucuronidation in humans: pitfalls and promises.* Biochem Pharmacol, 2006. **71**(11): p. 1531-9.
52. Chiang, J.Y., *Bile acid metabolism and signaling.* Compr Physiol, 2013. **3**(3): p. 1191-212.
53. Oda, S., et al., *A comprehensive review of UDP-glucuronosyltransferase and esterases for drug development.* Drug metabolism and pharmacokinetics, 2015. **30**(1): p. 30-51.
54. Lv, X., et al., *Recent progress and challenges in screening and characterization of UGT1A1 inhibitors.* Acta pharmaceutica sinica b, 2019. **9**(2): p. 258-278.
55. Kiang, T.K., M.H. Ensom, and T.K. Chang, *UDP-glucuronosyltransferases and clinical drug-drug interactions.* Pharmacology & therapeutics, 2005. **106**(1): p. 97-132.
56. Di Perri, G., *Clinical pharmacology of the single tablet regimen bictegravir/emtricitabine/tenofovir alafenamide (BIC/FTC/TAF).* Infez Med, 2019. **27**(4): p. 365-373.
57. Miners, J.O., et al., *Drug-drug interactions that alter the exposure of glucuronidated drugs: Scope, UDP-glucuronosyltransferase (UGT) enzyme selectivity, mechanisms (inhibition and induction), and clinical significance.* Pharmacology & Therapeutics, 2023. **248**: p. 108459.
58. Joseph, D., et al., *Effect of faldaprevir on raltegravir pharmacokinetics in healthy volunteers.* The Journal of Clinical Pharmacology, 2015. **55**(4): p. 384-391.
59. Song, I., et al., *Effects of enzyme inducers efavirenz and tipranavir/ritonavir on the pharmacokinetics of the HIV integrase inhibitor dolutegravir.* European Journal of Clinical Pharmacology, 2014. **70**(10): p. 1173-1179.
60. Song, I., et al., *Effect of carbamazepine on dolutegravir pharmacokinetics and dosing recommendation.* European Journal of Clinical Pharmacology, 2016. **72**(6): p. 665-670.
61. Devineni, D., et al., *Effects of rifampin, cyclosporine A, and probenecid on the pharmacokinetic profile of canagliflozin, a sodium glucose co-transporter 2 inhibitor, in healthy participants.* Int J Clin Pharmacol Ther, 2015. **53**(2): p. 115-28.
62. You, B.H., E.C. Gong, and Y.H. Choi, *Inhibitory Effect of Sauchinone on UDP-Glucuronosyltransferase (UGT) 2B7 Activity.* Molecules, 2018. **23**(2).
63. Li, X., et al., *Potential interactions among myricetin and dietary flavonols through the inhibition of human UDP-glucuronosyltransferase in vitro.* Toxicol Lett, 2022. **358**: p. 40-47.

64. Zhou, Q.H., et al., *A broad-spectrum substrate for the human UDP-glucuronosyltransferases and its use for investigating glucuronidation inhibitors.* Int J Biol Macromol, 2021. **180**: p. 252-261.
65. Zhang, Y.S., et al., *Strong inhibition of celastrol towards UDP-glucuronosyl transferase (UGT) 1A6 and 2B7 indicating potential risk of UGT-based herb-drug interaction.* Molecules, 2012. **17**(6): p. 6832-9.
66. Cao, Y.F., et al., *Drug-Drug Interactions Potential of Icariin and Its Intestinal Metabolites via Inhibition of Intestinal UDP-Glucuronosyltransferases.* Evid Based Complement Alternat Med, 2012. **2012**: p. 395912.
67. Liu, C., et al., *Strong inhibition of deoxyschizandrin and schisantherin A toward UDP-glucuronosyltransferase (UGT) 1A3 indicating UGT inhibition-based herb–drug interaction.* Fitoterapia, 2012. **83**(8): p. 1415-1419.
68. Jiang, L., et al., *Piceatannol exhibits potential food-drug interactions through the inhibition of human UDP-glucuronosyltransferase (UGT) in Vitro.* Toxicol In Vitro, 2020. **67**: p. 104890.
69. Fisher, M.B., et al., *The role of hepatic and extrahepatic UDP-glucuronosyltransferases in human drug metabolism.* Drug Metab Rev, 2001. **33**(3-4): p. 273-97.
70. Knights, K.M., A. Rowland, and J.O. Miners, *Renal drug metabolism in humans: the potential for drug-endobiotic interactions involving cytochrome P450 (CYP) and UDP-glucuronosyltransferase (UGT).* Br J Clin Pharmacol, 2013. **76**(4): p. 587-602.
71. Margaillan, G., et al., *Quantitative profiling of human renal UDP-glucuronosyltransferases and glucuronidation activity: a comparison of normal and tumoral kidney tissues.* Drug Metab Dispos, 2015. **43**(4): p. 611-9.
72. Dobrinska, M.R., *Enterohepatic circulation of drugs.* J Clin Pharmacol, 1989. **29**(7): p. 577-80.
73. Roberts, M.S., et al., *Enterohepatic circulation: physiological, pharmacokinetic and clinical implications.* Clin Pharmacokinet, 2002. **41**(10): p. 751-90.
74. Williams, J.A., et al., *Reaction phenotyping in drug discovery: moving forward with confidence?* Curr Drug Metab, 2003. **4**(6): p. 527-34.
75. Nagar, S., U.A. Argikar, and D.J. Tweedie, *Enzyme kinetics in drug metabolism: fundamentals and applications*. 2021: Springer.
76. Fu, S., et al., *Metabolism-mediated drug–drug interactions–study design, data analysis, and implications for in vitro evaluations.* Medicine in Drug Discovery, 2022. **14**: p. 100121.
77. Frere, J.M., B. Leyh, and A. Renard, *Lineweaver-Burk, Hanes, Eadie-Hofstee and Dixon plots in non-steady-state situations.* J Theor Biol, 1983. **101**(3): p. 387-400.
78. Sahi, J., S. Grepper, and C. Smith, *Hepatocytes as a tool in drug metabolism, transport and safety evaluations in drug discovery.* Curr Drug Discov Technol, 2010. **7**(3): p. 188-98.
79. Nishimura, M., et al., *Evaluation of gene induction of drug-metabolizing enzymes and transporters in primary culture of human hepatocytes using high-sensitivity real-time reverse transcription PCR.* Yakugaku Zasshi, 2002. **122**(5): p. 339-61.
80. Bünning, P., *Drug–Drug Interaction: Enzyme Induction*, in *Drug Discovery and Evaluation: Safety and Pharmacokinetic Assays*, H.G. Vogel, et al., Editors. 2013, Springer Berlin Heidelberg: Berlin, Heidelberg. p. 975-987.
81. Dawson, P.A. and S.J. Karpen, *Intestinal transport and metabolism of bile acids.* J Lipid Res, 2015. **56**(6): p. 1085-99.
82. Rowland, A., J.O. Miners, and P.I. Mackenzie, *The UDP-glucuronosyltransferases: Their role in drug metabolism and detoxification.* The International Journal of Biochemistry & Cell Biology, 2013. **45**(6): p. 1121-1132.
83. Chiang, J., J. Ferrell, and J. Chiang, *Up to date on cholesterol 7a-hydroxylase (CYP7A1) in bile acid synthesis.* Liver Research, 2020. **4**.
84. Shulpekova, Y., et al., *The Role of Bile Acids in the Human Body and in the Development of Diseases.* Molecules, 2022. **27**(11): p. 3401.

85. Kastrinou Lampou, V., et al., *Novel insights into bile acid detoxification via CYP, UGT and SULT enzymes.* Toxicol In Vitro, 2023. **87**: p. 105533.
86. W. Wolkoff, A. and P.D. Berk, *Bilirubin metabolism and jaundice.* Schiff's Diseases of the Liver, 2017: p. 103-134.
87. Trottier, J., et al., *Human UDP-glucuronosyltransferase (UGT)1A3 enzyme conjugates chenodeoxycholic acid in the liver.* Hepatology, 2006. **44**(5): p. 1158-1170.
88. Fang, Z.Z., et al., *A model of in vitro UDP-glucuronosyltransferase inhibition by bile acids predicts possible metabolic disorders.* J Lipid Res, 2013. **54**(12): p. 3334-44.
89. Zhou, J., T.S. Tracy, and R.P. Remmel, *Correlation between bilirubin glucuronidation and estradiol-3-gluronidation in the presence of model UDP-glucuronosyltransferase 1A1 substrates/inhibitors.* Drug Metab Dispos, 2011. **39**(2): p. 322-9.
90. Jeong, H., et al., *Regulation of UDP-glucuronosyltransferase (UGT) 1A1 by progesterone and its impact on labetalol elimination.* Xenobiotica, 2008. **38**(1): p. 62-75.
91. W. Wolkoff , A. and P.D. Berk, *Bilirubin Metabolism and Jaundice*, in *Schiff's Diseases of the Liver*. 2017. p. 103-134.
92. Ritter, J.K., *Intestinal UGTs as potential modifiers of pharmacokinetics and biological responses to drugs and xenobiotics.* Expert Opin Drug Metab Toxicol, 2007. **3**(1): p. 93-107.
93. Bock, K.W., *Roles of human UDP-glucuronosyltransferases in clearance and homeostasis of endogenous substrates, and functional implications.* Biochem Pharmacol, 2015. **96**(2): p. 77-82.
94. Badée, J., et al., *Optimization of Experimental Conditions of Automated Glucuronidation Assays in Human Liver Microsomes Using a Cocktail Approach and Ultra-High Performance Liquid Chromatography-Tandem Mass Spectrometry.* Drug Metab Dispos, 2019. **47**(2): p. 124-134.
95. Donato, M.T., et al., *Validated assay for studying activity profiles of human liver UGTs after drug exposure: inhibition and induction studies.* Analytical and Bioanalytical Chemistry, 2010. **396**(6): p. 2251-2263.
96. Ge, S., Y. Tu, and M. Hu, *Challenges and Opportunities with Predicting In Vivo Phase II Metabolism via Glucuronidation From In Vitro Data.* Current Pharmacology Reports, 2016. **2**(6): p. 326-338.
97. Goon, C.P., et al., *UGT1A1 Mediated Drug Interactions and its Clinical Relevance.* Curr Drug Metab, 2016. **17**(2): p. 100-6.
98. Oda, S., et al., *A comprehensive review of UDP-glucuronosyltransferase and esterases for drug development.* Drug Metab Pharmacokinet, 2015. **30**(1): p. 30-51.
99. Strassburg, C.P., et al., *Polymorphic gene regulation and interindividual variation of UDP-glucuronosyltransferase activity in human small intestine.* J Biol Chem, 2000. **275**(46): p. 36164-71.
100. Williams, J.A., et al., *Drug-drug interactions for UDP-glucuronosyltransferase substrates: a pharmacokinetic explanation for typically observed low exposure (AUCi/AUC) ratios.* Drug Metab Dispos, 2004. **32**(11): p. 1201-8.
101. Fallon, J.K., et al., *Targeted Quantitative Proteomics for the Analysis of 14 UGT1As and -2Bs in Human Liver Using NanoUPLC–MS/MS with Selected Reaction Monitoring.* Journal of Proteome Research, 2013. **12**(10): p. 4402-4413.
102. Trottier, J., et al., *Human UDP-glucuronosyltransferase (UGT)1A3 enzyme conjugates chenodeoxycholic acid in the liver.* Hepatology, 2006. **44**(5): p. 1158-70.
103. Lv, X., et al., *Recent progress and challenges in screening and characterization of UGT1A1 inhibitors.* Acta pharmaceutica Sinica. B, 2019. **9**(2): p. 258-278.
104. Wang, Z., et al., *Inhibition of human UDP-glucuronosyltransferase enzymes by midostaurin and ruxolitinib: implications for drug-drug interactions.* 2020. **41**(6): p. 231-238.
105. Kim, M.J. and D.J. Suh, *Profiles of serum bile acids in liver diseases.* The Korean journal of internal medicine, 1986. **1**(1): p. 37-42.

106. Hofmann, A.F., *The Continuing Importance of Bile Acids in Liver and Intestinal Disease.* Archives of Internal Medicine, 1999. **159**(22): p. 2647-2658.
107. Chiang, J.Y.L., *Bile acid metabolism and signaling in liver disease and therapy.* Liver Research, 2017. **1**(1): p. 3-9.
108. Evangelakos, I., et al., *Role of bile acids in inflammatory liver diseases.* Seminars in Immunopathology, 2021. **43**(4): p. 577-590.
109. Kiang, T.K., M.H. Ensom, and T.K. Chang, *UDP-glucuronosyltransferases and clinical drug-drug interactions.* Pharmacol Ther, 2005. **106**(1): p. 97-132.
110. Oda, S., et al., *Targeted Screen for Human UDP-Glucuronosyltransferases Inhibitors and the Evaluation of Potential Drug-Drug Interactions with Zafirlukast.* Drug Metabolism and Disposition, 2015. **43**(6): p. 812-818.
111. Couto, N., et al., *Quantitative Proteomics of Clinically Relevant Drug-Metabolizing Enzymes and Drug Transporters and Their Intercorrelations in the Human Small Intestine.* Drug Metabolism and Disposition, 2020. **48**(4): p. 245-254.
112. Akazawa, T., et al., *High Expression of UGT1A1/1A6 in Monkey Small Intestine: Comparison of Protein Expression Levels of Cytochromes P450, UDP-Glucuronosyltransferases, and Transporters in Small Intestine of Cynomolgus Monkey and Human.* Molecular Pharmaceutics, 2017. **15**(1): p. 127-140.
113. Fallon, J.K., et al., *Targeted Precise Quantification of 12 Human Recombinant Uridine-Diphosphate Glucuronosyl Transferase 1A and 2B Isoforms Using Nano-Ultra-High-Performance Liquid Chromatography/Tandem Mass Spectrometry with Selected Reaction Monitoring.* Drug Metabolism and Disposition, 2013. **41**(12): p. 2076-2080.
114. Cubitt, H.E., J.B. Houston, and A. Galetin, *Relative importance of intestinal and hepatic glucuronidation-impact on the prediction of drug clearance.* Pharm Res, 2009. **26**(5): p. 1073-83.
115. Walsky, R.L., et al., *Optimized assays for human UDP-glucuronosyltransferase (UGT) activities: altered alamethicin concentration and utility to screen for UGT inhibitors.* Drug Metab Dispos, 2012. **40**(5): p. 1051-65.
116. Chen, A., et al., *Design and optimization of the cocktail assay for rapid assessment of the activity of UGT enzymes in human and rat liver microsomes.* Toxicol Lett, 2018. **295**: p. 379-389.
117. Lu, D., Q. Xie, and B. Wu, *N-glucuronidation catalyzed by UGT1A4 and UGT2B10 in human liver microsomes: Assay optimization and substrate identification.* J Pharm Biomed Anal, 2017. **145**: p. 692-703.
118. Seo, K.A., et al., *In vitro assay of six UDP-glucuronosyltransferase isoforms in human liver microsomes, using cocktails of probe substrates and liquid chromatography-tandem mass spectrometry.* Drug Metab Dispos, 2014. **42**(11): p. 1803-10.
119. Attili, A.F., et al., *Bile acid-induced liver toxicity: relation to the hydrophobic-hydrophilic balance of bile acids.* Med Hypotheses, 1986. **19**(1): p. 57-69.
120. Zhang, D., et al., *In vitro inhibition of UDP glucuronosyltransferases by atazanavir and other HIV protease inhibitors and the relationship of this property to in vivo bilirubin glucuronidation.* Drug metabolism and disposition: the biological fate of chemicals, 2005. **33**(11): p. 1729-1739.
121. Ritter, J.K., *Intestinal UGTs as potential modifiers of pharmacokinetics and biological responses to drugs and xenobiotics.* Expert Opinion on Drug Metabolism & Toxicology, 2007. **3**(1): p. 93-107.
122. Korprasertthaworn, P., et al., *Inhibition of human UDP-glucuronosyltransferase (UGT) enzymes by kinase inhibitors: Effects of dabrafenib, ibrutinib, nintedanib, trametinib and BIBF 1202.* Biochem Pharmacol, 2019. **169**: p. 113616.
123. Gammal, R.S., et al., *Clinical Pharmacogenetics Implementation Consortium (CPIC) Guideline for UGT1A1 and Atazanavir Prescribing.* Clin Pharmacol Ther, 2016. **99**(4): p. 363-9.

124. Li, T. and U. Apte, *Bile Acid Metabolism and Signaling in Cholestasis, Inflammation, and Cancer.* Adv Pharmacol, 2015. **74**: p. 263-302.
125. Basu, N.K., et al., *Gastrointestinally distributed UDP-glucuronosyltransferase 1A10, which metabolizes estrogens and nonsteroidal anti-inflammatory drugs, depends upon phosphorylation.* J Biol Chem, 2004. **279**(27): p. 28320-9.
126. Harbourt, D.E., et al., *Quantification of Human Uridine-Diphosphate Glucuronosyl Transferase 1A Isoforms in Liver, Intestine, and Kidney Using Nanobore Liquid Chromatography–Tandem Mass Spectrometry.* Analytical Chemistry, 2011. **84**(1): p. 98-105.
127. Couto, N., et al., *Quantification of Proteins Involved in Drug Metabolism and Disposition in the Human Liver Using Label-Free Global Proteomics.* Molecular Pharmaceutics, 2019. **16**(2): p. 632-647.
128. Mullapudi, T.V.R., P.R. Ravi, and G. Thipparapu, *UGT1A1 and UGT1A3 activity and inhibition in human liver and intestinal microsomes and a recombinant UGT system under similar assay conditions using selective substrates and inhibitors.* Xenobiotica, 2021. **51**(11): p. 1236-1246.
129. Oda, S., et al., *Targeted screen for human UDP-glucuronosyltransferases inhibitors and the evaluation of potential drug-drug interactions with zafirlukast.* Drug Metab Dispos, 2015. **43**(6): p. 812-8.
130. Ghosal, A., et al., *Identification of human UDP-glucuronosyltransferase enzyme(s) responsible for the glucuronidation of ezetimibe (Zetia).* Drug Metab Dispos, 2004. **32**(3): p. 314-20.
131. Food and D. Administration, *Clinical drug interaction studies-cytochrome P450 enzyme-and transporter-mediated drug interactions guidance for industry.* Center for Drug Evaluation and Research (CDER), US Department of Health and Human Services Food and Drug Administration, Silver Springs, MD, 2020.
132. Mazur, C.S., et al., *Differences between human and rat intestinal and hepatic bisphenol A glucuronidation and the influence of alamethicin on in vitro kinetic measurements.* Drug Metab Dispos, 2010. **38**(12): p. 2232-8.
133. Oswald, S., et al., *Disposition and sterol-lowering effect of ezetimibe are influenced by single-dose coadministration of rifampin, an inhibitor of multidrug transport proteins.* Clin Pharmacol Ther, 2006. **80**(5): p. 477-85.
134. Sun, Y.L., et al., *Zafirlukast antagonizes ATP-binding cassette subfamily G member 2-mediated multidrug resistance.* Anticancer Drugs, 2012. **23**(8): p. 865-73.
135. Oswald, S., et al., *Impact of efavirenz on intestinal metabolism and transport: insights from an interaction study with ezetimibe in healthy volunteers.* Clin Pharmacol Ther, 2012. **91**(3): p. 506-13.
136. Ridlon, J.M., et al., *Bile acids and the gut microbiome.* Curr Opin Gastroenterol, 2014. **30**(3): p. 332-8.
137. Li, T. and J.Y. Chiang, *Nuclear receptors in bile acid metabolism.* Drug Metab Rev, 2013. **45**(1): p. 145-55.
138. Chiang, J.Y., *Recent advances in understanding bile acid homeostasis.* F1000Res, 2017. **6**: p. 2029.
139. Massafra, V., et al., *Progress and challenges of selective Farnesoid X Receptor modulation.* Pharmacol Ther, 2018. **191**: p. 162-177.
140. Massafra, V. and S.W.C. van Mil, *Farnesoid X receptor: A "homeostat" for hepatic nutrient metabolism.* Biochimica et Biophysica Acta (BBA) - Molecular Basis of Disease, 2018. **1864**(1): p. 45-59.
141. Hou, Y., et al., *Farnesoid X receptor: An important factor in blood glucose regulation.* Clin Chim Acta, 2019. **495**: p. 29-34.
142. Wang, H., et al., *FXR modulators for enterohepatic and metabolic diseases.* Expert Opin Ther Pat, 2018. **28**(11): p. 765-782.

143. Xi, Y. and H. Li, *Role of farnesoid X receptor in hepatic steatosis in nonalcoholic fatty liver disease.* Biomedicine & pharmacotherapy = Biomedecine & pharmacotherapie, 2020. **121**: p. 109609.
144. Fiorucci, S., A. Zampella, and E. Distrutti, *Development of FXR, PXR and CAR agonists and antagonists for treatment of liver disorders.* Curr Top Med Chem, 2012. **12**(6): p. 605-24.
145. Kim, I., et al., *Differential regulation of bile acid homeostasis by the farnesoid X receptor in liver and intestine.* J Lipid Res, 2007. **48**(12): p. 2664-72.
146. Kong, B., et al., *Mechanism of tissue-specific farnesoid X receptor in suppressing the expression of genes in bile-acid synthesis in mice.* Hepatology, 2012. **56**(3): p. 1034-43.
147. Jin, L., et al., *The antiparasitic drug ivermectin is a novel FXR ligand that regulates metabolism.* Nat Commun, 2013. **4**: p. 1937.
148. Qi, W., et al., *Ivermectin decreases triglyceride accumulation by inhibiting adipogenesis of 3T3-L1 preadipocytes.* Food Chem Toxicol, 2019. **131**: p. 110576.
149. van de Wiel, S.M.W., et al., *Identification of FDA-approved drugs targeting the Farnesoid X Receptor.* 2019. **9**(1): p. 2193.
150. Jin, L., et al., *Selective targeting of nuclear receptor FXR by avermectin analogues with therapeutic effects on nonalcoholic fatty liver disease.* Sci Rep, 2015. **5**: p. 17288.
151. Bernstein, H., et al., *Bile acids as endogenous etiologic agents in gastrointestinal cancer.* World J Gastroenterol, 2009. **15**(27): p. 3329-40.
152. Xie, G., et al., *Conjugated secondary 12alpha-hydroxylated bile acids promote liver fibrogenesis.* EBioMedicine, 2021. **66**: p. 103290.
153. Schadt, H.S., et al., *Bile acids in drug induced liver injury: Key players and surrogate markers.* Clin Res Hepatol Gastroenterol, 2016. **40**(3): p. 257-266.
154. Saran, C., et al., *Novel Bile Acid-Dependent Mechanisms of Hepatotoxicity Associated with Tyrosine Kinase Inhibitors.* 2022. **380**(2): p. 114-125.
155. James, S.C. and K. Fraser, *Concentrations of Fecal Bile Acids in Participants with Functional Gut Disorders and Healthy Controls.* 2021. **11**(9).
156. Perwaiz, S., et al., *Determination of bile acids in biological fluids by liquid chromatography-electrospray tandem mass spectrometry.* J Lipid Res, 2001. **42**(1): p. 114-9.
157. Burkard, I., A. von Eckardstein, and K.M. Rentsch, *Differentiated quantification of human bile acids in serum by high-performance liquid chromatography-tandem mass spectrometry.* J Chromatogr B Analyt Technol Biomed Life Sci, 2005. **826**(1-2): p. 147-59.
158. Ye, L., et al., *High-performance liquid chromatography-tandem mass spectrometry for the analysis of bile acid profiles in serum of women with intrahepatic cholestasis of pregnancy.* J Chromatogr B Analyt Technol Biomed Life Sci, 2007. **860**(1): p. 10-7.
159. Haag, M., et al., *Quantitative bile acid profiling by liquid chromatography quadrupole time-of-flight mass spectrometry: monitoring hepatitis B therapy by a novel Na(+)-taurocholate cotransporting polypeptide inhibitor.* Anal Bioanal Chem, 2015. **407**(22): p. 6815-25.
160. Xiang, X., et al., *High performance liquid chromatography-tandem mass spectrometry for the determination of bile acid concentrations in human plasma.* J Chromatogr B Analyt Technol Biomed Life Sci, 2010. **878**(1): p. 51-60.
161. Suzuki, Y., et al., *Simple and rapid quantitation of 21 bile acids in rat serum and liver by UPLC-MS-MS: effect of high fat diet on glycine conjugates of rat bile acids.* Nagoya J Med Sci, 2013. **75**(1-2): p. 57-71.
162. Scherer, M., et al., *Rapid quantification of bile acids and their conjugates in serum by liquid chromatography-tandem mass spectrometry.* J Chromatogr B Analyt Technol Biomed Life Sci, 2009. **877**(30): p. 3920-5.
163. Tagliacozzi, D., et al., *Quantitative analysis of bile acids in human plasma by liquid chromatography-electrospray tandem mass spectrometry: a simple and rapid one-step method.* Clin Chem Lab Med, 2003. **41**(12): p. 1633-41.

164. Luo, L., et al., *Assessment of serum bile acid profiles as biomarkers of liver injury and liver disease in humans.* PLoS One, 2018. **13**(3): p. e0193824.
165. Shiffka, S.J., et al., *Quantification of common and planar bile acids in tissues and cultured cells.* J Lipid Res, 2020. **61**(11): p. 1524-1535.
166. Li, Y., et al., *Simultaneous determination of sex hormones and bile acids in rat plasma using a liquid chromatography-tandem mass spectrometry method.* J Pharm Biomed Anal, 2023. **223**: p. 115139.
167. Hu, T., et al., *A sensitive and efficient method for simultaneous profiling of bile acids and fatty acids by UPLC-MS/MS.* J Pharm Biomed Anal, 2020. **178**: p. 112815.
168. Fu, X., et al., *Serum bile acids profiling by liquid chromatography-tandem mass spectrometry (LC-MS/MS) and its application on pediatric liver and intestinal diseases.* Clin Chem Lab Med, 2020. **58**(5): p. 787-797.
169. Wang, X., et al., *Semi-quantitative profiling of bile acids in serum and liver reveals the dosage-related effects of dexamethasone on bile acid metabolism in mice.* J Chromatogr B Analyt Technol Biomed Life Sci, 2018. **1095**: p. 65-74.
170. Danese, E., et al., *Bile Acids Quantification by Liquid Chromatography-Tandem Mass Spectrometry: Method Validation, Reference Range, and Interference Study.* Diagnostics (Basel), 2020. **10**(7).
171. Ando, M., et al., *High sensitive analysis of rat serum bile acids by liquid chromatography/electrospray ionization tandem mass spectrometry.* J Pharm Biomed Anal, 2006. **40**(5): p. 1179-86.
172. Tribe, R.M., et al., *Longitudinal profiles of 15 serum bile acids in patients with intrahepatic cholestasis of pregnancy.* Am J Gastroenterol, 2010. **105**(3): p. 585-95.
173. Wegner, K., et al., *Rapid analysis of bile acids in different biological matrices using LC-ESI-MS/MS for the investigation of bile acid transformation by mammalian gut bacteria.* Anal Bioanal Chem, 2017. **409**(5): p. 1231-1245.
174. Bobeldijk, I., et al., *Quantitative profiling of bile acids in biofluids and tissues based on accurate mass high resolution LC-FT-MS: compound class targeting in a metabolomics workflow.* J Chromatogr B Analyt Technol Biomed Life Sci, 2008. **871**(2): p. 306-13.
175. Yang, T., et al., *Quantitative profiling of 19 bile acids in rat plasma, liver, bile and different intestinal section contents to investigate bile acid homeostasis and the application of temporal variation of endogenous bile acids.* J Steroid Biochem Mol Biol, 2017. **172**: p. 69-78.
176. Zhang, X., et al., *Quantitative Profiling of Bile Acids in Feces of Humans and Rodents by Ultra-High-Performance Liquid Chromatography-Quadrupole Time-of-Flight Mass Spectrometry.* Metabolites, 2022. **12**(7).
177. Garcia-Canaveras, J.C., et al., *Targeted profiling of circulating and hepatic bile acids in human, mouse, and rat using a UPLC-MRM-MS-validated method.* J Lipid Res, 2012. **53**(10): p. 2231-2241.
178. Sarafian, M.H., et al., *Bile acid profiling and quantification in biofluids using ultra-performance liquid chromatography tandem mass spectrometry.* Anal Chem, 2015. **87**(19): p. 9662-70.
179. Gomez, C., et al., *Development and Validation of a Highly Sensitive LC-MS/MS Method for the Analysis of Bile Acids in Serum, Plasma, and Liver Tissue Samples.* Metabolites, 2020. **10**(7).
180. John, C., et al., *A liquid chromatography-tandem mass spectrometry-based method for the simultaneous determination of hydroxy sterols and bile acids.* J Chromatogr A, 2014. **1371**: p. 184-95.
181. Choucair, I., et al., *Quantification of bile acids: a mass spectrometry platform for studying gut microbe connection to metabolic diseases.* J Lipid Res, 2020. **61**(2): p. 159-177.
182. Reiter, S., et al., *Development of a Highly Sensitive Ultra-High-Performance Liquid Chromatography Coupled to Electrospray Ionization Tandem Mass Spectrometry Quantitation Method for Fecal Bile Acids and Application on Crohn's Disease Studies.* J Agric Food Chem, 2021. **69**(17): p. 5238-5251.

183. Shafaei, A., et al., *Extraction and quantitative determination of bile acids in feces.* Anal Chim Acta, 2021. **1150**: p. 338224.
184. Bathena, S.P., et al., *The profile of bile acids and their sulfate metabolites in human urine and serum.* J Chromatogr B Analyt Technol Biomed Life Sci, 2013. **942-943**: p. 53-62.
185. Huang, J., et al., *Simultaneous characterization of bile acids and their sulfate metabolites in mouse liver, plasma, bile, and urine using LC-MS/MS.* J Pharm Biomed Anal, 2011. **55**(5): p. 1111-9.
186. Han, J., et al., *Metabolic profiling of bile acids in human and mouse blood by LC-MS/MS in combination with phospholipid-depletion solid-phase extraction.* Anal Chem, 2015. **87**(2): p. 1127-36.
187. Want, E.J., et al., *Ultra performance liquid chromatography-mass spectrometry profiling of bile acid metabolites in biofluids: application to experimental toxicology studies.* Anal Chem, 2010. **82**(12): p. 5282-9.
188. Yang, L., et al., *Bile acids metabonomic study on the CCl4- and alpha-naphthylisothiocyanate-induced animal models: quantitative analysis of 22 bile acids by ultraperformance liquid chromatography-mass spectrometry.* Chem Res Toxicol, 2008. **21**(12): p. 2280-8.
189. Prinville, V., L. Ohlund, and L. Sleno, *Targeted Analysis of 46 Bile Acids to Study the Effect of Acetaminophen in Rat by LC-MS/MS.* Metabolites, 2020. **10**(1).
190. Mireault, M., et al., *Semi-Targeted Profiling of Bile Acids by High-Resolution Mass Spectrometry in a Rat Model of Drug-Induced Liver Injury.* Int J Mol Sci, 2023. **24**(3).
191. Alnouti, Y., I.L. Csanaky, and C.D. Klaassen, *Quantitative-profiling of bile acids and their conjugates in mouse liver, bile, plasma, and urine using LC-MS/MS.* J Chromatogr B Analyt Technol Biomed Life Sci, 2008. **873**(2): p. 209-17.
192. Guideline, I.H., *Bioanalytical method validation and study sample analysis M10.* ICH Harmonised Guideline: Geneva, Switzerland, 2022.
193. Xue, R., et al., *Bile Acid Receptors and the Gut-Liver Axis in Nonalcoholic Fatty Liver Disease.* Cells, 2021. **10**(11).
194. Hofmann, A.F., *The continuing importance of bile acids in liver and intestinal disease.* Arch Intern Med, 1999. **159**(22): p. 2647-58.
195. Jia, W., et al., *Targeting the alternative bile acid synthetic pathway for metabolic diseases.* Protein Cell, 2021. **12**(5): p. 411-425.
196. Chiang, J.Y., *Negative feedback regulation of bile acid metabolism: impact on liver metabolism and diseases.* Hepatology, 2015. **62**(4): p. 1315-7.
197. Sheweita, S.A., *Drug-metabolizing enzymes mechanisms and functions.* Current drug metabolism, 2000. **1**(2): p. 107-132.
198. Di, L., *The role of drug metabolizing enzymes in clearance.* Expert opinion on drug metabolism & toxicology, 2014. **10**(3): p. 379-393.
199. Muntane, J., *Regulation of drug metabolism and transporters.* Curr Drug Metab, 2009. **10**(8): p. 932-45.
200. Li, H. and H. Wang, *Activation of xenobiotic receptors: driving into the nucleus.* Expert Opin Drug Metab Toxicol, 2010. **6**(4): p. 409-26.
201. Krishnaswamy, S., et al., *Validation of serotonin (5-hydroxtryptamine) as an in vitro substrate probe for human UDP-glucuronosyltransferase (UGT) 1A6.* Drug Metabolism and Disposition, 2003. **31**(1): p. 133-139.
202. Wang, P.C., et al., *Catecholamine glucuronidation: an important metabolic pathway for dopamine in the rat.* Journal of neurochemistry, 1983. **40**(5): p. 1435-1440.
203. Guillemette, C., A. Bélanger, and J. Lépine, *Metabolic inactivation of estrogens in breast tissue by UDP-glucuronosyltransferase enzymes: an overview.* Breast Cancer Research, 2004. **6**(6): p. 246.

204. Zhang, D., et al., *In vitro inhibition of UDP glucuronosyltransferases by atazanavir and other HIV protease inhibitors and the relationship of this property to in vivo bilirubin glucuronidation.* Drug Metab Dispos, 2005. **33**(11): p. 1729-39.
205. Findlay, K.A.B., et al., *Characterization of the Uridine Diphosphate-Glucuronosyltransferase-Catalyzing Thyroid Hormone Glucuronidation in Man1.* The Journal of Clinical Endocrinology & Metabolism, 2000. **85**(8): p. 2879-2883.
206. Hirashima, R., et al., *Induction of the UDP-Glucuronosyltransferase 1A1 during the Perinatal Period Can Cause Neurodevelopmental Toxicity.* Mol Pharmacol, 2016. **90**(3): p. 265-74.
207. Trottier, J., et al., *Profiling serum bile acid glucuronides in humans: gender divergences, genetic determinants, and response to fenofibrate.* Clin Pharmacol Ther, 2013. **94**(4): p. 533-43.
208. McGlone, E.R. and S.R. Bloom, *Bile acids and the metabolic syndrome.* Ann Clin Biochem, 2019. **56**(3): p. 326-337.
209. Fuchs, C.D. and M. Trauner, *Role of bile acids and their receptors in gastrointestinal and hepatic pathophysiology.* Nat Rev Gastroenterol Hepatol, 2022. **19**(7): p. 432-450.
210. Hegade, V.S., et al., *Novel bile acid therapeutics for the treatment of chronic liver diseases.* Therapeutic Advances in Gastroenterology, 2016. **9**(3): p. 376-391.
211. Jansen, P.L.M., et al., *New developments in glucuronidation research: Report of a workshop on "Glucuronidation, its role in health and disease".* Hepatology, 1992. **15**(3): p. 532-544.
212. Wells, P.G., et al., *Glucuronidation and the UDP-glucuronosyltransferases in health and disease.* Drug Metab Dispos, 2004. **32**(3): p. 281-90.
213. Bigo, C., et al., *Nuclear receptors and endobiotics glucuronidation: the good, the bad, and the UGT.* Drug Metabolism Reviews, 2013. **45**(1): p. 34-47.
214. Erichsen, T.J., et al., *Regulation of the human bile acid UDP-glucuronosyltransferase 1A3 by the farnesoid X receptor and bile acids.* J Hepatol, 2010. **52**(4): p. 570-8.
215. Modica, S., R.M. Gadaleta, and A. Moschetta, *Deciphering the nuclear bile acid receptor FXR paradigm.* Nucl Recept Signal, 2010. **8**: p. e005.
216. Jiang, L., et al., *Farnesoid X receptor (FXR): Structures and ligands.* Comput Struct Biotechnol J, 2021. **19**: p. 2148-2159.
217. Barbier, O., et al., *FXR induces the UGT2B4 enzyme in hepatocytes: a potential mechanism of negative feedback control of FXR activity.* Gastroenterology, 2003. **124**(7): p. 1926-40.
218. Gallucci, G.M., et al., *Adjunct Fenofibrate Up-regulates Bile Acid Glucuronidation and Improves Treatment Response For Patients With Cholestasis.* Hepatol Commun, 2021. **5**(12): p. 2035-2051.
219. Miyazaki, T., et al., *Upregulation of Taurine Biosynthesis and Bile Acid Conjugation with Taurine through FXR in a Mouse Model with Human-like Bile Acid Composition.* Metabolites, 2023. **13**(7).
220. Mahmoud, H.M., et al., *Zafirlukast protects against hepatic ischemia-reperfusion injury in rats via modulating Bcl-2/Bax and NF-kappaB/SMAD-4 pathways.* Int Immunopharmacol, 2023. **122**: p. 110498.
221. Li, Y.Q., et al., *Bilirubin and bile acids may modulate their own metabolism via regulating uridine diphosphate-glucuronosyltransferase expression in the rat.* Journal of Gastroenterology and Hepatology, 2000. **15**(8): p. 865-870.
222. van der Schoor, L.W.E., et al., *Potential of therapeutic bile acids in the treatment of neonatal Hyperbilirubinemia.* Sci Rep, 2021. **11**(1): p. 11107.
223. Sugatani, J., *Function, genetic polymorphism, and transcriptional regulation of human UDP-glucuronosyltransferase (UGT) 1A1.* Drug Metab Pharmacokinet, 2013. **28**(2): p. 83-92.

Appendices

List of Publications (From Thesis Work)

1. **Mullapudi T.V.R.**, Ravi P.R., Thipparapu G. UGT1A1 and UGT1A3 activity and inhibition in human liver and intestinal microsomes and a recombinant UGT system under similar assay conditions using selective substrates and inhibitors. Xenobiotica. 2021 Nov;51(11):1236-1246. doi: 10.1080/00498254.2021.1998732. Epub 2021 Nov 10. PMID: 34698602.
2. **Mullapudi, T.V.R.,** Ravi, P.R. & Thipparapu, G. Simultaneous determination of seven bile acids to study the effect of ivermectin on their plasma levels in rat by UHPLC–MS/MS. *J Anal Sci Technol* **14**, 44 (2023). https://doi.org/10.1186/s40543-023-00408-y
3. **TV Radhakrishna Mullapudi.**, Ravi, P.R., Ganapathi Thipparapu. Drug-drug interaction of zafirlukast on UGT-mediated glucuronidation of ezetimibe in rat. (Under Review with Journal of Toxicology Mechanisms and Methods)

Other Publications

1. Khan MS, Ravi PR, **Mullapudi TVR**. Dose identification of triamcinolone acetonide for noninvasive pre-corneal administration in the treatment of posterior uveitis using a rapid, sensitive HPLC method with photodiode-array detector. Biomed Chromatogr. 2022;36(2):e5264. doi:10.1002/bmc.5264.

2. Taskar KS, Mariappan TT, Kurawattimath V, Singh Gautam S, **Radhakrishna Mullapudi TV**, Sridhar SK, Kallem RR, Marathe P, Mandlekar S. Unmasking the Role of Uptake Transporters for Digoxin Uptake Across the Barriers of the Central Nervous System in Rat. J Cent Nerv Syst Dis. 2017;9:1179573517693596. Published 2017 Mar 15. doi:10.1177/117957351769359

Workshops attended

1. 7th Asia Pacific International Society for the Study of Xenobiotic 2023 workshop 29 Jan 2023- 1st Feb 2023. Theme: Innovative approaches in Translation ADMET Science for Accelerating Drug Discovery and Development.
2. 2-day workshop on 'LC-MS training' conducted by Spinco Biotech Pvt Ltd and BITS–Pilani, Hyderabad Campus, on 3-4th November 2018, at BITS- Pilani, Hyderabad Campus.

Biography of Mr. Tv Radhakrishna Mullapudi

I am Mr. Tv Radhakrishna Mullapudi, a highly dedicated and accomplished individual with a strong background in the pharmaceutical industry. I hold a B Pharm and M Pharm degree, specializing in pharmacology, from the prestigious Rajiv Gandhi University of Health Sciences, Bangalore, Karnataka.

Immediately after completing my M Pharm, I had the privilege of joining Biocon Bristol Meyers Squibb R&D Center in Bangalore as a research scientist in the Department of Pharmaceutical Candidate Optimization. During my 4.5-year tenure, I contributed significantly to the development of new drugs and therapies, utilizing my expertise in DMPK (Drug Metabolism and Pharmacokinetics) to optimize pharmaceutical candidates. Following this enriching experience, I embarked on a new journey at Advinus Therapeutics Pvt Ltd (Eurofins - Advinus) as a Senior Research Scientist. For 4 years, I continued to excel in my role, leading research projects and collaborating with cross-functional teams to drive innovation and achieve breakthrough discoveries.

Currently, I am serving as an investigator at Pharmajen Labs in Hyderabad, where I continue to contribute to the advancement of pharmaceutical research and development. My passion for the field is evident in my decision to pursue a Ph.D., which I have registered for with BITS Pilani Hyderabad Campus. This endeavor allows me to delve deeper into the intricacies of pharmaceutical science and make a meaningful impact on the industry.

Biography of Prof. Punna Rao Ravi

Prof. Punna Rao Ravi is currently working as Professor in Department of Pharmacy, BITS Pilani Hyderabad Campus. He obtained his B.Pharm, M.Pharm and PhD degrees in Pharmaceutical Sciences from BITS Pilani, Rajasthan. He has been working as a faculty member in BITS-Pilani since year 2000. He has 52 publications in reputed international and national peer-reviewed journals and has presented papers in scientific conferences both in India and abroad. He has successfully completed government sponsored research projects and industry sponsored consultancy projects. He has designed and delivered several short term certificate courses on Pharmacokinetics, Pharmaceutical Biostatistics, Design of Experiments etc., for executives working in pharma industries. His research interests include bioanalytical method development and validation, nanoparticulate drug delivery systems for oral, ocular and nose-to-brain delivery and Pharmacokinetics. He had supervised 9 doctoral thesis students and currently 5 students are pursuing their doctoral thesis under his supervision.